Retinal imaging in epidemiological studies

age-related macular degeneration and the retina as a window to the brain

Doctoral thesis

to obtain a doctorate (PhD)

from the Faculty of Medicine

of the University of Bonn

Davide Garzone

from Bari, Italy

2024

Written with authorization of

the Faculty of Medicine of the University of Bonn

First reviewer: Prof. Dr. Dr. Robert P. Finger

Second reviewer: Prof. Dr. Dr. Monique M. B. Breteler

Day of oral examination: 14.08.2024

From the university hospital of Bonn, Ophthalmology

department

Director: Prof. Dr. Frank G. Holz

and the German center for neurodegenerative diseases

(DZNE), Population Health Sciences

Director: Prof. Dr. Dr. Monique M. B. Breteler

Table of contents

List of abbreviations

AD	Alzheimer's disease
AI	Artificial intelligence
AMD	Age-related macular degeneration
BM	Bruch's membrane
CFP	Color fundus photography
CI	Confidence interval
CCS	Chorioretinopatia centralis serosa
CNV	Choroidal neovascularization
DL	Deep learning
DZNE	Deutsches Zentrum für Neurodegenerative Erkrankungen/ German
	Center for Neurodegenerative Diseases, Bonn, Germany
ETDRS	Early treatment of diabetic retinopathy study
FDR	False-discovery rate / Benjamini-Hochberg correction
GA	Geographic atrophy
GCL	Ganglion cell layer
GRS	Genetic risk score
GWAS	Genome-wide association study
LDA	Large drusen area
OR	Odds ratio
OPL	Outer plexiform layer
ML	Machine learning
MS	Multiple Sclerosis
N	Number
NfL	Neurofilament light chain
OCT	Optical coherence tomography
P	p-value
PPE	Pachychoroid pigment epiteliopathy

(p)RNFL	(Peripapillary) retinal nerve fiber layer
PROS	Photoreceptor outer segment
Q	Adjusted p-value
RMSE	Root mean squared error
RPD	Reticular pseudodrusen
RPE	Retinal pigmented epithelium
SD	Standard deviation; Spectral-domain
SNP	Single nucleotide polymorphism

1. Abstract

Retinal imaging in population-based studies not only enhances our understanding of retinal diseases but, due to its high resolution and velocity, also holds great potential in the study of brain diseases. This is attributed to the possibility of direct visualization of retinal vascular and nervous tissue, being the retina part of the central nervous system. The Rhineland Study, based in Bonn, Germany, provides an ideal framework for investigating retinal and brain markers, as well as their relationship and changes across the lifespan. This population-based study integrates state-of-the-art imaging of both retina and brain, with a primary objective of examining healthy aging. In this thesis, I provide an outline of my work in this direction, largely conducted in the Rhineland Study.

Initially, I focus on grading methods and prevalence of age-related macular degeneration (AMD), the most common cause of blindness, in the first 5000 participants of the Rhineland Study. AMD classifications and consequently, epidemiological data, mainly rely on older imaging methods. I provide examples of how integration of better imaging, including optical coherence tomography (OCT), enables for better AMD endophenotyping, as it enables better detection of markers of high severity in intermediate AMD, such as reticular pseudodrusen (RPD). In the first 5000 individuals of the Rhineland Study, we observed a prevalence of 498 (10.5%) with early AMD, 401 (8.5%) with intermediate AMD and 35 (0.7%) with late AMD, while reticular pseudodrusen (RPD) were graded in 93 (1.96%) of individuals. Multimodal imaging also enables to better differentiate AMD from its main differential diagnoses in a population-based setting, such as pachychoroid disease, for which we observed a prevalence of 2.9% (N=206). Furthermore, utilizing OCT paves the way for the utilization of automated segmentation methods, such as an algorithm for automated drusen detection, which can lead to better AMD phenotyping. In this respect, I also investigated the distribution and comparability of drusen volume between two different algorithms in the MACUSTAR cohort, a multicenter cohort study focusing on generating clinical endpoints in intermediate AMD and integrating deep retinal imaging phenotyping of the recruited subjects.

Furthermore, to advance our understanding of the validity of retinal markers for neurodegeneration, I investigated the association between retinal markers and plasma levels of neurofilament light chain (NfL). Plasma NfL rises in most neurological diseases

and reflects neuroaxonal damage, thus being a marker of age-related brain atrophy and neurodegeneration.

We observed that in the general population, ageing is the main driver of an association between inner retinal atrophy and plasma NfL levels, and that the presence of neurological diseases or cardiovascular risk factors can determine their association. Hence, shared neuronal injury might drive neuronal pathology in the brain and in the retina, thereby determining their association. However, previous studies also observed that structures in the visual pathway, from the retina to the visual cortex in the occipital lobe, can undergo transneuronal neurodegeneration, in the presence of visual impairment or localized visual pathway structures pathology. This could partly explain the association between visual and cognitive impairment, since visual structures account for a large amount of brain activity and are in synaptic connection with temporal lobe cognitive structures. For these reasons I later investigated the conjoint associations between visual impairment, retinal and both global and local brain atrophy, including visual pathway and hippocampal lobe (as an important cognitive structure) in the Rhineland Study. I also aimed to estimate the relative contribution of transneuronal neurodegeneration versus common neuronal injury, to the previously observed association between retinal and brain atrophy. We observed that retinal atrophy can reflect loss of integrity in both visual and cognitive pathway structures, as well as global brain measures. Interestingly, we also observed that visual impairment showed similar associations. This is of particular interest as it highlights the importance of visual preservation as a preventative measure for brain health, even in a population-based study with a relatively low proportion of visually impaired individuals. I also observed that most of the effect of the association between retinal and brain atrophy can be attributed to a common neuronal injury mechanism. Overall, my research further reinforces the utilization of retinal readouts, in particular atrophy in the inner retina and in the ganglion cell layer, as universal markers of neurodegeneration.

Based on this work, I conclude that integration of forefront retinal imaging in population-based studies not only holds significant potential for advancing our understanding of retinal diseases such as AMD, but also for serving as overarching markers of brain structure and neurodegeneration.

2. Introduction

The last decades have witnessed large progress in retinal imaging: a notable example is the widespread adoption of spectral domain-optical coherence tomography (SD-OCT), enabling high-resolution, three-dimensional retinal visualization. Advancements in imaging have paralleled those in imaging analysis: Retinology is at the forefront of imaging-based machine learning (ML) and artificial intelligence (AI) application. These advancements have not only greatly improved the understanding of retinal diseases, such as age-related macular degeneration (AMD), but also offer overarching markers for systemic and brain diseases. In this context, population-based studies allow to investigate dynamic changes in diverse markers and with respect to the ageing process. The implementation of newer retinal imaging methods, such as SD-OCT, in population-based studies is imperative for establishing normative data on retinal markers obtained from newer imaging analysis methods and exploring their viability in both retinal diseases like AMD, and as markers of systemic and brain diseases.

My work largely focused on data from the Rhineland Study, a population-based study in Bonn, Germany with a focus on ageing and neurodegeneration. By employing state-of-the-art retinal and brain imaging as well as visual acuity and other systemic investigations, it provides an ideal framework at this scope.

2.1　Age-related macular degeneration

AMD represents the most common cause of visual impairment in Western countries. Current classifications of AMD rely on color fundus photography (CFP). For grading of AMD in the Rhineland Study, we mainly relied on the Beckmann classification, which emerged to codify a level of knowledge that was current in 2012 but that now is largely surpassed. The Beckmann classification divides early stages of AMD into early AMD (eAMD, largest diameter of the largest drusen observed on CFP between 62 and 125 µm) and intermediate AMD (iAMD, larger than 125 µm). Pigmentary abnormalities related to drusen also determine an iAMD status.(Ferris et al. 2013) Drusen provide the soil for the emergence of either choroidal neovascularization (CNV) or geographic atrophy, (GA) defining late AMD.(Mitchell et al. 2018) Early stages of AMD are common in the general population but only a minority of affected subjects will progress to late AMD.(Klaver et al.

2001) Hence, there is great interest in stratifying risk of progression of patients with early stages of AMD. So far, there is only weak evidence that some supplements might postpone late AMD onset.(Age-Related Eye Disease Study Research Group 2001)

With the advent of OCT, new imaging-based biomarkers of AMD became available, whose integration in population-based cohorts is needed. In manual AMD grading, large drusen area (LDA) was defined as total area of large drusen larger than a 650 µm circle, as described previously.(Misran and Islam 2014) Categorizing a variable that is continuous (as LDA in our analysis for capturing heavy drusen burden) represents by definition a simplification and leads to a loss of data variance larger than 30%.(Douglas G. Altman and Royston 2006) The case of drusen volume exemplifies how better imaging allows for deeper phenotyping by moving away from categorical, arbitrary threshold: in this case, from two-dimensional categories of drusen area, such as e-, iAMD and LDA to a three-dimensional quantification of drusen volume. Several algorithms exist for segmentation and quantification of drusen load and other AMD markers, some of which also implemented on OCT for drusen volume. (Wintergerst et al. 2017) A possible approach is to utilize in-built software for layers segmentation and assess drusen volume as the BM-RPE complex. This has been adopted in some studies, however it entails two main limitations: 1) manual correction would be required in the vast majority of cases, as in-built retinal layers segmentation software is insufficient in retinal pathologies and 2) both the "elevated" (drusen) and the non-elevated RPE volume would be assessed as BM-RPE complex. Furthermore, the RPE undergoes changes with ageing and other factors, which might confound drusen volume association. (Ko et al., 2017).

The MACUSTAR study is a multicenter study aiming to generate clinical end-points in iAMD (iAMD). At this scope, MACUSTAR implements deep retinal imaging phenotyping from different devices and software, providing an ideal framework for investigating imaging markers in AMD.

Against this background:

- I present grading methods and prevalence of AMD in the first 5000 participants of the Rhineland Study.
- I present preliminary results in the Rhineland Study on pachychoroid disease as a main differential diagnosis of AMD in a population-based setting, and I present some markers of pachychoroid disease observed in the Rhineland Study.

- I present the distribution and comparability of drusen volume measurements obtained from a recently developed algorithm running on Spectralis OCT against a previously FDA-approved algorithm in the MACUSTAR cohort.

  This work also serves as basis for implementation of automated drusen volume assessment in the Rhineland Study, which is mentioned in this thesis´ discussion.

2.2 Retinal markers of brain´s health and disease

Being the retina part of the CNS and a brain extension with shared vascularization, there is great interest in studying retinal markers of brain´s health and disease. Retinal imaging can offer a much higher resolution than brain imaging (for example a commercially available OCT-Angiography can reach 6 μm axially, while a state-of-the-art 7-Tesla magnetic resonance (MRI) only reaches up to 0.2 mm), is faster and less costly. For several decades CFP was the main imaging method available, thus imaging retinal markers were mainly CFP-derived. This mainly fell in the cerebro-vascular domain, as CFP-derived measures were arterioles and venules calibers or fractal dimension as well as presence of individual vascular lesions, such as microaneurysms or exudates. With the advent of OCT, direct three-dimensional retinal layers observation became possible. The retina consists of ten layers, with different cellular composition and physiology; new generation OCTs and their in-built segmentation algorithms also allow visualization, segmentation and quantification of individual retinal layers volume, hence obtaining retinal markers in a more granular fashion.

Many studies have reported OCT-derived retinal changes in patients with neurological disorders, such as AD and MS, often compared against age- and sex-matched controls.(Chan et al. 2018; Petzold et al. 2017) Previous research from population-based studies observed that OCT-derived retinal layers are associated with brain volume independently of age in the general population, and assessed their determinants as prevalent risk factors in the general population, such as smoking and systolic blood pressure.(Mauschitz et al. 2018; Mutlu et al. 2017). However, much remains unexplored, as retinal markers are not established markers of brain diseases in real-world scenario. One main limitation of current research is that we cannot distinguish between age-related and brain disease-related changes in the retina, as current research has described unspecific retinal layers atrophy and inner retinal neurodegeneration in association with

both. Large population-based studies can help overcome this limitation by providing normative data on both retinal and brain pathology in ageing, and investigate their relationship. The Rhineland Study finds itself in an ideal position for this scope, integrating state-of-the-art retinal and brain imaging in its examination battery.

In the last years, plasma neurofilament light chain (NfL) has emerged as a new sensitive marker of neuroaxonal damage, reflecting age-related brain atrophy and exhibiting increased levels in most neurological diseases(Mattsson et al. 2017; Khalil et al. 2020; Fyfe 2019; Duering et al. 2018). Assessing the relationship between OCT-derived retinal markers and plasma NfL in the general population is of great importance to understand the value of retinal atrophy as a universal marker of neurodegeneration. In this thesis, I discuss my study on the association and differential determinants of OCT-derived retinal layers and neurofilament light chain (NfL). Interestingly, due to the direct synaptic connection between retinal cells and structures within the visual pathway of the brain, retinal atrophy can serve not just as a global brain atrophy and neurodegeneration marker, but I hypothesized that it might also as an indicator of specific integrity loss in the structures of the visual pathway. This phenomenon might occur as a result of transneuronal neurodegeneration, whose evidence comes from many brain and retinal imaging studies in numerous ocular diseases, including AMD, amblyopia and glaucoma. (Noppeney et al. 2005; Lu et al. 2019; Prins, Hanekamp, and Cornelissen 2016; Malania et al. 2017; Yoshimine et al. 2018)

 A previous population-based study also performed an hypothesis-free association study between retinal layers and brain voxels, observing a preferential association with occipital lobe structures.(Mutlu et al. 2018). Interestingly, previous studies also observed an association between inner retinal neurodegeneration and cognitive loss.(Ward et al. 2020) Given that cognitive areas also receive large sensorial information from visual areas, it is also possible that transneuronal neurodegeneration might extend beyond the visual pathway and extend to downstream synaptic areas, such as the hippocampus, which is important for cognition and often employed as a marker of AD, and also serves as an important structure in visuospatial orientation, with some groups of neurons showing intact retinotopic organization. (Lee, Yeung, and Barense 2012; Silson et al. 2021) For these reasons I investigated the conjoint associations between visual impairment, retinal and both global and local brain atrophy, including visual pathway and hippocampal lobe in the

Rhineland Study. I also aimed to estimate the relative contribution of transneuronal neurodegeneration versus common neuronal injury, to the previously observed association between retinal and brain atrophy.

2.3   Thesis outline

The following chapters provide, after a general introduction on AMD, a summary of the grading methods and prevalence of the AMD in the Rhineland Study, with a focus on imaging methods and pachychoroid manifestations as an important differential diagnosis. Afterwards, I introduce our study on automated drusen volume measurements in the MACUSTAR Cohort. Later, I discuss our study on the association between retinal atrophy and plasma NfL as a measure of neuroaxonal damage, and our study on the conjoint assessment of visual impairment, retinal and both global and local brain atrophy.

In the discussion section, the importance of the work done in the context of AMD research and its relevance to the Rhineland Study cohort are discussed, together with possible research next steps and data collection. Lastly, I provide an outline of the relevance of this work in the field of retinal markers of brain disease and hypothesize possible next research steps in relation to future developments of the field.

Bibliography

Age-Related Eye Disease Study Research Group, Age-Related Eye Disease Study Research. 2001. "A Randomized, Placebo-Controlled, Clinical Trial of High-Dose Supplementation with Vitamins C and E, Beta Carotene, and Zinc for Age-Related Macular Degeneration and Vision Loss: AREDS Report No. 8." *Archives of Ophthalmology (Chicago, Ill. : 1960)* 119 (10): 1417–36. https://doi.org/10.1001/archopht.119.10.1417.

Altman, Douglas G., and Patrick Royston. 2006. "Statistics Notes: The Cost of Dichotomising Continuous Variables." *BMJ : British Medical Journal* 332 (7549): 1080. https://doi.org/10.1136/BMJ.332.7549.1080.

Chan, Victor T.T., Zihan Sun, Shumin Tang, Li Jia Chen, Adrian Wong, Clement C. Tham, Tien Y. Wong, et al. 2018. "Spectral-Domain OCT Measurements in Alzheimer's Disease: A Systematic Review and Meta-Analysis." *Ophthalmology* 4: 1–14. https://doi.org/10.1016/j.ophtha.2018.08.009.

Duering, Marco, Marek J. Konieczny, Steffen Tiedt, Ebru Baykara, Anil Man Tuladhar, Esther van Leijsen, Philippe Lyrer, et al. 2018. "Serum Neurofilament Light Chain Levels Are Related to Small Vessel Disease Burden." *Journal of Stroke* 20 (2): 228–38. https://doi.org/10.5853/jos.2017.02565.

Ferris, Frederick L., C.P. Wilkinson, Alan Bird, Usha Chakravarthy, Emily Chew, Karl Csaky, and SriniVas R. Sadda. 2013. "Clinical Classification of Age-Related Macular Degeneration." *Ophthalmology* 120 (4): 844–51. https://doi.org/10.1016/J.OPHTHA.2012.10.036.

Fyfe, Ian. 2019. "Neurofilament Light Chain — New Potential for Prediction and Prognosis." *Nature Reviews Neurology* 15 (10): 557–557. https://doi.org/10.1038/s41582-019-0265-2.

Khalil, Michael, Lukas Pirpamer, Edith Hofer, Margarete M. Voortman, Christian Barro, David Leppert, Pascal Benkert, et al. 2020. "Serum Neurofilament Light Levels in Normal Aging and Their Association with Morphologic Brain Changes." *Nature Communications* 11 (1): 812. https://doi.org/10.1038/s41467-020-14612-6.

Klaver, Caroline C W, Jacqueline J M Assink, Redmer van Leeuwen, Roger C W Wolfs, Johannes R Vingerling, Theo Stijnen, Albert Hofman, and Paulus T V M de Jong. 2001. "Incidence and Progression Rates of Age-Related Maculopathy: The Rotterdam Study." *Investigative Ophthalmology & Visual Science* 42 (10): 2237–41.

Lee, Andy C. H., Lok-Kin Yeung, and Morgan D. Barense. 2012. "The Hippocampus and Visual Perception." *Frontiers in Human Neuroscience* 6 (April): 91. https://doi.org/10.3389/fnhum.2012.00091.

Lu, Lu, Qian Li, Lianqing Zhang, Shi Tang, Xubo Yang, Longqian Liu, John A. Sweeney, Qiyong Gong, and Xiaoqi Huang. 2019. "Altered Cortical Morphology of Visual Cortex in Adults with Monocular Amblyopia." *Journal of Magnetic Resonance Imaging*, March. https://doi.org/10.1002/jmri.26708.

Malania, Maka, Julia Konrad, Herbert Jägle, John S. Werner, and Mark W. Greenlee. 2017. "Compromised Integrity of Central Visual Pathways in Patients With Macular Degeneration." *Investigative Opthalmology & Visual Science* 58 (7): 2939. https://doi.org/10.1167/iovs.16-21191.

Mattsson, Niklas, Ulf Andreasson, Henrik Zetterberg, Kaj Blennow, and for the Alzheimer's Disease Neuroimaging Initiative. 2017. "Association of Plasma Neurofilament Light With Neurodegeneration in Patients With Alzheimer Disease." *JAMA Neurology* 74 (5): 557. https://doi.org/10.1001/jamaneurol.2016.6117.

Mauschitz, Matthias M., Pieter W.M. Bonnemaijer, Kersten Diers, Franziska G. Rauscher, Tobias Elze, Christoph Engel, Markus Loeffler, et al. 2018. "Systemic and Ocular Determinants of Peripapillary Retinal Nerve Fiber Layer Thickness Measurements in the European Eye Epidemiology (E3) Population." *Ophthalmology* 125 (10): 1526–36. https://doi.org/10.1016/j.ophtha.2018.03.026.

Misran, Norbahiah, and MT Islam. 2014. "Harmonizing the Classification of Age-Related Macular Degeneration in the Three Continent AMD Consortium." *Ophthalmic Epidemiol* 5 (4): 427–34. https://doi.org/10.3109/09286586.2013.867512.Harmonizing.

Mitchell, Paul, Gerald Liew, Bamini Gopinath, and Tien Y. Wong. 2018. "Age-Related Macular Degeneration." *The Lancet* 392 (10153): 1147–59. https://doi.org/10.1016/S0140-6736(18)31550-2.

Mutlu, Unal, Pieter W.M. Bonnemaijer, M. Arfan Ikram, Johanna M. Colijn, Lotte G.M. Cremers, Gabriëlle H.S. Buitendijk, Johannes R. Vingerling, et al. 2017. "Retinal Neurodegeneration and Brain MRI Markers: The Rotterdam Study." *Neurobiology of Aging* 60 (December): 183–91. https://doi.org/10.1016/j.neurobiolaging.2017.09.003.

Mutlu, Unal, Mohammad K. Ikram, Gennady V. Roshchupkin, Pieter W. M. Bonnemaijer, Johanna M. Colijn, Johannes R. Vingerling, Wiro J. Niessen, Mohammad A. Ikram,

Caroline C. W. Klaver, and Meike W. Vernooij. 2018. "Thinner Retinal Layers Are Associated with Changes in the Visual Pathway: A Population-Based Study." *Human Brain Mapping* 39 (11): 4290–4301. https://doi.org/10.1002/hbm.24246.

Noppeney, Uta, Karl J. Friston, John Ashburner, Richard Frackowiak, and Cathy J. Price. 2005. "Early Visual Deprivation Induces Structural Plasticity in Gray and White Matter." *Current Biology* 15 (13): R488–90. https://doi.org/10.1016/J.CUB.2005.06.053.

Petzold, Axel, Laura Balcer, Peter A. Calabresi, Fiona Costello, Teresa Frohman, Elliot Frohman, Elena H. Martinez-Lapiscina, et al. 2017. "Retinal Layer Segmentation in Multiple Sclerosis: A Systematic Review and Meta-Analysis." *The Lancet Neurology* 16 (10): 797–812. https://doi.org/10.1016/S1474-4422(17)30278-8.

Prins, Doety, Sandra Hanekamp, and Frans W. Cornelissen. 2016. "Structural Brain MRI Studies in Eye Diseases: Are They Clinically Relevant? A Review of Current Findings." *Acta Ophthalmologica* 94 (2): 113–21. https://doi.org/10.1111/aos.12825.

Silson, Edward H, Peter Zeidman, Tomas Knapen, and Chris I Baker. 2021. "Representation of Contralateral Visual Space in the Human Hippocampus." https://doi.org/10.1523/JNEUROSCI.1990-20.2020.

Ward, David D., Matthias M. Mauschitz, Meta M. Bönniger, Natascha Merten, Robert P. Finger, and Monique M.B. Breteler. 2020. "Association of Retinal Layer Measurements and Adult Cognitive Function: A Population-Based Study." *Neurology* 95 (9): e1144–52. https://doi.org/10.1212/WNL.0000000000010146.

Wintergerst, Maximilian W.M., Thomas Schultz, Johannes Birtel, Alexander K. Schuster, Norbert Pfeiffer, Steffen Schmitz-Valckenberg, Frank G. Holz, and Robert P. Finger. 2017. "Algorithms for the Automated Analysis of Age-Related Macular Degeneration Biomarkers on Optical Coherence Tomography: A Systematic Review." *Translational Vision Science & Technology* 6 (4): 10. https://doi.org/10.1167/tvst.6.4.10.

Yoshimine, Shoyo, Shumpei Ogawa, Hiroshi Horiguchi, Masahiko Terao, Atsushi Miyazaki, Kenji Matsumoto, Hiroshi Tsuneoka, Tadashi Nakano, Yoichiro Masuda, and Franco Pestilli. 2018. "Age-Related Macular Degeneration Affects the Optic Radiation White Matter Projecting to Locations of Retinal Damage." *Brain Structure and Function* 223 (8): 3889–3900. https://doi.org/10.1007/s00429-018-1702-5.

3. Age-related macular degeneration in the Rhineland Study cohort

3.1 Imaging protocol, grading methods and results

Macula-centered CFP are obtained in the Rhineland study following pharmacological pupil dilation (Visucam 500, Carl Zeiss Meditec AG). AMD status was graded by two main trained graders and three junior graders using the K-DRS software (University of Regensburg, Regensburg, Germany). We categorized AMD based on the clinical classification of AMD, also referred to as Beckmann classification. (Ferris et al. 2013) We defined macular area inside an early treatment for diabetic retinopathy (ETDRS) grid. ("Grading Diabetic Retinopathy from Stereoscopic Color Fundus Photographs—An Extension of the Modified Airlie House Classification: ETDRS Report Number 10" 1991) Additionally, other lesions were graded:

- Large load of small drusen (LLD) was defined as more than 20 small, hard drusen in the macula (macular LLD) or in the periphery (peripheral LLD).
- Large drusen area (LDA) was defined as a total area of large drusen larger than a 650 µm circle as described previously. (Misran and Islam 2014)
- Reticular pseudodrusen (RPD) were shown in multiple studies to increase the risk of AMD progression, but multimodal imaging is needed for their assessment, as they are poorly recognizable on CFP. (Rabiolo et al. 2017; Finger et al. 2016)Hence, images graded with any AMD were re-assessed with multimodal imaging to assess for RPD, defined as infrared imaging and with OCT as drusenoid deposits occurring in correspondence with or above the RPE.

We graded these lesions to address limitations of the Beckmann classification. In particular, small drusen can occur in ageing or in younger individuals. However, it is unknown whether many small, hard drusen as in LLD might precede the onset of early AMD or increase the risk of AMD progression among individuals who also display features of AMD. Previous studies have also shown that higher drusen burden is associated with increased AMD risk and severity, hence we tried to capture this by, among individuals with AMD, grading those with LDA. (Abdelfattah et al. 2016; Nassisi et al. 2019) We employed multimodal imaging to adjudicate between disagreements, for which an expert grader adjudicated. All AMD cases and doubtful cases graded by junior graders were also reviewed with multimodal imaging by a main grader. Since RPD and LDA were only

assessed by main graders and among already graded AMD cases, inter-rater kappa was not determined. We reported kappa across raters for AMD-defining lesions, LLD and other drusen in **Table 3.1.**

A kappa coefficient between 0.6-0.8 (highlighted in yellow in Table 2.1.1) and larger than 0.8 constitutes substantial and optimal agreement between raters, respectively. (D.G. Altman 1991)In our study a high agreement was not reached for smaller and peripheral drusen, indicating a higher variability in their assessment. Agreement for LLD was not uniform across raters, ranging from 0.39 to 0.78; the value of 0 refers to a small cohort with only one LLD case and should be thus far disregarded and re-assessed in a larger sample. Our results are comparable with previous studies reporting inter-agreement. (Mitchell et al. 1995; Klein, Klein, and Linton 2013)

In our study, both CFP and OCT with multimodal imaging (mainly infra-red and autofluorescence) were employed, although multimodal imaging was only consulted as a second-line method. Our method is somewhat novel for AMD grading in a population-based study. While CFP is barely utilized for AMD assessment in ophthalmological clinics, as it has been largely replaced by OCT and multimodal imaging (mainly, infrared and autofluorescence), most epidemiological studies still employ CFP as the method of choice for AMD grading, being the Beckmann classification based on it. (Ferris et al. 2013)

A previous study has provided formulas for translating drusen read-outs from Beckmann classification onto OCT. (Kim et al. 2021)It should be pointed out that OCT provides for retinal visualization in three- , rather than two-dimensions as in CFP, hence newer AMD classifications taking into account multimodal imaging, integrating different imaging methods, are needed. A recent study compared the grading of AMD with CFP vs. multimodal imaging, showing marked differences in obtained AMD prevalence. (Hogg et al. 2022)Interestingly, they also reported that an age-related effect was more marked in OCT-, rather than CFP-based grading, attributed to over-grading of small drusen in CFP at a younger age and an increase in lens opacifications masking real drusen at older age (CFP being more subject to lens opacifications than OCT). Also in my observation, a univocal correspondence between drusen-like lesions on CFP and OCT is not always present, while on OCT deeper phenotyping is possible (for example, distinguishing between complete and incomplete GA). Multimodal imaging also allowed to better

differentiate between AMD and AMD-mimicking differentials such as pachychoroid, discussed later.

In conclusion, we employed a combination of CFP and multimodal imaging (mainly infrared, OCT and autofluorescence) for AMD grading in the Rhineland Study, although CFP represented the first-line grading. The reached agreement between graders was at least substantial (kappa > 0.6).

Table 3.1 Agreement between raters in a dataset of 7901 participants of the Rhineland Study.

	Rater DG – Rater MMM							
Lesion	Small Drusen	Int. Drusen	Large Drusen	LLD	PA, AMD-related	Large peripheral Drusen	Int. peripheral Drusen	Small peripheral Drusen
Agreement	82.865	97.753	100	98.596	99.438	74.438	89.045	97.191
Kappa	0.642	0.859	1	0.776	0.83	0.5	0.502	0.601
Percentages, DG	0.587	0.081	0.037	0.025	0.017	0.031	0.098	0.379
Percentages MMM	0.624	0.093	0.037	0.039	0.017	0.042	0.152	0.545
	Rater DG – Rater JR							
Lesion	Small Drusen	Int. Drusen	Large Drusen	LLD	PA, AMD-related	Large peripheral Drusen	Int. peripheral Drusen	Small peripheral Drusen
Agreement	79.918	96.311	99.044	98.634	99.18	71.585	90.574	98361
Kappa	0.599	0.663	0.795	0.66	0.663	0.454	0.466	0.592
Percentages, DG	0.546	0.048	0.02	0.018	0.008	0.02	0.108	0.602
Percentages, JR	0.485	0.068	0.027	0.023	0.016	0.02	0.087	0.4
	Rater DG – Rater VM							
Lesion	Small Drusen	Int. Drusen	Large Drusen	LLD	PA, AMD-related	Large peripheral Drusen	Int. peripheral Drusen	Small peripheral Drusen
Agreement	78	97	98	98	98.667	80	90.333	97
Kappa	0.563	0.836	0.802	0.39	0.744	0.599	0.559	0.511
Percentages, DG	0.537	0.093	0.047	0.013	0.02	0.033	0.137	0.493
Percentages.VM	0.45	0.11	0.06	0.02	0.033	0.03	0.113	0.367
	Rater DG – Rater NF							
Lesion	Small Drusen	Int. Drusen	Large Drusen	LLD	PA, AMD-related	Large peripheral Drusen	Int. peripheral Drusen	Small peripheral Drusen
Agreement	72.308	97.692	97.692	98.462	98.462	70	90.769	96.154
Kappa	0.446	0.812	0.758	0	0.743	0.395	0.63	0.266
Percentages, DG	0.562	0.054	0.062	0	0.023	0.023	0.154	0.646

		Intra-rater DG						
Percentages.NF	0.5	0.077	0.038	0.015	0.038	0.031	0.138	0.515
Lesion	Small Drusen	Int. Drusen	Large Drusen	LLD	PA, AMD-related	Large peripheral Drusen	Int. peripheral Drusen	Small peripheral Drusen
Agreement	82.824	99.237	98.855	98.855	99.237	74.427	90.84	96.183
Kappa	0.641	0.937	0.763	0.764	0.746	0.484	0.563	0.48
Percentages, DG	0.58	0.069	0.027	0.019	0.015	0.038	0.095	0.351
Percentages. DG, intra-rater	0.637	0.061	0.023	0.031	0.015	0.038	0.141	0.485

Green indicates almost perfect agreements reached between raters (kappa > 0.8), yellow indicates substantial agreement between raters (kappa between 0.61 and 0.80)

3.2   AMD prevalence and demographics

We assessed absolute and age-standardized prevalence of AMD in the Rhineland Study population, as well as of the three aforementioned high-risk phenotypes (LDA, RPD, LLD). For assessing the overall AMD status, we considered the worse eye, an approach typically adopted in population-based studies. AMD is by definition an age-related disease. However, AMD-related phenotypes, such as drusen or pigmentary abnormalities can also occur in younger subjects. It is currently unknown whether these lesions share common pathophysiological significance as in AMD. Interestingly, while drusen represent the hallmark lesion of early stages of AMD, drusen and drusen-like lesions can also occur in other maculopathies such as dystrophic maculopathies or pachychoroid spectrum disease (in this case, named pachydrusen.(Khan et al. 2016) For this reason, the prevalence of AMD-related phenotypes in individuals younger than 50 years old in the Rhineland Study are also reported.

Among 7901 individuals with graded images, in 725 (9.2%) individuals no gradable data was available in either eye. Of these, 264 individuals (3.3%) were excluded during grading because of low quality of images, while for 461 subjects (5.8%) no images were available. The main reasons for missing images were technical problems (n=166, 2.1%), lack of time (n=73, 0.9%) and refused examination (n=44, 0,6%). In this dataset, in 254 individuals only was eye was graded, as the other eye was discarded during grading due to low quality. We excluded individuals younger than 50 years of age, leaving 4729 subjects with complete data on AMD in at least one eye for data analysis. Characteristics of this study population are presented in **Table 3.2.**

Associations between increasing AMD stages, high-risk endophenotypes and dependent variables were assessed with logistic regression. When assessing LDA, only individuals with iAMD were considered.

In the analytical population, in 3795 (80.2%) individuals no AMD was observed, while 498 (10.5%) were graded with eAMD, 401 (8.5%) with iAMD and 35 (0.7%) with late AMD. Standardized AMD prevalence by age decade is shown in **Image 3.1.** Early AMD prevalence rose from 6.7% in the 50-60 to 17.9% in the 80+ age group, similarly iAMD rose from only 3.1% to 28.7% in the oldest, and late AMD from just one case (0.05%) in the 50-60 decade to 5.7% in the 80+ age group. Similar trends were observed for largest macular and peripheral drusen (**Table 3.3**).

RPD were graded in 93 (1.96%) of individuals; however, it must be noted that our initial assessment was only based on CFP and images graded with AMD were re-assessed for RPD. Hence, only 6 (0.1%) individuals were graded with RPD in the no AMD group (thus in the absence of other signs of AMD) which might be an underestimate of the real prevalence obtained if images were assessed on first-line with multimodal imaging, as RPD might be poorly visible on CFP. Macular LLD were graded in 220 (4.6%) of individuals; of which 104 were graded with no AMD and 116 were graded with AMD (12.4% of all AMD cases). Prevalence data of LDA, RPD and LLD stratified by AMD stages and age groups are showed in **Table 3.4**.

One increasing year of age was associated with higher odds of AMD (est. [95%CI], p = 1.091 [1.082 − 1.100] <0.0001, RPD 1.106 [1.076 − 1.140], <0.0001) and LDA among individuals with AMD (est. [95%CI], p = 1.082 [1.051 − 1.116], <0.0001). LLD was associated with increasing age but not independently of AMD (included as covariate). Sex was not associated with AMD, nor with presence of RPD, LLD or LDA in our population after age adjustment; however, male sex was associated with lower odds of larger peripheral drusen (est. [95%CI], p = 0.505 [0.444 − 0.575], <0.0001). No and small drusen were present in 694 (28.4%) and 1666 (68.3%) of individuals, while medium and large drusen were present in 73 (2.99%) and 8 (0.33%) of individuals. Also in the age range 30-50, increasing age was associated with higher odds of larger drusen presence (est. [95%CI], p = 1.041 [1.025 − 1.057], <0.0001).

Several population-based studies have reported AMD prevalence, with estimates ranging from 16.2% to 27.7% in two recent meta-analyses. (Colijn, et al., 2017; Li et al., 2020).

Our results are generally in range with these previous results. Small disparities are explained by factors intrinsic to the population, such as heterogeneity across age groups and different grading methods and imaging devices utilized. No sex preference for AMD is expected after adjustment for age (which accounts for a survival bias of women at older age), which is in line with our results.

RPD were present in 93 (1.9%) of the population sample and 87 (9.3%) of individuals with AMD, while LDA in 78 (8.3%) of individuals with intermediate or late AMD. A marked age-effect was observed for both lesions, with their prevalence going from 0.2% to around 9% from youngest to oldest age group. These two are markers of high AMD severity and progression risk and their assessment is an important factor for risk stratification. (Abdelfattah et al. 2016; Rabiolo et al. 2017)

Prevalence of AMD-related lesions in individuals younger than 50 have been also reported by previous studies, with estimates to the ones provided in our analysis (Brandl et al. 2016; Silvestri et al. 2012)

Despite agreement for peripheral drusen being lower than for macular drusen in our population, a similar sex effect has been observed in previous studies. It is currently unknown whether larger peripheral drusen constitute a risk factor for the development of AMD. In conclusion, in this dataset the prevalence of AMD in the Rhineland Study was 19.7% and ranged from 9.8% to 52.3% from youngest to oldest age group.

Table 3.2 Characteristics of the study population included for AMD prevalence data in the Rhineland Study. Excluded individuals tended to be older and have higher SBP, but no differences in smoking habits and BMI were observed.

	Missing/excluded participants	Analytical population	p
N	549	4729	
Age (mean (SD))	67.6131 (10.5026)	63.4070 (9.2597)	<0.001
Sex = m (%)	227 (41.3)	2099 (44.4)	0.190
SBP (mean (SD))	132.0382 (17.8567)	129.2991 (16.1424)	<0.001
BMI (mean (SD))	26.0113 (4.1507)	26.3667 (4.5836)	0.103
Smoking (%)			0.228
Current	45 (9.9)	547 (11.8)	
Former	223 (49.0)	2091 (45.2)	
Never	187 (41.1)	1984 (42.9)	

N= number, m=male, SD= Standard Deviation, SBP= Systolic blood pressure

Table 3.3, Age-standardized prevalence of largest drusen in the Rhineland Study.

	No	Small	Medium	Large
Largest macular drusen				
50-60	482 (23.7%)	1348 (66.4%)	146 (7.2%)	55 (2.7%)
60-70	329 (21.6%)	936 (61.3%)	170 (11.1%)	91 (5.96%)
70-80	187 (20.9%)	379 (42.4%)	167 (18.7%)	160 (17.9%)
80+	48 (17.2%)	86 (30.8%)	60 (21.5%)	85 (30.5%)
Largest peripheral drusen				
	No	Small	Medium	Large
50-60	517 (25.5%)	1123 (55.3%)	305 (15.0%)	86 (4.23%)
60-70	436 (28.6%)	646 (42.3%)	319 (20.9%)	125 (8.19%)
70-80	301 (33.7%)	244 (27.3%)	196 (21.9%)	152 (17.0%)
80+	89 (31.9%)	57 (20.4%)	75 (26.9%)	58 (20.8%)

Table 3.4, Age standardized prevalence of high-risk endophenotypes (RPD, LDA, LLD).

LDA		RPD		LLD	
Age group	N (%)	Age group	N (%)	Age group	N (%)
50-60	4 (0.19)	50-60	4 (0.20)	50-60	88 (0.043)
60-70	14 (0.92)	60-70	12 (0.79)	60-70	60 (0.039)
70-80	35 (3.92)	70-80	48 (5.4)	70-80	50 (0.056)
80+	25 (8.96)	80+	29 (10.4)	80+	22 (0.079)
AMD stage	N (%)	Age group	N (%)	AMD stage	N (%)
Intermediate	70 (17.46)	No	6 (0.16)	No	164 (0.026)
Late	8 (22.86)	Early	23 (4.6)	Early	65 (0.13)
		Intermediate	49 (12.2)	Intermediate	44 (0.11)
		Late	15 (42.9)	Late	7 (0.2)

N= number, LDA= Large drusen area, RPD= Reticular pseudodrusen, LLD= Large load of small drusen, AMD = Age-related macular degeneration
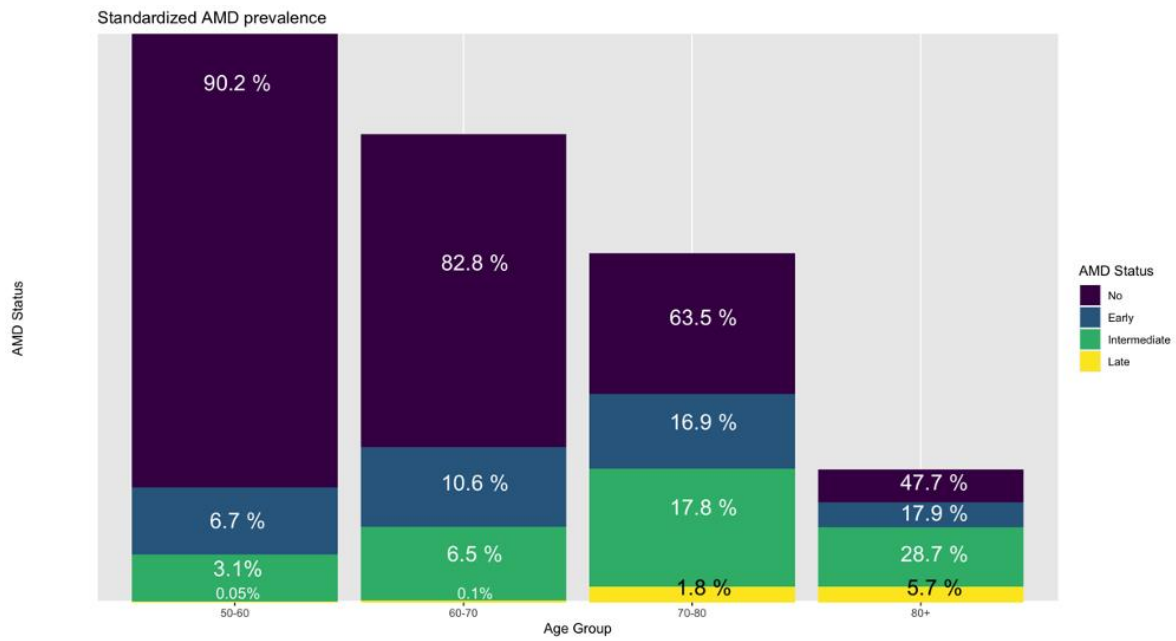
Image 3.1, Bar plot showing AMD-prevalence standardized per age decade. Percentages indicate proportion of individuals with each AMD stage per age decade group.

Bibliography

Abdelfattah, Nizar Saleh, Hongyang Zhang, David S. Boyer, Philip J. Rosenfeld, William J. Feuer, Giovanni Gregori, and SriniVas R. Sadda. 2016. "Drusen Volume as a Predictor of Disease Progression in Patients With Late Age-Related Macular Degeneration in the Fellow Eye." *Investigative Opthalmology & Visual Science* 57 (4): 1839. https://doi.org/10.1167/iovs.15-18572.

Altman, D.G. 1991. *Practical Statistics for Medical Research.* Chapman and Hall, London.

Brandl, Caroline, Valentin Breinlich, Klaus J. Stark, Sabrina Enzinger, Matthias Aenmacher, Matthias Olden, Felix Grassmann, et al. 2016. "Features of Age-Related Macular Degeneration in the General Adults and Their Dependency on Age, Sex, and Smoking: Results from the German KORA Study." *PloS One* 11 (11). https://doi.org/10.1371/JOURNAL.PONE.0167181.

Ferris, Frederick L., C.P. Wilkinson, Alan Bird, Usha Chakravarthy, Emily Chew, Karl Csaky, and SriniVas R. Sadda. 2013. "Clinical Classification of Age-Related Macular Degeneration." *Ophthalmology* 120 (4): 844–51. https://doi.org/10.1016/J.OPHTHA.2012.10.036.

Finger, Robert P., Elaine Chong, Myra B. McGuinness, Luba D. Robman, Khin Zaw Aung, Graham Giles, Paul N. Baird, and Robyn H. Guymer. 2016. "Reticular Pseudodrusen and Their Association with Age-Related Macular Degeneration: The Melbourne Collaborative Cohort Study." *Ophthalmology* 123 (3): 599–608. https://doi.org/10.1016/J.OPHTHA.2015.10.029.

"Grading Diabetic Retinopathy from Stereoscopic Color Fundus Photographs—An Extension of the Modified Airlie House Classification: ETDRS Report Number 10." 1991. *Ophthalmology* 98 (5): 786–806. https://doi.org/10.1016/S0161-6420(13)38012-9.

Hogg, Ruth E, David M Wright, Nicola B Quinn, Katherine Alyson Muldrew, Barbra Hamill, Laura Smyth, Amy Jayne Mcknight, et al. 2022. "Prevalence and Risk Factors for Age-Related Macular in a Population-Based Cohort Study of older Adults in Northern Ireland Using Multimodal: NICOLA Study." *Br J Ophthalmol* 0: 1–7. https://doi.org/10.1136/bjophthalmol-2021-320469.

Khan, Kamron N., Omar A. Mahroo, Rehna S. Khan, Moin D. Mohamed, Martin McKibbin, Alan Bird, Michel Michaelides, Adnan Tufail, and Anthony T. Moore. 2016.

"Differentiating Drusen: Drusen and Drusen-like Appearances Associated with Ageing, Age-Related Macular Degeneration, Inherited Eye Disease and Other Pathological Processes." *Progress in Retinal and Eye Research*. Elsevier Ltd. https://doi.org/10.1016/j.preteyeres.2016.04.008.

Kim, Dong Yoon, Jessica Loo, Sina Farsiu, and Glenn J. Jaffe. 2021. "Comparison of Single Drusen Size on Color Fundus Photography and Spectral-Domain Optical Coherence Tomography." *Retina (Philadelphia, Pa.)* 41 (8): 1715–22. https://doi.org/10.1097/IAE.0000000000003099.

Klein, Ronald, Barbara E.K. Klein, and Kathryn L.P. Linton. 2013. "Prevalence of Age-Related Maculopathy." *Ophthalmology* 99 (6): 933–43. https://doi.org/10.1016/s0161-6420(92)31871-8.

Misran, Norbahiah, and MT Islam. 2014. "Harmonizing the Classification of Age-Related Macular Degeneration in the Three Continent AMD Consortium." *Ophthalmic Epidemiol* 5 (4): 427–34. https://doi.org/10.3109/09286586.2013.867512.Harmonizing.

Mitchell, Paul, Wayne Smith, Karin Attebo, and Jie Jin Wang. 1995. "Prevalence of Age-Related Maculopathy in Australia: The Blue Mountains Eye Study." *Ophthalmology* 102 (10): 1450–60. https://doi.org/10.1016/S0161-6420(95)30846-9.

Nassisi, Marco, Jianqin Lei, Nizar Saleh Abdelfattah, Ayesha Karamat, Siva Balasubramanian, Wenying Fan, Akihito Uji, et al. 2019. "OCT Risk Factors for Development of Late Age-Related Macular Degeneration in the Fellow Eyes of Patients Enrolled in the HARBOR Study." *Ophthalmology* 126 (12): 1667–74. https://doi.org/10.1016/J.OPHTHA.2019.05.016.

Rabiolo, Alessandro, Riccardo Sacconi, Maria Vittoria Cicinelli, Lea Querques, Francesco Bandello, and Giuseppe Querques. 2017. "Spotlight on Reticular Pseudodrusen." *Clinical Ophthalmology (Auckland, N.Z.)* 11: 1707–18. https://doi.org/10.2147/OPTH.S130165.

Silvestri, G., M. A. Williams, C. McAuley, K. Oakes, E. Sillery, D. C. Henderson, S. Ferguson, V. Silvestri, and K. A. Muldrew. 2012. "Drusen Prevalence and Pigmentary Changes in Caucasians Aged 18-54 Years." *Eye (London, England)* 26 (10): 1357–62. https://doi.org/10.1038/EYE.2012.165.

4. Pachychoroid spectrum lesions as a differential in age-related macular degeneration grading

Manifestations of pachychoroid spectrum have been described since several years as single entities, but their synoptic attribution to pachychoroid spectrum is a somehow novel clinical entity that emerged in the last decade.(Cheung et al. 2019). Pachychoroid spectrum disease comprises different subtypes:

1. Central serous chorioretinopathy (CCS)
2. Pachychoroid pigment epiteliopathy (PPE)
3. Focal choroidal excavation (FCE)
4. Peripapillary pachychoroid syndrome (PPS)
5. Pachychoroid neovasculopathy (PNV)

CCS is mainly characterized by subretinal exudation and presents typically in an acute fashion as sudden visual changes or loss, and may completely resolve or recur and become chronic, with subretinal fluid persisting over time which can predispose to the development of neovascularization.(Berger, Bühler, and Yzer 2021) PPS is a less commonly described clinical form characterized by similar changes near the optic disc; while FCE is characterized by a foveolar excavation pointing towards the choroid with hyperreflective changes and is less described in literature.(Phasukkijwatana et al., n.d.) PPE has been introduced in the last years as fundus pigmentary changes associated with hyperreflectivity and pachydrusen at OCT and has been described as a "forme fruste" of CCS, with similar but less pronounced pathogenesis that does not lead to subretinal fluid.(Warrow, Hoang, and Freund 2013) This is supported by the observation that pigmentary changes might remain after acute CCS resolution.(Berger, Bühler, and Yzer 2021; Warrow, Hoang, and Freund 2013; Cheung et al. 2019) All of these lesions share a large choroid and/or dysfunctional choriocapillaris, constituting the retina-choroid interface.(Cheung et al. 2019)

Pachychoroid lesions constituted a main differential diagnostic for AMD in the Rhineland Study population. They may mimic an early- or intermediate-AMD phenotype on fundus and/or on OCT, since they might also display drusen or drusen-like lesions, in this case named pachydrusen, which represent the hallmark lesion of

AMD, and pigmentary abnormalities.(Khan et al. 2016; Cheung et al. 2019) However, different pathophysiology and disease course underlie pachychoroid spectrum.(Cheung et al. 2019; Rämö et al. 2023; Yamashiro et al. 2020) Multimodal imaging allows for their better distinction based on criteria such as sub-foveal or sub-lesion choroid size on OCT or individual lesions feature (e.g. choroidal hypertransmission in smaller drusen on OCT) or patients demographics (AMD rarely happens at the age of 50, while pachychoroid spectrum lesions can occur in younger individuals).(Yamashiro et al. 2020) Many population-based studies did not employ multimodal imaging, hence it is safe to assume that AMD cohort might have included eyes with diseases mimicking AMD, such as pachychoroid lesions or dystrophies. Smoking, male sex, stress with related type A-personality and cortisol levels have been implicated in pachychoroid spectrum manifestations; an association with hyperopic refractive errors has been noted.(Cheung et al. 2019; Yamashiro et al. 2020)

Interestingly, recent studies hypothesized that protective genetic variants in genes involved in complement regulation, such as CFH, might confer an elevated risk of pachychoroid spectrum manifestations. (Rämö et al. 2023) In general, much is still unknown of pachychoroid spectrum and no large epidemiological or population-based studies have assessed its prevalence, determinants and associations. This is largely due to these lesions possibly affecting vision only in a minority of cases and to the recent emergence as a distinct, clinical entity. Furthermore, both end-stadium of pachychoroid lesions and AMD can present as neovascular lesions, which are mainly treated with anti-VEGF therapy irrespective of their etiology.(Pang and Freund 2015) However, with the current advancement in imaging and -omics for phenotypic delineation of these clinical entities, as well as with rapid development of therapeutic options in medical retina, delineation and stratification of individual phenotypes might aid better therapeutic options.(Schmitz-Valckenberg et al. 2022) For these reasons, we assessed prevalence and association of graded pachychoroid spectrum in the Rhineland Study.

For assessing CCS prevalence, 7170 individuals were included. The same population was included for AMD Grading, but no age cut-offs were employed for this analysis. Main criteria were lesions distribution (for example following gravity,

previously termed gravitational tracks), thick sub-foveal or sub-lesional choroidal vessels on SD-OCT and enhanced depth imaging, exudative sub-retinal lesions with or without associated pachydrusen, choroidal hypertransmission, pigmentary abnormalities on CFP. Drusen and pigmentary abnormalities were graded. Example of cases primarily graded as CCS are shown in **Image 7.1 and Image 7.2.**

Associations between CCS and factors acting on a subject level (e.g., age or genetics) were assessed by considering CCS as a binary variable in the worse eye and modeled with multivariable logistic regression. Associations with ocular factors, such as spherical equivalent, were assessed with logistic mixed-models with a random effect for each eye to account for eye inter-correlation.

In total, 206 individuals (2.9%) were graded as displaying pachychoroid spectrum features in either eye. Among these, 52 (25.2%) showed features of pachychoroid spectrum in both eyes and 150 (72.8%) only in one eye. Pigmentary abnormalities were detected In 86 individuals (41.74%), while small, medium and drusen were observed in 124 (60.2%), 13 (6.3%) and 6 (2.9%) of individuals, respectively. Focal excavation and peripapillary pachychoroidal lesion were observed in only 4 (1.9%) and 2 (1%) of individuals, respectively.

Individuals graded with pachychoroid spectrum tended to be more often males (OR [95% CI] for male sex: 3.078 [2.021 - 4.80], $p<0.0001$) and younger (0.974 [0.951 - 0.996], $p=0.03$). Trends of pachychoroid spectrum disease for best-corrected visual acuity (VA) are shown in **Table 7.1**. 383 (93%) of eyes graded with pachychoroid disease had a VA of 20/25 or higher, while VA was 0.4 or lower only in four eyes (1.2%). Among eyes with low VA, two were graded with active CCS and two with PPE and small, hard drusen. Individuals graded with pachychoroid spectrum disease tended to show more often hyperopic refractive errors (after age and sex adjustment, OR [95% CI] for SE: 1.081 [1.03 - 1.13], $p<0.0005$).

Interestingly, a diagnosis of CCS was associated with lower GRS and complement subscore for AMD (OR [95% CI] = 0.81 [0.65 − 0.98] and 0.81 [0.65 − 0.99], respectively).

In this population, pachychoroid spectrum had a prevalence of 2.9%. I observed that pachychoroid spectrum constitutes an important differential of AMD, as they might

display similar lesions (namely, pigmentary changes and pachydrusen) and that multimodal imaging might be a key element for differentiating them. I observed that isolated PPE or pachydrusen were the most common pachychoroid phenotypes, with only a minority of individuals showing active exudative or excavation lesions. The associations with male sex and with hyperopic refractive errors have been reported previously. Interestingly, most individuals had a high visual acuity, suggesting that most of these lesions might go undetected throughout life and/or be misdiagnosed for early AMD or normal age-related changes. We also observed that pachychoroid spectrum lesions were more common at younger age. It is possible that at a younger age, pachychoroid spectrum lesion might have a higher incidence and that most of them might eventually resolve with time, with only a minority of individuals eventually developing chronic forms. In this regard, it must be noted that given our population-based sample, invasive tests like indocyanine green angiography could not be employed as in a clinical setting. This implies that that individuals with more severe pachychoroid lesions possibly occurring at older age with longer disease course, such as pachychoroid neovasculopathy, might have been more often misclassified as neovascular AMD.

The observations that pachychoroid lesions had a negative association with a GRS and complement subscore for AMD, strengthens and confirms the notion that the two diseases might have opposite genetic background. Interestingly, this has been recently theorized by some authors for CFH variants, while we observed this for a while complement subscore and GRS for AMD. (Yamashiro et al. 2020) A main strength of this analysis is standardized data collection and the large population-based setting attributing novelty of our findings, as so far studies on pachychoroid spectrum disease were limited to clinical settings. A main limitation of our study is the somehow qualitative definition of pachychoroid spectrum, which was not supported by quantitative criteria such as choroidal thickness.

In conclusion, I reported a prevalence of 2.8% pachychoroid spectrum disease in a population-based setting. One-fourth of individuals showed bilateral lesions; pigmentary abnormalities and pachydrusen larger than 63 μm were observed in approximately 41% and 9% of individuals respectively. Pachychoroid spectrum

disease was associated with higher spherical equivalent, younger age, male sex and lower genetic risk for AMD. More research on pachychoroid spectrum is needed.

Table 4.1, Distribution of eyes with pachychoroid disease per level of visual acuity

	N (percentage)
0.32	1 (0.242%)
0.4	2 (0.485%)
0.5	2 (0.485%)
0.63	24 (5.825%)
0.8	54 (13.106%)
1	60 (14.563%)
1.25	269 (65.291%)
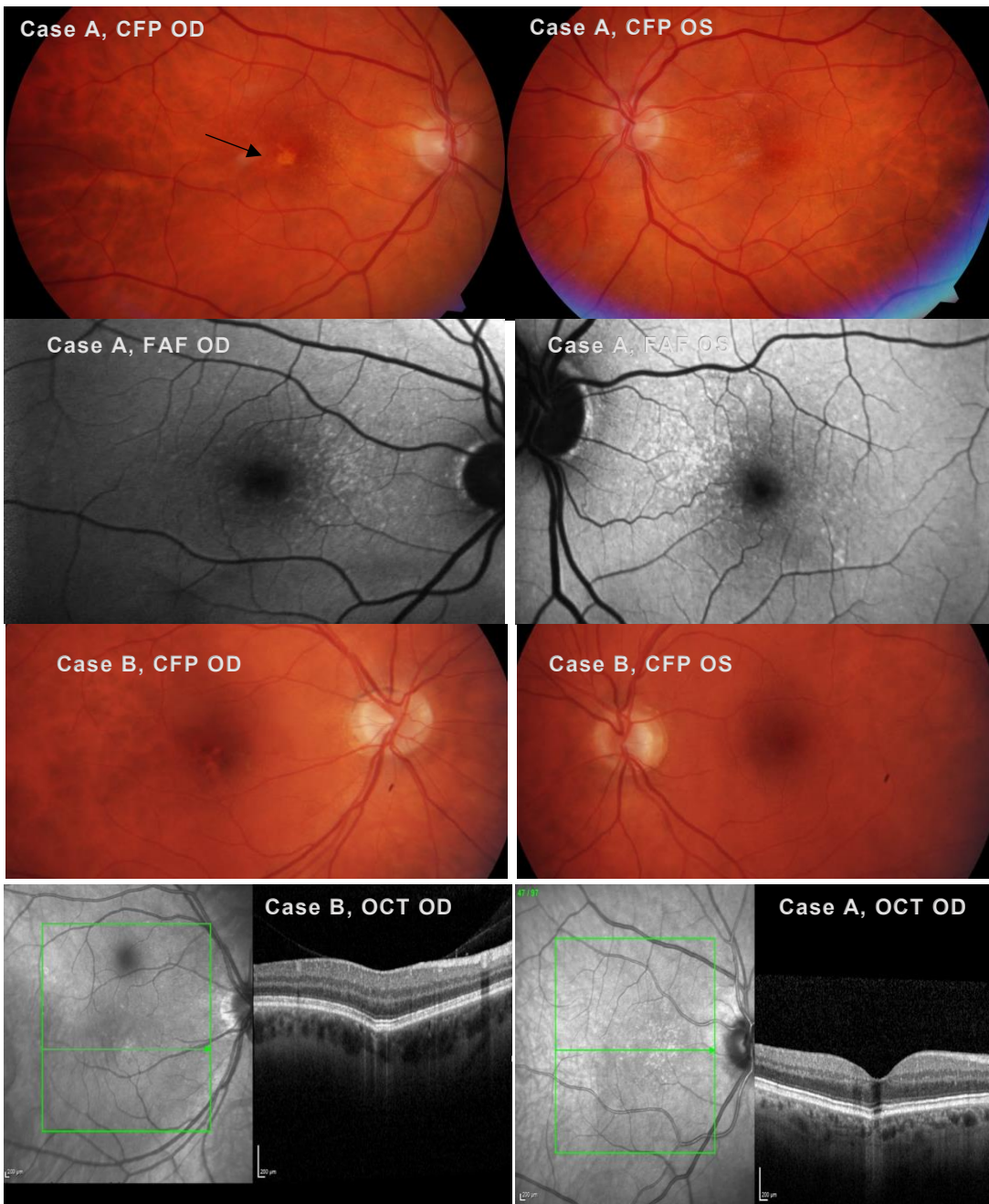
Image 4.1, Focal choroidal excavation in pachychoroid spectrum mimicking AMD.
In Case A (81 yo, male), on CFP numerous, hard, closely packed small drusen like structures seen and an ovoid soft drusen-like lesion (black arrow) are observed; hyperreflective dot-like lesions are observed on FAF, while in OCT a focal choroidal excavation with choroidal hypertransmission corresponds to the lesion observed on CFP. In Case B (41 yo male), in the right eye large soft drusen-like lesions with hyperpigmentary changes are noted, which correspond to a focal foveal choroidal excavation with choroidal hypertransmission on OCT and hyperreflectivity on infrared. A large choroid for age is observed in both cases.
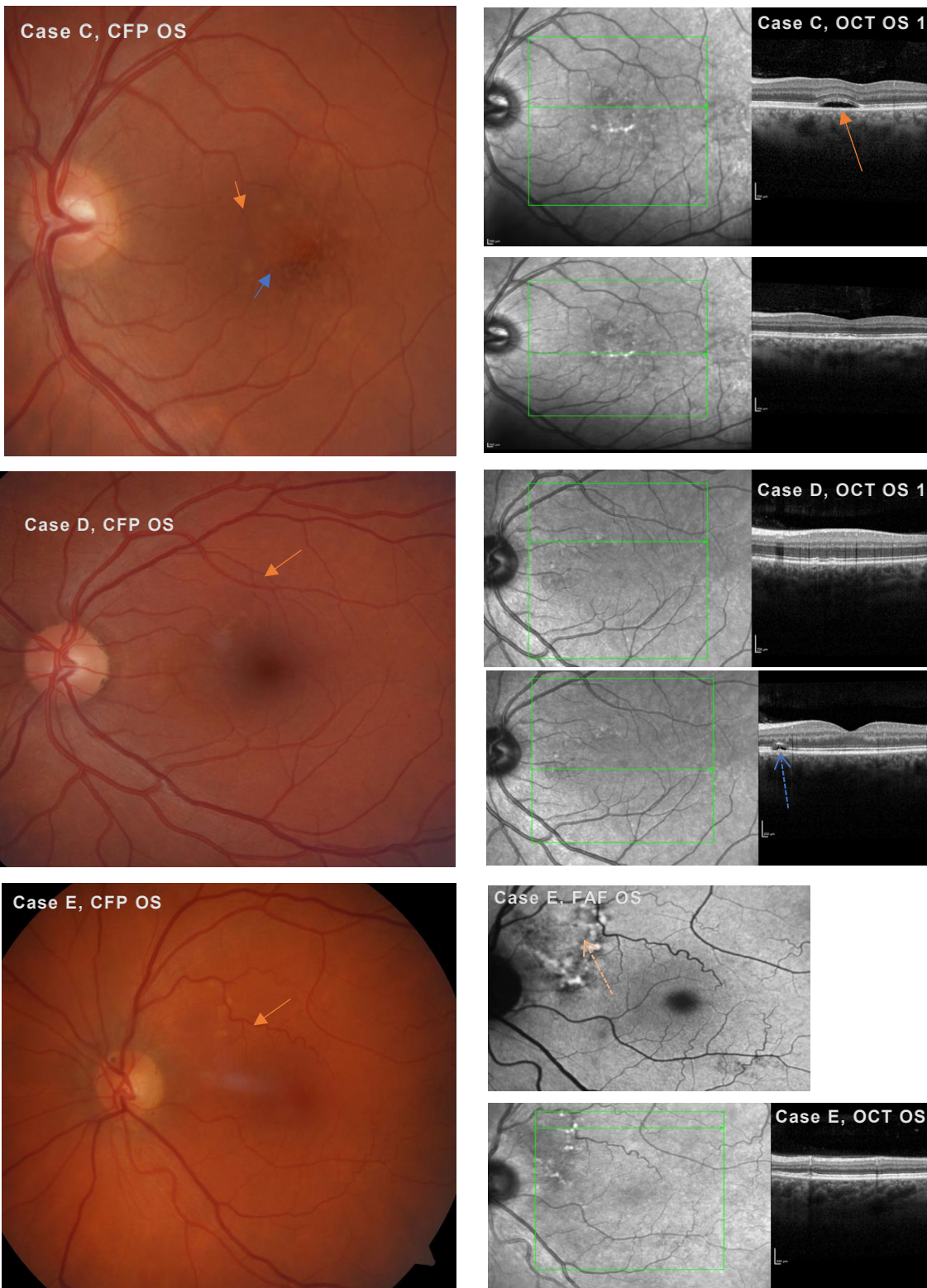
Image 4.2, AMD-mimicking phenotypes in pachychoroid spectrum

In case C (43 yo, Male), diffuse hyperpigmentation (blue arrow) and pachydrusen (orange arrow) are noted on CFP, while on OCT pachydrusen and a central serous elevation with large choroid is noted, consistent with a diagnosis of central serous chorioretinopathy.

In case D (40 yo, Male), drusenoid lesions are noted on CFP, corresponding in OCT to subretinal drusenoid lesions with choroidal hypertransmission on OCT and a large choroid; however, a serous hyporeflective lesions with corresponding hyperreflective photoreceptors is noted (dashed blue arrow).

In case E (70 yo, Female), on CFP drusenoid lesions are noted in the nasal superior macular and peripapillary area corresponding to pachydrusen on OCT; a large choroid and peripapillary subretinal pachydrusen with lesions gravitational tracks on FAF (dashed orange arrow) suggest a diagnosis of peripapillary pachychoroid syndrome.

Bibliography

Berger, Lieselotte, Virginie Bühler, and Suzanne Yzer. 2021. "Central Serous Chorioretinopathy - An Overview." *Klinische Monatsblatter Fur Augenheilkunde* 238 (9): 971–79. https://doi.org/10.1055/A-1531-5605/ID/R2426-32.

Cheung, Chui Ming Gemmy, Won Ki Lee, Hideki Koizumi, Kunal Dansingani, Timothy Y Y Lai, and K Bailey Freund. 2019. "Pachychoroid Disease." *Eye (London, England)* 33 (1): 14–33. https://doi.org/10.1038/s41433-018-0158-4.

Khan, Kamron N., Omar A. Mahroo, Rehna S. Khan, Moin D. Mohamed, Martin McKibbin, Alan Bird, Michel Michaelides, Adnan Tufail, and Anthony T. Moore. 2016. "Differentiating Drusen: Drusen and Drusen-like Appearances Associated with Ageing, Age-Related Macular Degeneration, Inherited Eye Disease and Other Pathological Processes." *Progress in Retinal and Eye Research*. Elsevier Ltd. https://doi.org/10.1016/j.preteyeres.2016.04.008.

Pang, Claudine E., and K. Bailey Freund. 2015. "Pachychoroid Neovasculopathy." *Retina (Philadelphia, Pa.)* 35 (1): 1–9. https://doi.org/10.1097/IAE.0000000000000331.

Phasukkijwatana, Nopasak PhD, MD, K. Bailey MD Freund, Rosa MD, PhD Dolz-Marco, Mayss MD Al-Sheikh, Pearse A. MD Keane, CATHERINE A. MD Egan, and Sandeep MD Randhawa. n.d. "PERIPAPILLARY PACHYCHOROID SYNDROME."

Rämö, Joel T., Erik Abner, Elon H. C. van Dijk, Xin Wang, Joost Brinks, Tiit Nikopensius, Margit Nõukas, et al. 2023. "Overlap of Genetic Loci for Central Serous Chorioretinopathy With Age-Related Macular Degeneration." *JAMA Ophthalmology*, April. https://doi.org/10.1001/JAMAOPHTHALMOL.2023.0706.

Schmitz-Valckenberg, Steffen, Moussa A. Zouache, Gregory S. Hageman, and Monika Fleckenstein. 2022. "From Genes, Proteins, and Clinical Manifestation: Why Do We Need to Better Understand Age-Related Macular Degeneration?" *Ophthalmology Science* 2 (2): 100174. https://doi.org/10.1016/j.xops.2022.100174.

Warrow, David J., Quan V. Hoang, and K. Bailey Freund. 2013. "Pachychoroid Pigment Epitheliopathy." *Retina (Philadelphia, Pa.)* 33 (8): 1659–72. https://doi.org/10.1097/IAE.0B013E3182953DF4.

Yamashiro, Kenji, Yoshikatsu Hosoda, Masahiro Miyake, Sotaro Ooto, and Akitaka Tsujikawa. 2020. "Characteristics of Pachychoroid Diseases and Age-Related Macular Degeneration:

Multimodal Imaging and Genetic Backgrounds." *Journal of Clinical Medicine* 9 (7). https://doi.org/10.3390/jcm9072034.

scientific reports

OPEN

Comparability of automated drusen volume measurements in age-related macular degeneration: a MACUSTAR study report

Davide Garzone[1,2], Jan Henrik Terheyden[1], Olivier Morelle[1,3], Maximilian W. M. Wintergerst[1], Marlene Saßmannshausen[1], Steffen Schmitz-Valckenberg[1,4], Maximilian Pfau[1], Sarah Thiele[1], Stephen Poor[5], Sergio Leal[6], Frank G. Holz[1], Robert P. Finger[1✉] & MACUSTAR Consortium*

Drusen are hallmarks of early and intermediate age-related macular degeneration (AMD) but their quantification remains a challenge. We compared automated drusen volume measurements between different OCT devices. We included 380 eyes from 200 individuals with bilateral intermediate (iAMD, n = 126), early (eAMD, n = 25) or no AMD (n = 49) from the MACUSTAR study. We assessed OCT scans from Cirrus (200 × 200 macular cube, 6 × 6 mm; Zeiss Meditec, CA) and Spectralis (20° × 20°, 25 B-scans; 30° × 25°, 241 B-scans; Heidelberg Engineering, Germany) devices. Sensitivity and specificity for drusen detection and differences between modalities were assessed with intra-class correlation coefficients (ICCs) and mean difference in a 5 mm diameter fovea-centered circle. Specificity was > 90% in the three modalities. In eAMD, we observed highest sensitivity in the denser Spectralis scan (68.1). The two different Spectralis modalities showed a significantly higher agreement in quantifying drusen volume in iAMD (ICC 0.993 [0.991–0.994]) than the dense Spectralis with Cirrus scan (ICC 0.807 [0.757–0.847]). Formulae for drusen volume conversion in iAMD between the two devices are provided. Automated drusen volume measures are not interchangeable between devices and softwares and need to be interpreted with the used imaging devices and software in mind. Accounting for systematic difference between methods increases comparability and conversion formulae are provided. Less dense scans did not affect drusen volume measurements in iAMD but decreased sensitivity for medium drusen in eAMD.

Trial registration: ClinicalTrials.gov NCT03349801. Registered on 22 November 2017.

Age-related macular degeneration (AMD) continues to be a major cause of visual impairment and in order to better predict the risk of disease progression and outcomes, better phenotyping and thus AMD staging is needed[1,2]. The Beckmann classification is widely adopted for AMD staging; it is based on maximal drusen diameter cut-offs measured on color fundus photography (CFP), with measurements between 63 and 125 μm defining early AMD (eAMD) and larger than 125 μm defining intermediate AMD (iAMD)[3]. Using solely two-dimensional CFP for AMD disease staging is somewhat outdated; semi-quantitative assessment of multi-modal imaging has become a more common approach for retinal experts in day to day clinical routine. In particular, optical coherence tomography (OCT) lends itself to biomarker quantification, i.e. the calculation of drusen load using three-dimensional information for the quantification of drusen volume[4]. Previous studies observed an

[1]Department of Ophthalmology, University Hospital Bonn, Ernst-Abbe Str. 2, 53127 Bonn, Germany. [2]Population Health Sciences, German Center for Neurodegenerative Diseases (DZNE), Bonn, Germany. [3]B-IT and Institute of Informatics, University of Bonn, Bonn, Germany. [4]John A. Moran Eye Center, University of Utah, Salt Lake City, USA. [5]Ophthalmology, Novartis Institutes for Biomedical Research, Cambridge, MA, USA. [6]Bayer Pharmaceuticals, Berlin, Germany. *A list of authors and their affiliations appears at the end of the paper. ✉email: robert.finger@ukbonn.de

association between larger drusen volumes and an increased risk of AMD progression[5,6], while drusen volume regression can precede conversion to late AMD lesions[7]. Drusen volume might be also more precisely measurable and repeatable than drusen area[5,8], thus making it a promising biomarker and structural endpoint in AMD. OCT also allows for accurate assessment of reticular pseudodrusen (RPD), which are not included in the Beckmann classification but have emerged as an important biomarker of AMD severity and progression risk[9].

Automated algorithms for drusen volume quantification are available including a software for the high definition-OCT Cirrus (Carl Zeiss Meditec, Dublin, CA), achieving approval by the Food and Drug Administration (FDA) in 2012[4].

Several studies in the last decade have compared drusen measurements obtained from this software against manual quantification of drusen or similar readouts on different imaging modalities (mainly CFP-based), often showing that measurements across different imaging methods and devices yield different results and are not directly interchangeable[10,11]. One previous work compared drusen volume measurements from two different devices, with similar findings[12]. However, drusen volumes obtained from the FDA-cleared algorithms on Cirrus have not been compared with those from the Spectralis SD (spectral domain)-OCT device (Heidelberg Engineering, Heidelberg, Germany).

Another study found that drusen volume measurements obtained from 145 B- and 15 B-scans in iAMD are similar[13]. Nevertheless, different scan patterns on the same device have not been compared as to their sensitivity and specificity for drusen detection in eAMD and iAMD.

In order to better understand how the use of different devices, softwares and scan patterns might affect drusen volume measurements, we compared all these factors in persons with no AMD, eAMD and iAMD. We included automated drusen volume measures from the FDA-approved software in Cirrus and from two scans (a denser volume scan, 241 B-scans and a less dense volume scan, 25 B-scans) in Spectralis, assessed through a newly developed software, in the MACUSTAR study cohort.

Methods

We assessed an initial dataset of 258 subjects from the cross-sectional part of MACUSTAR, a multi-center clinical cohort study focused on early stages of AMD[14,15].

In brief, the major objective of the MACUSTAR consortium is to develop novel clinically validated endpoints in the area of functional, structural, and patient-reported outcome measures in patients with iAMD[14,15]. AMD staging (no, early, intermediate and late) for all subjects is reading center–confirmed using multimodal imaging[14,15]. Since drusen assessment was the main focus of this analysis, individuals with late AMD were not included in the study population.

Inclusion criteria, design and goals of MACUSTAR have been previously described[14,15].

For 10 patients, no imaging data could be retrieved for data analysis due to data management issues. Seven individuals were excluded because of a time gap between Cirrus and Spectralis examinations (>6 weeks). Two individuals were excluded because of low-quality scans in both eyes (internal Cirrus quality parameter < 6 or internal Spectralis quality parameter < 20 dB). Incomplete date (at least one scan lacking in both eyes) lead to the exclusion of 39 participants. In the analytical population, 20 eyes were excluded due to either a missing scan in one of the three modalities (N = 8), low scan quality (N = 5 Cirrus, N = 3 Spectralis) or artifacts in drusen segmentation (N = 1 for Cirrus, N = 3 for Spectralis), leaving 380 eyes from 200 individuals (no AMD, n = 49 (22.3%), eAMD, n = 25 (13.1%), iAMD, n = 126 (64.6%)) with high-quality, complete data.

This study has been conducted according to the provisions of the Declaration of Helsinki and was approved by local licensing ethic committees of participating countries, including University Hospital Bonn ethics committee (384/17), as listed previously[15]. All participants provided informed consent.

Imaging. Participants underwent pupil dilation with tropicamide 0.5% and phenylephrine 2.5% after which multimodal imaging according to standard operational procedures was performed[15]. The Spectralis imaging protocol included a 20°×20° (25 B-scans, approximate distance between scans 240 μm, 4 frames per B-scan) and a 30°×25° macular volume scan (241 B-scans, approximate distance between scans 30 μm, 9 frames per B-scan)[15]. The SD-OCT Cirrus imaging protocol included a 200×200 macular cube (200 B-scans) covering an area of 6×6 mm.

Image grading. Details on the MACUSTAR Image grading have been described previously[15,16].

In brief, MACUSTAR participants are recruited at 20 clinical sites from seven European countries. Imaging data are graded at the central reading center (GRADE Reading Center, Bonn, Germany) by one junior reader followed by one senior reader grading review according to standardized and predefined grading procedures. For AMD status grading, the dense SD-OCT raster scan was used as the reference imaging modality. The B-scan with the largest possible drusen was preselected and its measurement was used to assess the maximum drusen size, which allowed for classification into small (≤63 μm), medium (>63 μm and ≤125 μm) and large (>125 μm) drusen. RPD were defined as hyperreflective irregularities and elevations above the RPE/BM complex on OCT that had to display corresponding lesions on either infrared imaging or fundus autofluorescence. Prerequisite for grading was a minimum of five individual lesions, each of a diameter of approximately 100 μm.

Drusen segmentation and quantification. Drusen volume measurements on Cirrus were derived from an established and FDA-approved software, whose measures are repeatable and reproducible[4,5,17,18].

In brief, in the Cirrus algorithm the observed and expected contours of the RPE layer are obtained by interpolating and fitting the shape of the segmented RPE layer, respectively. The areas located between the interpolated and fitted RPE shapes (which have nonzero area when drusen occurs) are marked as drusen[4,17].

Drusen quantification on Spectralis is based on OCT layer predictions. BM and RPE layer heights are predicted with a state-of-the-art deep learning model for order-constrained layer regression (predicting layer heights while guaranteeing their correct anatomical order). For the drusen computation, a healthy RPE height is derived from BM and RPE predictions under the assumption that it has a fixed distance to the BM which varies only based on individual physiology and image resolution. The drusen height, required for filtering small false positives, is determined based on connected components in a drusen enface projection. The algorithm on Spectralis was built as an extension of a previously published tool for drusen volume segmentation and is freely available[19–21]. Interestingly, the algorithm on Cirrus and the one on Spectralis adopt a similar method: drusen are computed as the area between the predicted and the computed healthy RPE. In both algorithms, small false positive RPE elevations less than 5 pixels (19.5 μm) high are filtered out[4,20,21].

To ensure full automation of measurements, neither drusen nor retinal layers segmentation was manually corrected. However, we performed post-hoc quality assurance in both scans and enface projection of drusen segmentation in both devices, ensuring that all scans were fully centered and drusen segmentation maps were plausible. Both algorithms report drusen volume measures both inside a fovea-centered 3- and a 5-mm diameter circle[4]; we only investigated values from the 5-mm circle as they reflect the grid used for Beckmann AMD grading. Pixel-microns conversion was based on the respective formula provided by the Heidelberg Eye Explorer and Cirrus Zeiss software. A previous study showed high comparability between their axial and lateral retinal measurements[22].

Statistical analyses.

We assessed inter-device and inter-scan differences with intra-class correlation coefficients (ICCs), root mean squared error (RMSE), and mean difference.

Differences between devices were assessed with Wilcoxon paired signed rank test; increases across AMD stages were assessed with the Jonckheere-Terpstra test for ordered variables.

Sensitivity, specificity and area under the curve (AUC) of both algorithms in the population sample were tested with a receiver operating characteristic (ROC) analysis. We tested accuracy of drusen volume measurements in discriminating eyes with any e- and iAMD, as well as subsets with only i- and eAMD, vs controls. We selected drusen volume measurement thresholds maximizing the optimality criterion expressed by the formula below[23]

$$ min\left((1 - sensitivities)^2 + \left(1 - specificities\right)^2 \right). $$

To assess the relative magnitude of the mean difference in each AMD group, we standardized it by dividing it by the mean average value of the two devices, respectively. We only calculated ICC in the iAMD group due to low variability of drusen volume in no and eAMD, leading to poorly interpretable ICC[24].

Current algorithms are trained for segmenting the BM-RPE complex; since RPDs are located between the RPE and ellipsoid zone, algorithms may be less consistent in RPD detection and segmentation. For this reason, we stratified ICC by excluding individuals with reticular pseudodrusen (RPD) in iAMD to assess its effect on measures comparability. We reported both consistency and agreement using two-way ICC. In brief, ICC type consistency compares two measures without adding a penalty for a systematic error ($x = y + e$), contrarily to ICC type agreement($x = y$), hence their conjoint assessment is highly informative of measurements' interchangeability[24]. We visualized differences between measurements from different algorithms and modalities with Bland–Altman plots[25]. Conversion formulae were obtained with Deming regression on the dense Spectralis scan. To assess their accuracy, we randomly split the dataset into approximately 80% of observations for training and 20% for testing and assessed prediction accuracy with mean error and RMSE between converted and observed values. We compared results in the whole iAMD dataset against an optimal iAMD subset based on the Bland–Altman analysis.

While continuous drusen volume measures might provide more detailed phenotyping, differences among quantitative measures might be less relevant when considering quantitative cut-offs (e.g., one indicating high risk to progression). Hence, we assessed comparability across modalities in iAMD against a binary cut-off indicating higher progression risk, previously shown at 0.03 mm³ in Cirrus[5]. The cut-off was 0.083 mm³ in Spectralis and was derived by converting the value of 0.03 mm³ with the conversion formula obtained in this paper. All statistical analyses were performed in R (base version 3.4).

Results

Individuals with AMD were significantly older and had worse VA than individuals without AMD (Table 1). Of the 58 eyes with RPD, 54 (93.1%) had iAMD and 4 (6.9%) had eAMD (Table 1).

Sensitivity and specificity.

In the dense Spectralis scan, we observed at the selected threshold a specificity of 93.7% and a sensitivity of 91.9% (68.1% for eAMD and 94.7% for iAMD). In the 25 B-scans modality, we observed a higher specificity (97.9%) but a lower sensitivity of 87.0% (36.2% in eAMD and 97.1% in iAMD). When assessing measurements obtained from the algorithm on Cirrus, we observed a specificity of 91.6%. Sensitivity was lower than for both Spectralis scan patterns (14.9% in eAMD, 87.0% in iAMD and 75.1% in the whole sample). ROC curves with AUC of each algorithm for drusen volume assessment and respective thresholds are reported in Supplementary Fig. 1.

Drusen volume measurements.

The denser Spectralis scan yielded on average larger drusen volumes (mean (SD) = 0.082 (0.139)), followed by the less dense Spectralis scan (mean (SD) = 0.0787 (0.135)) and Cirrus (mean (SD) = 0.0398 (0.0857)) (Table 2). We report summary statistics for drusen volume measurements stratified by AMD status in Table 2. All drusen volume measurements showed right-skewed distributions. Differ-

	Missing/excluded participants	Analytical population[1] (N = 200)			Among incl./excl.	Among AMD groups
		No AMD	eAMD	iAMD	P	P
N (%)	48	49 (22.3)	25 (13.1)	126 (64.6)		
Age in years	70.5 (6.9)	68.1 (6.3)	72.0 (6.4)	71.3 (7.5)	0.92	0.021
Sex = m (%)	16 (33.3)	19 (38.8)	6 (24.0)	47 (37.3)	0.403	0.143
BCVA	83.4 (6.13)	86.23 (5.09)	83.20 (5.63)	81.88 (6.75)	< 0.001	< 0.001

Table 1. Characteristics of the study population. *SD* standard deviation, *IQR* interquartile range, *AMD* age-related macular degeneration, *eAMD* early AMD, *iAMD* intermediate AMD, *BCVA* best-corrected visual acuity. [1]For 180 individuals, both eyes were included; for 20 individuals only one eye was included.

	Drusen volume in 5 mm circle (mm³)				
	Spectralis, 241 B-scans				
	Mean (SD)	**Median (IQR)**	**10–90%[1]**	**Range**	**% = 0[2]**
No AMD	0.0002 (0.001)	0 (0)	0–0.00041	0–0.0143	90.5
Early AMD	0.0014 (0.004)	0.0003 (0.008)	0–0.0025	0–0.0188	31.9
iAMD	0.131 (0.158)	0.074 (0.147)	0.035–0.297	0–0.891	0.8
Ret. drusen	0.114 (0.127)	0.068 (0.107)	0.0148–0.255	0–0.672	1.7
	Spectralis, 25 B-scans				
	Mean (SD)	**Median (IQR)**	**10–90%[1]**	**Range**	**% = 0[2]**
No AMD	0.00002 (0.0001)	0 (0)	0–0	0–0.00125	97.9
Early AMD	0.00102 (0.0027)	0 (0.0007)	0–0.002	0–0.016	63.8
Int. AMD	0.126 (0.154)	0.069 (0.149)	0.002–0.296	0–0.789	2.9
Ret. drusen	0.104 (0.128)	0.056 (0.0972)	0.0119–0.249	0–0.688	1.7
	Cirrus				
	Mean (SD)	**Median (IQR)**	**10–90%[1]**	**Range**	**% = 0[2]**
No AMD	0.00081 (0.0033)	0 (0)	0–0.0053	0–0.021	91.6
Early AMD	0.00094 (0.0033)	0 (0)	0–0.001	0–0.016	85.1
Int. AMD	0.063 (0.101)	0.022 (0.0702)	0–0.175	0–0.611	13.0
Ret. drusen	0.040 (0.0632)	0.015 (0.0417)	0.0007–0.094	0–0.287	10.3

Table 2. Summary statistics for different drusen volume measurements. *SD* standard deviation, *IQR* interquartile range, *AMD* age-related macular degeneration, *eAMD* early AMD, *iAMD* intermediate AMD, *SBP* systolic blood pressure, *BCVA* best-corrected visual acuity. [1]10–90% indicates 10 and 90% distribution quantiles. [2]% = 0 indicates percentage of values with undetected drusen (equal to 0).

ences between drusen volume measurements across all modalities and algorithms were statistically significant (Wilcoxon paired signed rank test p < 0.0001). Drusen volume increased from the no AMD group to early and intermediate AMD in all modalities (Jonckheere-Terpstra test < 0.0001). In all three modalities, mean drusen volume in individuals with RPD (n = 58, of which 54 with iAMD) was slightly lower than in individuals with iAMD without RPD. In Fig. 1 we show a comparison of drusen volume segmentation on the Cirrus (Fig. 1a,c,e) and dense Spectralis scan (Fig. 1B,D) by the respective algorithms.

Agreement and differences between drusen volume measurements. The mean systematic difference between the dense Spectralis scan and Cirrus was 0.0679 mm³ in iAMD and corresponded to 70% of the mean average value (Table 3).

When comparing drusen volumes between the two algorithms in iAMD, ICC type consistency was higher and more stable than type agreement (ICC [95% CI] 0.713 [0.294–0.859] vs 0.807 [0.757–0.847]), indicating that a systematic error partially accounts for differences in the iAMD group (Table 3). ICC increased when excluding individuals with RPD (n = 184, type consistency ICC [95% CI] 0.831 [0.781–0.871], type agreement ICC [95% CI] 0.752 [0.367–0.879]). When considering only individuals with RPD, the ICC was lower (type consistency ICC [95% CI] 0.645 [0.466–0.774]) and the mean difference (RMSE) were higher than for other subgroups (0.0737 and 0.1116 mm³, respectively). The CI of the ICC in individuals with and without RPD did not overlap, indicating a statistically significant difference between the two groups.

Applying the aforementioned high-risk threshold, agreement (kappa) between the dense Spectralis scan and Cirrus was 89.5 (78.9) (Table 3).

Drusen volume measurements of the two Spectralis scans had very high agreement (ICC agreement > 0.99) and the mean difference was 0.0055, corresponding to only 4% of the mean average value.
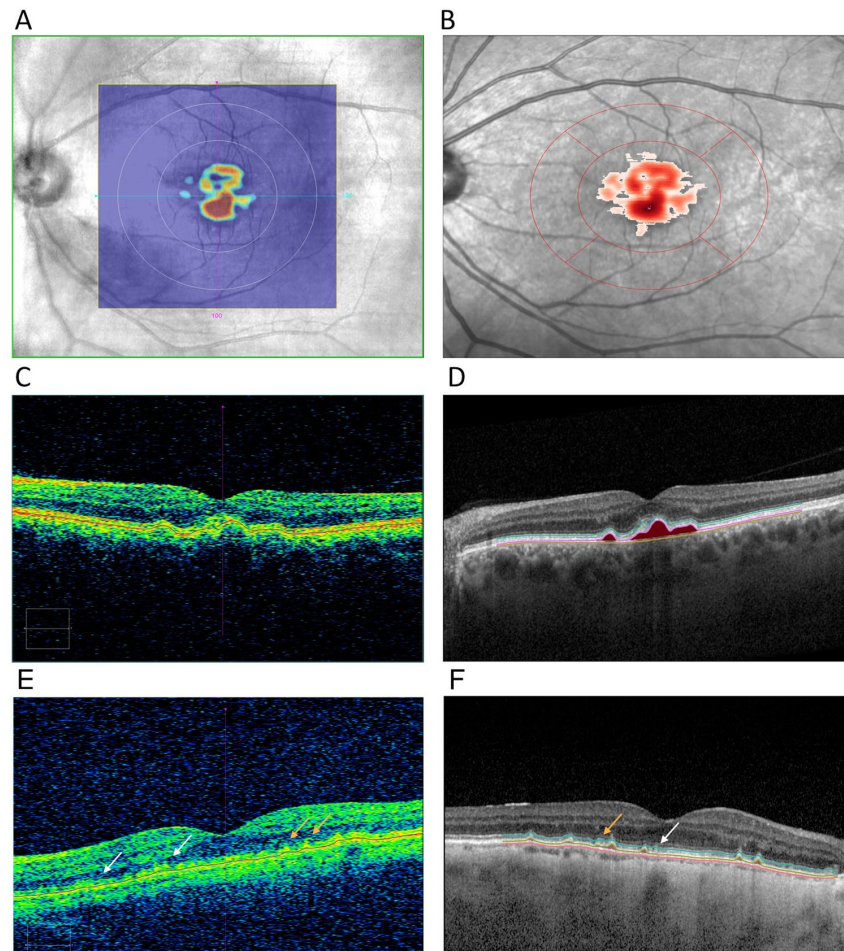
Figure 1. Comparison of Drusen segmentation of the same eye with iAMD, assessed with Cirrus ((**A**) enface projection, (**C**) foveolar B-scan) and Spectralis OCT ((**B**) enface projection, (**D**) foveolar B-scan), showing similar identification. (**E**) (Cirrus) and (**F**) (Spectralis) showing failure to detect (white arrows) or adequately segment (orange arrows) RPE elevations by automated segmentation algorithms in a corresponding macular B-scan.

In the inter-device comparison of the Bland–Altman plot, we observed, both in e- and iAMD, larger drusen detection on the dense Spectralis scan (in iAMD, n = 223 (93.6%) eyes, the difference between the two modalities was positive) and larger drusen volume measurement on Spectralis at larger average drusen volume measurement on the two devices (Fig. 2a,b). In iAMD, we observed a linear trend between drusen volume measurements in cirrus and the dense Spectralis scan for most data points. At the lower end of drusen volume a small number of participants (n = 13) had larger values on Cirrus and at the upper end, we observed a flattening of the linear trend with an increasingly broader confidence interval, indicating lower comparability. (Fig. 2b). In the inter-scan comparison, we observed smaller drusen measurement on the dense Spectralis scan and a random measurement error between the two modalities (random scatter around the x-axis) (Fig. 2c,d).

Formulae for algorithms conversion. We identified an optimal dataset with a linear trend between the two measurements consisting of 194 eyes for inter-device drusen volume measurements conversion based on Fig. 2b, i.e. we excluded eyes with measurement obtained from the Cirrus algorithm higher than Spectralis (N = 13) and mean values larger than 0.2 mm^3, corresponding to a flatter trend with large confidence interval (N = 31). When predicting drusen volume from Cirrus to the dense Spectralis scan in the test dataset, the mean error (RMSE) decreased in the whole iAMD dataset from − 0.0113 (0.0640) mm^3 to 0.0074 (0.0313) mm^3 in the optimal dataset. When predicting drusen volume from the dense Spectralis scan to Cirrus, the mean error (RMSE) amounted to 0.0173 (0.0458) mm^3 in the whole iAMD dataset and − 0.0003 (0.0168) mm^3 in the optimal dataset.

Subgroup	Intermediate AMD					
Measure	ICC Cons. [95%CI]		ICC Agreem. [95%CI]		Mean diff. (std.)[3,5]		RMSE[5]
Inter-device comparison[1]	0.807 [0.757–0.847]		0.713 [0.294–0.859]		0.0679 (0.70)		0.107
Inter-scan comparison[2]	0.993 [0.991–0.995]		0.993 [0.991–0.995]		0.0055 (0.04)		0.0188
Subgroup	No AMD		Early AMD		Whole population		
Measure	Mean diff.[5] (std.)[3]	RMSE[5]	Mean diff.[5] (std.)[3]	RMSE[5]	Mean diff.[5] (std.)[3]	RMSE[5]	Agreement4 (kappa)
Inter-device comparison[1]	−0.0006 (1.22)	0.0037	0.0005 (0.41)	0.0051	0.0424 (0.69)	0.084	89.5 (78.9)
Inter-scan comparison[2]	0.0001 (1.57)	0.0014	0.0004 (0.32)	0.0018	0.0055 (0.04)	0.0149	96.2 (92.4)

Table 3. Measures of agreement, in the whole population and stratified by AMD stage, across different drusen measurements. *ICC* intra-class correlation coefficient, *Cons.* consistency type, *Agreem.* agreement type, *RMSE* root mean squared error, *Spec.* spectralis, *AMD* age-related macular degeneration, *std.* standardized, *diff.* difference. [1]Inter-device comparison refers to the 241 B-scans Spectralis modality and Cirrus. [2]Inter-scan comparison refers to the 241 and 25 B-scans modalities in Spectralis. [3]The standardized mean value corresponds to mean difference divided the mean average value of the twodevices, respectively. [4]Assessed against a binary cut-off indicating high progression risk. [5]Measured in mm^3.

Data from the two algorithms can be converted in optimal iAMD cases with following formulas: Drusen volume from cirrus algorithm = (drusen volume from Spectralis algorithm) × 0.473 − 0.0091 mm^3; Drusen volume from Spectralis = (Drusen volume from Cirrus algorithm) × 2.112 + 0.0193 mm^3.

Discussion

We present a study systematically comparing drusen volume measurements obtained from two different algorithms on two different SD-OCT devices (Cirrus, Spectralis) and from two modalities at different B-scan density from the same device (Spectralis), as well as evaluating their classification accuracy in no AMD, eAMD and iAMD individuals.

The algorithm using Spectralis images showed a higher sensitivity in both the e- and iAMD groups than the Cirrus algorithm, while specificity was similar. In iAMD, after accounting for a systematic difference, comparability between the two algorithms was good (ICC consistency type > 0.75) and more stable (CI width decreased by 84%). The mean difference in iAMD was 0.0679 mm^3. The conversion formulae that were provided could be used to collate and compare data from the two algorithms and devices. The formulae were derived in an optimal iAMD dataset; hence they might be less accurate at average drusen volume measurement larger than 0.2 mm^3 and in case of higher quantification from the Cirrus algorithm.

Comparability between drusen volume measurements from the two devices was lower in individuals with RPD. This might be due to factors both intrinsic to imaging and performance of algorithms for drusen segmentation[26]. In particular, RPD and soft drusen have a different relationship with respect to the RPE, hence current algorithms often fail to accurately segment RPD.

Furthermore, we observed a good agreement between the two devices against a high-risk cut-off in drusen volume in iAMD. This indicates a substantial agreement in detecting individuals at high-risk, which might prove useful in clinical settings to efficiently triage patients[5].

To the best of our knowledge, a comparison between drusen volume measurements from two different algorithms on Spectralis and Cirrus SD-OCT has not been performed. However, previous studies have observed a systematic difference when investigating other biomarkers (such as retinal thickness or the BM-RPE complex derived with built-in softwares) across the two devices[12,22,27,28].

Any such differences may be due to differences in image acquisition, resolution and scaling[22,27,28], device specific softwares (e.g. computational methods, minimal elevation of the RPE necessary to identify drusen) or chosen scan modality (number of A- and B-scans[22]). In our study, the number of significant decimal figures of the two algorithms is different, which might in part account for observed sensitivity differences.

Interestingly, a previous study found comparable retinal thickness measurements from Cirrus and Spectralis utilizing a third-party segmentation algorithm[28].

Similarly, another study found that differences in drusen volume measurements between two SD-OCT devices decreased when measuring drusen volume with the same third-party software, as compared to measuring drusen volume with in-built algorithms on each device[12]. These findings suggest that differences in software might be more relevant than in hardware; however our study design did not account for dissecting intrinsic image differences against software differences in drusen segmentation.

When assessing drusen segmentation between the dense, 241 B-scans and the less dense, 25-B-scans modalities in Spectralis, we observed almost complete agreement between the two scan patterns in iAMD. Similar findings were observed in a recent study, comparing manually delineated drusen volume with Spectralis in an iAMD cohort between 145 B-scans and 15 B-scans modalities[13]. Our results extend these previous findings, with the observation that a less dense grid might suffice for drusen volume quantification in iAMD but has lower
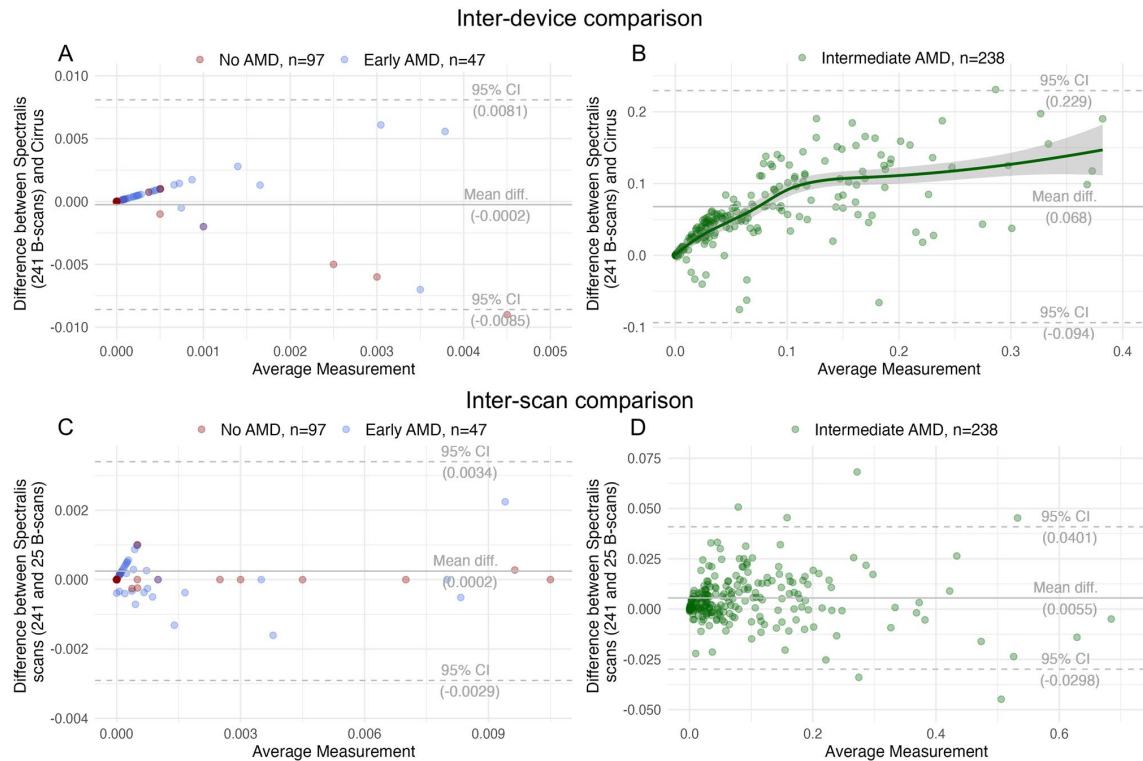
Figure 2. Bland–Altman plot showing differences stratified per AMD stage between the two algorithms (**A**,**B**) and the two scans (**C**,**D**), respectively. A Least Absolute Shrinkage and Selection Operator (LASSO) regression line was added in (**B**) to highlight a linear inter-device trend at lower drusen volume measurements and flattening of the curve with increasingly broader confidence intervals at higher values, indicating lower comparability. *AMD* age-related macular degeneration, *diff.* difference.

sensitivity in eAMD. This difference is explained by the observation that interpolation of large drusen between the scans might account for a smaller number of B-scans, but medium drusen (between 63 and 125 μm) might occur between B-scans and be more easily missed in less dense scan. In this context, part of the lower sensitivity in Cirrus for eAMD might also be explained by less densely placed B-scans compared to the Spectralis scan (200 vs 241 B-scans, respectively). More studies are needed investigating drusen detection at intermediate B-scan densities, to derive an optimal number of B-scans optimizing examination velocity and detection of smaller biomarkers (such as medium-sized drusen or hyperreflective foci).

Strengths of our study include the well phenotyped sample of participants with no, early and iAMD, the implementation of standardized image acquisition protocols, training of study site personnel, use of a central reading center and implementation of automated image analysis softwares. Limitations include the relatively small sample size, lack of an external validation of our findings and lack of data on repeatability and reproducibility of the Spectralis software while such studies exist for Cirrus[8,17]. However, the high agreement we observed between the two Spectralis scans might be indicative of good reproducibility of its findings.

In conclusion, drusen volume measurements obtained from the two devices and algorithms are not directly interchangeable. In iAMD, accounting for a systematic error largely increased their comparability, possibly allowing for data integration from the two modalities. Presence of RPD further complicated drusen detection and quantification. Comparability between a 25- and 241 B-scans modality was high, but dense scan patterns are required in eAMD. Further research is required to better characterize optimal scan patterns and image analysis softwares for best possible drusen detection and quantification.

Data availability

Data are not publicly available. However, the datasets used in the present study can be made available from the MACUSTAR consortium upon reasonable request at dataaccess@macustar.eu.

References

1. Wong, W. L. *et al.* Global prevalence of age-related macular degeneration and disease burden projection for 2020 and 2040: A systematic review and meta-analysis. *Lancet Glob. Health* **2**, e106–e116 (2014).
2. Mitchell, P., Liew, G., Gopinath, B. & Wong, T. Y. Age-related macular degeneration. *The Lancet* **392**, 1147–1159 (2018).
3. Klein, R. *et al.* Harmonizing the classification of age-related macular degeneration in the three-continent AMD consortium. *Ophthalmic Epidemiol.* **21**, 14–23 (2014).
4. Chen, Q. *et al.* Automated drusen segmentation and quantification in SD-OCT images. *Med. Image Anal* **17**, 1058–1072 (2013).
5. Abdelfattah, N. S. *et al.* Drusen volume as a predictor of disease progression in patients with late age-related macular degeneration in the fellow eye. *Investig. Opthalmol. Vis. Sci.* **57**, 1839 (2016).
6. Nassisi, M. *et al.* OCT risk factors for development of late age-related macular degeneration in the fellow eyes of patients enrolled in the HARBOR study. *Ophthalmology* **126**, 1667–1674 (2019).
7. Schlanitz, F. G. *et al.* Drusen volume development over time and its relevance to the course of age-related macular degeneration. *Br. J. Ophthalmol.* **101**, 198–203 (2017).
8. Nittala, M. G., Ruiz-Garcia, H. & Sadda, S. R. Accuracy and reproducibility of automated drusen segmentation in eyes with non-neovascular age-related macular degeneration. *Investig. Ophthalmol. Vis. Sci.* **53**, 8319–8324 (2012).
9. Rabiolo, A. *et al.* Spotlight on reticular pseudodrusen. *Clin. Ophthalmol.* **11**, 1707–1718 (2017).
10. Wintergerst, M. W. M. *et al.* Algorithms for the automated analysis of age-related macular degeneration biomarkers on optical coherence tomography: A systematic review. *Transl. Vis. Sci. Technol.* **6**, 10 (2017).
11. Kim, D. Y., Loo, J., Farsiu, S. & Jaffe, G. J. Comparison of single drusen size on color fundus photography and spectral-domain optical coherence tomography. *Retina* **41**, 1715–1722 (2021).
12. Beck, M. *et al.* Comparison of Drusen volume assessed by two different OCT devices. *J. Clin. Med.* **9**, 2657 (2020).
13. Thiele, S., Fleckenstein, M. & Fang, P. Longitudinal analysis of drusen volume in intermediate age-related macular degeneration using two spectral-domain optical coherence tomography scan patterns. *Ophthalmologica.* https://doi.org/10.1159/000485260 (2018).
14. Finger, R. P. *et al.* MACUSTAR: Development and clinical validation of functional, structural, and patient-reported endpoints in intermediate age-related macular degeneration. *Ophthalmologica* **241**, 61–72 (2019).
15. Terheyden, J. H. *et al.* Clinical study protocol for a low-interventional study in intermediate age-related macular degeneration developing novel clinical endpoints for interventional clinical trials with a regulatory and patient access intention-MACUSTAR. *Trials* **21**, 659 (2020).
16. Saßmannshausen, M. *et al.* Intersession repeatability of structural biomarkers in early and intermediate age-related macular degeneration: A MACUSTAR study report. *Trans. Vis. Sci. Technol.* **11**, 27 (2022).
17. Gregori, G. *et al.* Spectral domain optical coherence tomography imaging of drusen in nonexudative age-related macular degeneration. *Ophthalmology* **118**, 1373–1379 (2011).
18. Yehoshua, Z. *et al.* Natural history of drusen morphology in age-related macular degeneration using spectral domain optical coherence tomography. *Ophthalmology* **118**, 2434–2441 (2011).
19. Wintergerst, M. W. M. *et al.* Replication and refinement of an algorithm for automated drusen segmentation on optical coherence tomography. *Sci. Rep.* **10**, 7395 (2020).
20. Zadeh, S. G. *et al.* CNNs enable accurate and fast segmentation of drusen in optical coherence tomography. *LNCS* vol. 10553, 65–73.
21. Morelle, O. *EyeLab.* https://doi.org/10.5281/ZENODO.6798770 (2022).
22. Folgar, F. A., Yuan, E. L., Farsiu, S. & Toth, C. A. Lateral and axial measurement differences between spectral-domain optical coherence tomography systems. *J. Biomed. Opt.* **19**, 016014 (2014).
23. Robin, X. *et al.* pROC: An open-source package for R and S+ to analyze and compare ROC curves. *BMC Bioinform.* **12**, 1–8 (2011).
24. Koo, T. K. & Li, M. Y. A guideline of selecting and reporting intraclass correlation coefficients for reliability research. *J. Chiropr. Med.* **15**, 155–163 (2016).
25. Martin Bland, J. & Altman, D. G. Statistical methods for assessing agreement between two methods of clinical measurement. *The Lancet* **327**, 307–310 (1986).
26. Switzer, D. W., Engelbert, M. & Freund, K. B. Spectral domain optical coherence tomography macular cube scans and retinal pigment epithelium/drusen maps may fail to display subretinal drusenoid deposits (reticular pseudodrusen) in eyes with non-neovascular age-related macular degeneration. *Eye* **25**, 1379 (2011).
27. Giani, A. *et al.* Reproducibility of retinal thickness measurements on normal and pathologic eyes by different optical coherence tomography instruments. *Am. J. Ophthalmol.* **150**, 815 (2010).
28. Sander, B., Al-Abiji, A. H., Kofod, M. & Jørgensen, T. M. Do different spectral domain OCT hardwares measure the same? Comparison of retinal thickness using third-party software. *Graefes Arch. Clin. Exp. Ophthalmol.* **253**, 1915. https://doi.org/10.1007/s00417-015-3075-2 (2015).

Disclaimer

Author contributions

D.G.: study design; data acquisition, analysis and interpretation; manuscript writing. J.H.T.: study design; data acquisition and interpretation; manuscript editing. O.M.: manuscript editing; data acquisition and interpretation, creation of new software used for this work. M.W.M.W.: manuscript editing; data interpretation, creation of new software for this work. M.S.: study design; data acquisition and interpretation; manuscript editing. M.M.B.: study design; manuscript editing. S.S.V.: study design; data acquisition and interpretation; manuscript editing. M.P.: study design; data acquisition and interpretation; manuscript editing. S.H.T.: study design; data acquisition and interpretation; manuscript editing. S.P.: study design; manuscript editing. S.L.: study design; manuscript editing. F.G.H.: study design; data acquisition and interpretation; manuscript editing. R.P.F.: study design, data acquisition and interpretation; manuscript editing. All authors approved the final version of the manuscript to be published.

Funding

Competing interests

DG: None. JHT: Heidelberg Engineering (F), Optos (F), Zeiss (F), CenterVue (F), Novartis (R), Okko (R). OM: None. MWMW: MWMW: Heidelberg Engineering (F, R), Optos (F), Carl Zeiss Meditec (F), CenterVue (F), Heine Optotechnik GmbH (C, R, F), Berlin-Chemie AG (F), Novartis Pharma GmbH (R, F), D-Eye Srl (F), Eyenuk Inc. (F), ASKIN & CO GmbH (R), DigiSight Technologies (R). MS: Heidelberg Engineering (F), CenterVue (F), Carl Zeiss MedicTec (F). SSV: AlphaRET (C), Apellis (C, R), Bayer (F), Bioeq (C), Carl Zeiss MediTec (F), Heidelberg Engineering (F, R), Katairo (C), Kubota Vision (C), Novartis (C, F), Oxurion (C), Pixium (C), Roche (C, F), SparingVision (C), STZ GRADE Reading Center (O). MP: Apellis Pharmaceuticals (C). SHT: Heidelberg Engineering (R, F); Optos (F), Zeiss (F), CenterVue (F); Novartis (R); Bayer (R); Allergan (R). SP: Novartis (E). SL: Bayer (E). FGH: Acucela (C,F), Allergan (F), Apellis (C, F), Bayer (C, F), Boehringer-Ingelheim (C), Bioeq/Formycon (F,C), CenterVue (F), Ellex (F), Roche/Genentech (C,F), Geuder (C,F), Graybug (C), Gyroscope (C), Heidelberg Engineering (C,F), IvericBio (C, F), Kanghong (C,F), LinBioscience (C), NightStarX (F), Novartis (C,F), Optos (F), Oxurion (C), Pixium Vision (C,F), Oxurion (C), Stealth BioTherapeutics (C), Zeiss (F,C), GRADE Reading Center (O). RPF: Bayer, Santen, Ophtea, Apellis, Roche/Genentech, Böhringer-Ingelheim, Novelion, ProQR, Oxford Innovation, Roche, Alimera, Santhera, Inositec, Ellex.

Additional information

Supplementary Information The online version contains supplementary material available at https://doi.org/10.1038/s41598-022-26223-w.

Correspondence and requests for materials should be addressed to R.P.F.

Reprints and permissions information is available at www.nature.com/reprints.

Publisher's note Springer Nature remains neutral with regard to jurisdictional claims in published maps and institutional affiliations.

MACUSTAR Consortium

H. Agostini[7], L. Altay[8], R. Atia[9], F. Bandello[10], P. G. Basile[11], C. Behning[12], M. Belmouhand[13], M. Berger[12], A. Binns[14], C. J. F. Boon[15], M. Böttger[16], C. Bouchet[17], J. E. Brazier[18], T. Butt[19], C. Carapezzi[20], J. Carlton[18], A. Carneiro[21], A. Charil[17], R. Coimbra[11], M. Cozzi[22], D. P. Crabb[14], J. Cunha-Vaz[11], C. Dahlke[8], L. de Sisternes[23], H. Dunbar[19], E. Fletcher[24], C. Francisco[11], M. Gutfleisch[25], R. Hogg[26], C. B. Hoyng[27], A. Kilani[28], J. Krätzschmar[16], L. Kühlewein[29], M. Larsen[13], Y. T. E. Lechanteur[27], U. F. O. Luhmann[30], A. Lüning[1], I. Marques[11], C. Martinho[11], G. Montesano[14], Z. Mulyukov[17], M. Paques[9], B. Parodi[10], M. Parravano[31], S. Penas[21], T. Peters[29], T. Peto[26], S. Priglinger[32], D. Rowen[18], G. S. Rubin[19], J. Sahel[9], C. Sánchez[27], O. Sander[17], M. Schmid[12], H. Schrinner-Fenske[33], J. Siedlecki[32], R. Silva[11], A. Skelly[17], E. Souied[34], G. Staurenghi[22], L. Stöhr[33], D. J. Taylor[14], A. Tufail[35], M. Varano[31], L. Vieweg[33], L. Wintergerst[1], A. Wolf[28] & N. Zakaria[17]

[7]Department of Ophthalmology, Universitaetsklinikum Freiburg (UKLFR), University of Freiburg, Freiburg, Germany. [8]Department of Ophthalmology, University Hospital of Cologne, Cologne, Germany. [9]Quinze-Vingts National Ophthalmology Hospital, UPMC-Sorbonne Université, Paris, France. [10]Department of Ophthalmology, University Vita Salute-Scientific Institute of San Raffaele, Milan, Italy. [11]AIBILI Association for Innovation and Biomedical Research on Light and Image (AIBILI), Coimbra, Portugal. [12]Institute for Medical Biometry, Informatics and Epidemiology, University of Bonn, Bonn, Germany. [13]Department of Ophthalmology, Rigshospitalet-Glostrup, Copenhagen University, Glostrup, Denmark. [14]City University London, London, UK. [15]Department of Ophthalmology, Leiden University Medical Center, Leiden, The Netherlands. [16]BAYER AG, Leverkusen, Germany. [17]Novartis Pharma AG, Basel, Switzerland. [18]University of Sheffield, Sheffield, UK. [19]University College London (UCL), London, UK. [20]Fondation Voir et Etendre, Paris, France. [21]Department of Ophthalmology, Porto Medical School, Centro Hospitalar de Sao Joao EPE (Hospital Sao Joao), Porto, Portugal. [22]Department of Ophthalmology

Luigi Sacco Hospital, University of Milan, Milan, Italy. [23]Carl Zeiss Meditec, AG, Jena, Germany. [24]Clinical Trial Unit, Department of Ophthalmology, Gloucestershire Hospitals NHS Foundation Trust, Cheltenham, UK. [25]Department of Ophthalmology, St. Franziskus Hospital, Münster, Germany. [26]Ophthalmology and Vision Sciences, The Queen's University and Royal Group of Hospitals Trust, Belfast, Northern Ireland, UK. [27]Stichting Katholieke Universiteit/ Radboud University Medical Center (SRUMC), Nijmegen Medical Center, Radbound University, Nijmegen, The Netherlands. [28]Department of Ophthalmology, University of Ulm, Ulm, Germany. [29]STZ Biomed and STZ Eyetrial at the Center of Ophthalmology, University Hospital Tuebingen, Tübingen, Germany. [30]F. Hoffmann-La Roche Ltd, Basel, Switzerland. [31]G. B. Bietti Eye Foundation-IRCCS, Rome, Italy. [32]Ludwig-Maximilians-Universitaet Muenchen (LMU), University Eye Hospital, Munich, Germany. [33]European Clinical Research Infrastructure Network (ECRIN), Paris, France. [34]Centre Hospitalier Intercommunal de Creteil (HIC), Centre Hospitalier Creteil, University Eye Clinic, Paris, France. [35]Moorfields Eye Hospital NHS Foundation Trust (MBRC), London, UK.

BRIEF COMMUNICATION

Neurofilament light chain and retinal layers' determinants and association: A population-based study

Davide Garzone[1,2] (iD), Robert P. Finger[2] (iD), Matthias M. Mauschitz[1,2], Marina L. S. Santos[1], Monique M. B. Breteler[1,3] (iD) & N. Ahmad Aziz[1,4] (iD)

[1]Population Health Sciences, German Center for Neurodegenerative Diseases (DZNE), Bonn, Germany
[2]Department of Ophthalmology, Faculty of Medicine, University of Bonn, Bonn, Germany
[3]Institute for Medical Biometry, Informatics and Epidemiology (IMBIE), Faculty of Medicine, University of Bonn, Bonn, Germany
[4]Department of Neurology, Faculty of Medicine, University of Bonn, Bonn, Germany

Correspondence
N. Ahmad Aziz, Population Health Sciences, German Center for Neurodegenerative diseases (DZNE), Bonn, Germany. Tel: +49-228-43302-954; Fax: +49-228-43302-948; E-mail: ahmad.aziz@dzne.de

Abstract

Both retinal atrophy measured through optical coherence tomography and plasma neurofilament light chain (NfL) levels are markers of neurodegeneration, but their relationship is unknown. Therefore, we assessed their determinants and association in 4369 participants of a population-based study. Both plasma NfL levels and inner retinal atrophy increased exponentially with age. In the presence of risk factors for neurodegeneration (including age, smoking, and a history of neurological disorders), plasma NfL levels were associated with inner retinal atrophy and outer retinal thickening. Our findings indicate that inner retinal atrophy can reflect neuroaxonal damage as mirrored by rising plasma NfL levels.

Introduction

Both plasma neurofilament light chain (NfL) levels and retinal layers' measures assessed through optical coherence tomography (OCT) have emerged as sensitive markers of neurodegeneration.[1,2] NfL is a blood-based biomarker, released in the circulation upon neuroaxonal damage, whereas the retina is an extension of the brain susceptible to similar injuries. Both markers change with advancing age, likely reflecting age-related neuronal loss,[3,4] and are considered sensitive but unspecific markers in several neurological diseases.[5–7] In the general population, baseline blood NfL levels were recently shown to predict future cognitive decline and brain atrophy.[3] Measures of inner retinal layers, the main location of retinal neurons, including the ganglion cell layer (GCL) and inner plexiform layer (IPL), are associated with brain volume.[7,8] Although a recent study investigated the association between plasma NfL levels and retinal measures in a cohort of multiple sclerosis patients,[9] normative population-based data regarding this relationship are still lacking. Therefore, using a population-based design, we aimed to: First, compare the determinants of plasma NfL levels and volume of GCL, the retinal layer most closely reflecting brain volume[8]; and second, examine the association between different retinal layers' measures and NfL levels, and assess whether their relation is modified by risk factors for neurodegeneration.

Methods

Study population

We analyzed baseline data from the first 5000 participants of the Rhineland Study, a population-based cohort study in Bonn, Germany.[4] Only the right eye was included per participant. We excluded participants with missing or low-quality NfL (N = 397) and/or right eye OCT data (N = 200). Furthermore, we excluded values larger than 3 standard deviations from both the mean of log-transformed NfL levels (N = 27) and retinal volume (N = 28), leaving a sample of 4369 subjects for data analysis.

Refraction and retinal layers

We assessed retinal layers using Spectralis spectral domain-OCT (Heidelberg Engineering, Heidelberg, Germany). Our workflow and OCT segmentation algorithm have been detailed before.[4] In brief, volumes of six macular layers, total retinal volume, and peripapillary retinal nerve fiber layer (pRNFL) thickness were computed using the inbuilt segmentation algorithm of the Heidelberg Eye Explorer (HEYEX).

Neurofilament light chain

Blood samples were collected in Vacutainer EDTA tubes and centrifuged at 2000 g for 10 minutes at room temperature and plasma samples were aliquoted and stored at -80 °C. NfL levels were assessed using the Simoa® NF-light Kit (103186) in a HD-1 Analyzer (Quanterix, Billerica, USA), following manufacturer's instructions.[10]

Other covariates

Blood volume was calculated with Nadler's formula.[11] Glomerular filtration rate (GFR) was estimated based on the CKD-EPI formula.[12]

Statistical analysis

Data are summarized as mean ± standard deviation (SD) or counts with proportions, for continuous and categorical variables, respectively. We adjusted NfL levels for batch and lot using a generalized mixed-effects model and used the log-transformed residuals in subsequent analyses. First, we assessed the effects of age, age-squared, sex, GFR, smoking status, blood volume, systolic blood pressure (SBP), history of ocular diseases and neurological disorders on both GCL volume and plasma NfL levels. Then, we investigated the relationship between retinal measures (independent variables), and plasma NfL levels (outcome) using three different models: Model 1 was based on univariate regression estimates, Model 2 was adjusted for GFR, blood volume, spherical equivalent, ocular diseases and sex, Model 3 was additionally adjusted for age and age-squared. Lastly, we assessed effect modification through the inclusion of an interaction term in the fully adjusted models. All statistical analyses were performed in R (base version 1.4.1106) and p-values <0.05 were considered statistically significant after false discovery rate adjustment for multiple comparisons.[13]

Results

Demographics

The mean (SD) age of the study population was 55.1 years (±13.8, range: 30.2–94.1) and 2450 participants (56%) were female. The mean (SD) GFR, SBP, and blood volume were 90.8 (18.7), 126.1 (15.9) and 4.7 (0.9), respectively; 531 (12.1%) participants were current smokers. The mean retinal volume was 8.6 mm^3 (0.4) and the median NfL value was 7.65 pg/ml (interquartile range: 5.6–11.0). Participants with missing data were significantly older, showed thinner retinas and higher NfL levels. A history of ocular disorders was reported in 99 participants (glaucoma ($N = 91$) and diabetic retinopathy ($N = 8$)). Intermediate age-related macular degeneration (iAMD) graded on fundoscopy was observed in 135 individuals, while no individuals with late AMD were included in the study population. Neurological disorders were reported by 113 participants (stroke ($N = 67$), dementia ($N = 5$), multiple sclerosis ($N = 23$), and Parkinson's disease ($N = 18$)).

Determinants of plasma NfL and retinal volume

We found that advancing age was the strongest determinant of both measures (1 SD increase in age was associated with 0.57 SD increase in plasma NfL levels (95% CI = [0.54–0.60], p-value = <0.0001) and 0.36 SD decrease in GCL volume (95% CI = [-0.40 to -0.32], p-value = <0.0001) (Figure 1). Plasma NfL increased by 3.0%/year and levels in the eldest group were 3.8 times higher compared to those in the youngest group (Figure 1A), while mean GCL volume decreased by 0.30% per year and showed a decline of 13.9% from the youngest to the eldest decade (Figure 1B). The highest relative change per decade for both biomarkers occurred in the seventh decade: Plasma NfL increased by 35.2% and GCL volume decreased by 3.74%. A history of neurological disorders was significantly associated with both biomarkers (Figure 1C). GFR and blood volume were important determinants of NfL (std. effect size [95% CI] for GFR = -0.216 [-0.244 to -0.189], for blood volume = -0.283 [-0.315 to -0.252]), while SBP had a quadratic relationship with plasma NfL but a linear one with GCL volume. No effect of smoking was noted. History of ocular diseases and refraction with a lower spherical equivalent were associated with thinner GCL (Figure 1C).
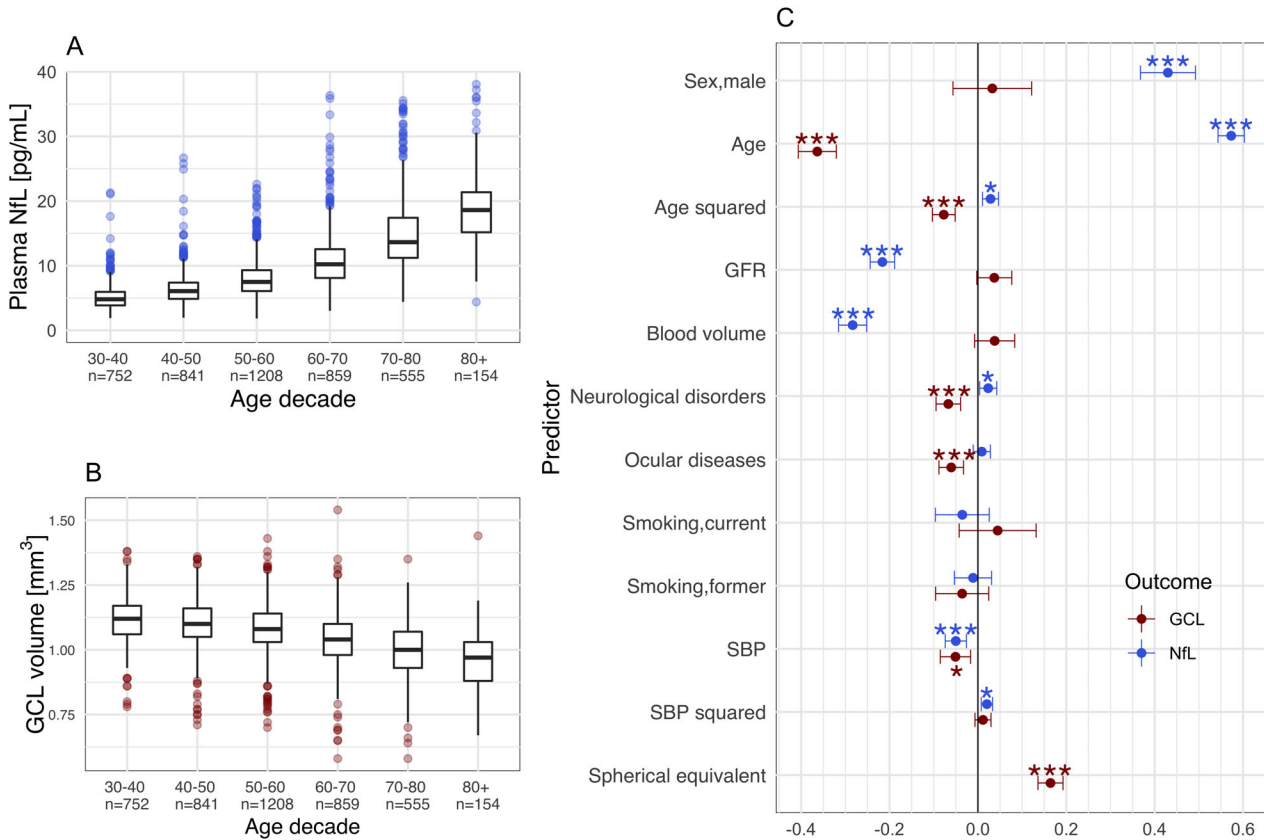
Figure 1. Differential age-effects and determinants of plasma NfL levels and GCL volume. Advancing age was associated with an exponential increase in plasma NfL levels (A), and an exponential decrease in GCL volume (B). Standardized estimates derived from a multivariable regression model, assessing the independent effect of each specified determinant, showed both similarities and differences between determinants of plasma NfL levels and GCL (C). Abbreviations: GFR, glomerular filtration rate; SBP, systolic blood pressure; BMI, body-mass index; GCL, ganglion cell layer volume; NfL, neurofilament light chain. * q < 0.05, ** q < 0.001, *** q < 0.0001.

The relation between plasma NfL and retinal measures

All inner neuronal retinal layers (including GCL and IPL) and total retinal volume were negatively associated with plasma NfL levels in the univariate and partially adjusted models; however, the direction of these associations reversed after adjustment for age (Table 1). In contrast, retinal pigmented epithelium volume (RPE) remained positively associated with NfL levels even after age adjustment (Table 1).

Modifiers of the relation between plasma NfL levels and retinal volume

Effect modification was assessed for those retinal measures with the highest neuronal density (i.e., GCL and IPL) plus RPE, for which also a robust association with plasma NfL levels was observed (Table 1). The association between GCL and plasma NfL was strongest in the oldest age tertile (Figure 2A), but an interaction between GCL and age was not significant in the fully adjusted model. In active smokers and in participants with a history of neurological disorders, GCL thinning was associated with higher NfL levels (Table 1, Figure 2B,C). Results remained similar when utilizing IPL volume (Table 1).

The exclusion of individuals with intermediate age-related macular degeneration (iAMD) did not change the statistical significance of any of our findings (data not shown).

Discussion

We present the first large-scale population-based study assessing the comparative determinants and association of plasma NfL levels with OCT-based retinal measures. Age, a history of neurological disorders and smoking largely accounted for the relationship between OCT-based retinal layer measures and plasma NfL levels. This indicates that brain atrophy could underlie their association. Indeed,

Table 1. Association between total retinal volume and individual retinal layers with plasma NfL.

| Method	Model 1, unadjusted[†]	Model 2, partially adjusted[†]	Model 3, fully adjusted[†]	Interaction terms			
Predictor		Std. Beta (95% CI)		Age	Neurological disorders	Smoking	Systolic blood pressure
RPE	0.027 (−0.003 to 0.057)	0.049*** (0.026 to 0.071)	0.028* (0.008 to 0.047)	0.006 (−0.013 to 0.024)	−0.010 (−0.028 to 0.008)	0.026 (−0.033 to 0.086)	0.016 (−0.003 to 0.035)
IPL	−0.259*** (−0.288 to −0.231)	−0.079*** (−0.102 to −0.056)	0.024* (0.003 to 0.044)	0.006 (−0.013 to 0.026)	−0.017' (−0.033 to −0.000)	−0.078* (−0.138 to −0.018)	−0.008 (−0.027 to 0.011)
GCL	−0.297*** (−0.326 to −0.269)	−0.098*** (−0.122 to −0.074)	0.024* (0.002 to 0.045)	0.005 (−0.015 to 0.025)	−0.020* (−0.036 to −0.003)	−0.078* (−0.138 to −0.017)	−0.011 (−0.030 to 0.008)
pRNFL	−0.166*** (−0.196 to −0.137)	−0.044** (−0.067 to −0.021)	0.019 (−0.001 to 0.039)				
TRET	−0.211*** (−0.240 to −0.182)	−0.056*** (−0.079 to −0.033)	0.021 (0.001 to 0.041)				
ONL	−0.116*** (−0.146 to −0.087)	−0.044** (−0.067 to −0.021)	0.007 (−0.013 to 0.027)				
OPL	0.026 (−0.004 to 0.056)	0.015 (−0.008 to 0.037)	−0.003 (−0.023 to 0.016)				
INL	−0.171*** (−0.200 to −0.142)	−0.071*** (−0.094 to −0.048)	−0.003 (−0.023 to 0.018)				

Abbreviations: GCL, ganglion cell layer volume; INL, inner nuclear layer volume; IPL, inner plexiform layer volume; ONL, outer nuclear layer volume; OPL, outer plexiform layer volume; pRNFL, peripapillary retinal nerve fiber layer thickness; RPE, retinal pigmented epithelium volume; TRET, total retinal volume.

*q < 0.05
**q < 0.001
***q < 0.0001 after multiple comparison correction.
[†]Model 1: unadjusted univariate regression analysis, Model 2: adjusted for GFR, blood volume, spherical equivalent, ocular diseases, sex, Model 3: additional adjustment for age and age-squared. In Model 3, we also checked for multi-collinearity by examining the variance inflation factors, which did not indicate any relevant degree of collinearity; all variance inflation factors were <<5: GCL = 1.26; sex = 2.6; SE_OD = 1.1; ocular diseases = 1.0; GFR = 2.1; blood volume = 2.6; age = 2.4; Age squared = 1.1.
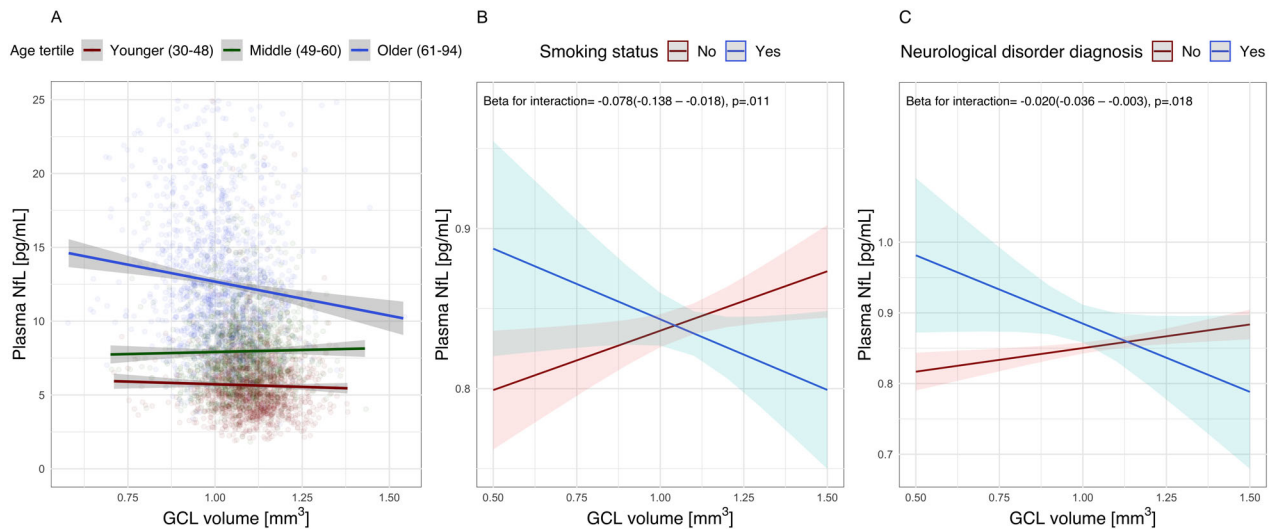
Figure 2. Modifiers of the relation between retinal measures and plasma NfL levels. The unadjusted association between GCL and plasma NfL largely depended on age (A). After accounting for all potential confounders, the relation between GCL volume and NfL levels was strongly dependent on the presence of (risk factors for) neurodegeneration, including smoking (B) and a history of neurological disorders (C). Abbreviations: SBP, systolic blood pressure; GCL, ganglion cell layer volume; NfL, neurofilament light chain.

previous imaging studies found that age-related brain atrophy starts in early adulthood, proceeds gradually throughout life and accelerates in old age. In line with these findings, we observed a similar age trend in both plasma NfL levels and GCL volume.[14]

Furthermore, we observed a non-linear, U-shaped, association between SBP and NfL levels, suggesting that both hypo- and hypertension may lead to neuronal injury,[15] as well as a linear association between SBP and GCL. Hypertension is an established risk factor for small-vessel disease and brain atrophy,[16] further supporting the idea of brain atrophy underlying the association between plasma NfL and retinal neurodegeneration.

The RPE showed a positive association with NfL levels independent of age. This epithelial layer is a component of the blood–retinal barrier (BRB) and undergoes thickening, rather than thinning, during aging.[17] Given the structural and functional similarities between the BRB and the blood–brain barrier (BBB),[18] this finding might be explained by RPE volume reflecting BBB integrity rather than brain size.

The effects of GFR and blood volume on plasma NfL, reflecting its clearance and dilution rates, respectively, were also reported in two separate previous studies.[19,20] Our findings extend these findings by showing that their effects are mutually independent, which should be considered in future studies utilizing plasma NfL levels.

Correcting for age reversed the direction of association between GCL volume and NfL levels. To understand this phenomenon, one should distinguish between *brain atrophy* (brain volume change observed between two measurements) and *brain size* (cross-sectional brain volume). We observed that in individuals with risk factors for brain atrophy, retinal neurodegeneration reflects rising plasma NfL levels. However, in individuals with the same rate of neuronal loss, once these risk factors are accounted for, a larger absolute brain size might lead to higher baseline NfL levels due to a larger amount of neuronal tissue available. Hence, both increasing brain atrophy and brain size may lead to higher NfL levels. Given that age is by far the strongest risk factor for neurodegeneration in the general population, adjusting for it largely removes the effect of brain atrophy, and amounts to comparing the association between NfL levels and GCL volume as a proxy for brain size.[3,7,8] Supporting this notion are findings from a previous study showing a trend for a positive association between plasma NfL levels and brain volume in 99 individuals, although these findings need further confirmation in a larger population-based cohort.[3]

The strengths of our study include a large population-based sample, inclusion of measures of all retinal layers, and assessment and consideration of all known relevant confounders in our statistical analyses. Limitations include self-reported history of medical conditions and lack of longitudinal data.

In conclusion, in the presence of risk factors for neuronal injury, plasma NfL levels are associated with inner retinal neurodegeneration and outer retinal thickening. Our study supports the integration of OCT-based retinal measures as both clinical and research tools for tracking central neurodegeneration.

Acknowledgments

Conflict of Interest

The author Robert P Finger declares grants and personal fees from Novartis; grants from Biogen; personal fees from Bayer, Santen, Ophtea, Apellis, Roche/Genentech, Böhringer-Ingelheim, Novelion, ProQR, Oxford Innovation, Roche, Alimera, Santhera, Inositec, Ellex. Other authors declare no conflict of interest.

References

1. Khalil M, Teunissen C, Otto M, et al. Neurofilaments as biomarkers in neurological disorders. Nat Rev Neurol. 2018;14(10):577-589.

2. London A, Benhar I, Schwartz M. The retina as a window to the brain—from eye research to CNS disorders. Nat Rev Neurol. 2013;9:44-53.

3. Khalil M, Pirpamer L, Hofer E, et al. Serum neurofilament light levels in normal aging and their association with morphologic brain changes. Nat Commun. 2020;11(1).

4. Mauschitz MM, Holz FG, Finger RP, Breteler MMB. Determinants of macular layers and optic disc characteristics on SD-OCT: the Rhineland study. Transl Vis Sci Technol. 2019;8(3):34.

5. Fyfe I. Neurofilament light chain—new potential for prediction and prognosis. Nat Rev Neurol. 2019;15:557-557.

6. Mirzaei N, Shi H, Oviatt M, et al. Alzheimer's retinopathy: seeing disease in the eyes. Front Neurosci. 2020;14.

7. Saidha S, Al-Louzi O, Ratchford JN, et al. Optical coherence tomography reflects brain atrophy in multiple sclerosis: a four-year study. Ann Neurol. 2015;78(5):801-813.

8. Mutlu U, Bonnemaijer PWM, Ikram MA, et al. Retinal neurodegeneration and brain MRI markers: the Rotterdam study. Neurobiol Aging. 2017;60:183-191. https://doi.org/10.1016/j.neurobiolaging.2017.09.003

9. Tavazzi E, Jakimovski D, Kuhle J, et al. Serum neurofilament light chain and optical coherence tomography measures in MS. Neurol Neuroimmunol Neuroinflamm. 2020;7(4):e737.

10. Quanterix Corporation Simoa® NF-light Advantage Kit. 1–3 (2018). Available at: https://www.quanterix.com/wp-content/uploads/2020/12/NF-light-Data-Sheet-HD-1/HD-X-2.pdf

11. Nadler SB, Hidalgo JH, Bloch T. Prediction of blood volume in normal human adults. Surgery. 1962;51:224-232.

12. Inker LA, Schmid CH, Tighiouart H, et al. Estimating glomerular filtration rate from serum creatinine and cystatin C. N Engl J Med. 2012;367(1):20-29. https://doi.org/10.1056/nejmoa1114248

13. Benjamini Y, Hochberg Y. Controlling the false discovery rate: a practical and powerful approach to multiple testing on JSTOR. J R Stat Soc. 1995;57:289-300.

14. Peters R. Ageing and the brain. Postgrad Med J. 2006;82:84-88.

15. Korte N, Nortley R, Attwell D. Cerebral blood flow decrease as an early pathological mechanism in Alzheimer's disease. Acta Neuropathol. 2020;140:793-810.

16. Zlokovic BV. Neurovascular pathways to neurodegeneration in Alzheimer's disease and other disorders. Nat Rev Neurosci. 2011;12:723-738.

17. Okubo A, Rosa, RH Jr, Bunce, CV, et al. The relationships of age changes in retinal pigment epithelium and Bruch's membrane. Investig Ophthalmol Vis Sci. 1999;40:443-449.

18. Steuer H, Jaworski A, Elger B, et al. Functional characterization and comparison of the outer blood–retina barrier and the blood–brain barrier. Investig Opthalmology Vis Sci. 2005;46(3):1047.

19. Manouchehrinia A, Piehl F, Hillert J, et al. Confounding effect of blood volume and body mass index on blood neurofilament light chain levels. Ann Clin Transl Neurol. 2020;7(1):139-143. https://doi.org/10.1002/acn3.50972

20. Akamine S, Marutani N, Kanayama D, et al. Renal function is associated with blood neurofilament light chain level in older adults. Sci Rep. 2020;10(1). https://doi.org/10.1038/s41598-020-76990-7

RESEARCH ARTICLE

WILEY

Visual impairment and retinal and brain neurodegeneration: A population-based study

Davide Garzone[1,2] | Robert P. Finger[2] | Matthias M. Mauschitz[1,2] | Alexandra Koch[1] | Martin Reuter[3,4,5] | Monique M. B. Breteler[1,6] | N. Ahmad Aziz[1,7]

[1]Population Health Sciences, German Center for Neurodegenerative Diseases (DZNE), Bonn, Germany

[2]Department of Ophthalmology, Faculty of Medicine, University of Bonn, Bonn, Germany

[3]Image Analysis, German Center for Neurodegenerative Diseases (DZNE), Bonn, Germany

[4]A.A. Martinos Center for Biomedical Imaging, Massachusetts General Hospital, Boston, Massachusetts, USA

[5]Department of Radiology, Harvard Medical School, Boston, Massachusetts, USA

[6]Faculty of Medicine, Institute for Medical Biometry, Informatics and Epidemiology (IMBIE), University of Bonn, Bonn, Germany

[7]Department of Neurology, Faculty of Medicine, University of Bonn, Bonn, Germany

Correspondence

N. Ahmad Aziz, Population Health Sciences, German Center for Neurodegenerative Diseases (DZNE) and Department of Neurology, University Hospital Bonn, Venusberg-Campus 1/99, 53127 Bonn, Germany.
Email: ahmad.aziz@dzne.de

Funding information

Alzheimer Forschung Initiative, Grant/Award Number: AARG-19-616534; Bundesministerium für Bildung und Forschung; H2020 European Research Council, Grant/Award Number: 101041677; Ministerium für Kultur und Wissenschaft des Landes Nordrhein-Westfalen

Abstract

Visual impairment and retinal neurodegeneration are intrinsically connected and both have been associated with cognitive impairment and brain atrophy, but the underlying mechanisms remain unclear. To investigate whether transneuronal degeneration is implicated, we systematically assessed the relation between visual function and retinal, visual pathway, hippocampal and brain degeneration. We analyzed baseline data from 3316 eligible Rhineland Study participants with visual acuity (VA), optical coherence tomography (OCT), and magnetic resonance imaging (MRI) data available. Regional volumes, cortical volume, and fractional anisotropy (FA) were derived from T1-weighted and diffusion-weighted 3 T MRI scans. Statistical analyses were performed using multivariable linear regression and structural equation modeling. VA and ganglion cell layer (GCL) thinning were both associated with global brain atrophy (SD effect size [95% CI] −0.090 [−0.118 to −0.062] and 0.066 [0.053–0.080], respectively), and hippocampal atrophy (−0.029 [−0.055 to −0.003] and 0.114 [0.087–0.141], respectively). The effect of VA on whole brain and hippocampal volume was partly mediated by retinal neurodegeneration. Similarly, the effect of retinal neurodegeneration on brain and hippocampal atrophy was mediated through intermediate visual tracts, accounting for 5.2%–23.9% of the effect. Visual impairment and retinal neurodegeneration were robustly associated with worse brain atrophy, FA, and hippocampal atrophy, partly mediated through disintegration of intermediate visual tracts. Our findings support the use of OCT-derived retinal measures as markers of neurodegeneration, and indicate that both general and transneuronal neurodegeneration along the visual pathway, partly reflecting visual impairment, account for the association between retinal neurodegeneration and brain atrophy.

KEYWORDS

brain, modeling, neurodegeneration, retina, structural equation, visual impairment

1 | OBJECTIVES

The retina is the first relay of the visual pathway, responsible for converting light signals into axon potentials. Retinal pathology has consistently been associated with degeneration of various components of the visual pathway, including the primary visual area (V1), the optic radiation, and the lateral geniculate nucleus (Boucard et al., 2009; Hernowo et al., 2011, 2014; Malania et al., 2017; Mutlu et al., 2018; Prins et al., 2016). This could be due to transneuronal degeneration, since these structures are components of the geniculostriate pathway: axons of the retinal ganglion cells (GCL) bundle together in the retinal nerve fiber layer (RNFL), and subsequently synapse at the level of the lateral geniculate nucleus, conveying visual information to V1 through the optic radiation. From V1, visual information is then carried forward through the ventral (parietal) and dorsal (temporal) streams for further integration and multimodal processing (Mishkin et al., 1983). In particular, retinal thinning in the inner neuronal layers (including GCL, the inner plexiform layer [IPL], and RNFL), which can be assessed noninvasively with spectral domain−optical coherence tomography (SD-OCT), is attributed to neurodegeneration and likely reflects neuronal damage accrued with age and other pathologies (Garzone et al., 2022; Mauschitz et al., 2018; Pfeiffer et al., 2020). Indeed, retinal neurodegeneration has been associated with both global and regional brain atrophy, as well as cognitive impairment (Hernowo et al., 2011, 2014; Ward et al., 2020; Mutlu et al., 2017).

Retinal neurodegeneration is intrinsically linked to visual function. For example, in glaucoma inner retinal neurodegeneration is the key event leading to visual loss, but an association between retinal neurodegeneration and visual loss is also seen in other retinal pathologies without primary inner retinal involvement. (Abdolrahimzadeh et al., 2019; Chiang et al., 2020; Li et al., 2021; Pillay et al., 2018; van Dijk et al., 2011) Decreased visual stimulation might also induce retinal degeneration through reduced levels of neurotrophic factors (Fleitas et al., 2020). Interestingly, visual impairment has also been associated with a higher risk of cognitive impairment (Chen et al., 2017; Shang et al., 2021, Ward et al., 2020), which is not surprising given that up to half of the total cortical surface area is devoted to the processing of visual information (Zilles & Amunts, 2012). Recently, it was shown that retinal neurodegeneration is preferentially associated with changes in the visual pathway, including the occipital lobe gray matter (Mutlu et al., 2018), and the medial temporal lobe structures, including the hippocampus (Kravitz et al., 2011). Indeed, temporal lobe structures are crucial for higher order visuospatial integration of downstream signals originating from the occipital lobe visual areas (Silson et al., 2020; Zilles & Amunts, 2012). Visual impairment and retinal pathology have also been associated with altered connectivity between visual and other brain areas (Sanda et al., 2018; Sabbah et al., 2017; Mendola et al., 2018; Huang et al., 2016; Collignon et al., 2013). However, to the best of our knowledge, systematic studies assessing the conjoint relations among visual impairment, retinal layer measures, major brain regions of the central visual system and involved in cognition and neurodegeneration, such as whole brain and hippocampal volume, in the general population are still lacking.

Accumulating evidence indicates that multisensory stimulation may enhance brain plasticity, and ward off neurodegeneration (Yang et al., 2021). In particular, visual stimulation has been demonstrated to decrease Alzheimer disease-associated pathology and improve cognition in various mouse models (Iaccarino et al., 2016; Martorell et al., 2019). Nevertheless, the major underlying neuroanatomical pathways through which visual stimulation or impairment could affect brain structure and connectivity in humans remain elusive. Elucidating the pathways underlying the association between visual impairment, retinal neurodegeneration, and brain atrophy in the general population is of paramount importance for the development of more effective, targeted preventive and therapeutic paradigms against age-associated neurodegeneration and cognitive decline. Therefore, using a population-based approach, in this study, we aimed to systematically assess (1) the interrelations among visual impairment, retinal degeneration, and regional and general brain atrophy, and (2) whether transneuronal degeneration along the visual pathway could be implicated.

2 | MATERIALS AND METHODS

2.1 | Study design and population

We analyzed baseline data from the first 5000 participants of the Rhineland Study, a community-based prospective cohort study including inhabitants older than 30 years from two distinct regions in the city of Bonn, Germany (Mauschitz et al., 2019). We excluded participants with self-reported neurological disorders (including stroke $N = 78$, dementia $N = 5$, and multiple sclerosis $N = 25$) and participants with insufficient SD-OCT image quality (internal quality parameter ≤20 dB, $N = 23$; Figure 1). When assessing the relationship between ipsilateral (right eye) retinal volume and best-corrected visual acuity (VA), 4687 participants were included (Table 2). The Rhineland study has been conducted according to the provisions of the Declaration of Helsinki, approved by the local ethic committee and all participants provided written informed consent.

2.2 | Magnetic resonance imaging image acquisition

Magnetic resonance imaging (MRI) scans were acquired on 3 T Siemens MAGNETOM Prisma MRI scanners (Siemens Healthcare, Erlangen, Germany) equipped with 64-channel head–neck coils at two examination sites in Bonn. The imaging protocol included a 3D T1-weighted multiecho magnetization-prepared rapid gradient-echo sequence with 2D acceleration and elliptical sampling (acquisition time [TA] $= 6.5$ min; Brenner et al., 2014; 4 echo times between 1.7 and 6.5 ms, repetition time $= 2560$ ms, inversion time $= 1100$ ms, flip angle $= 7°$, field of view $= 256 \times 256$ mm^2, 224 slices, 0.8 mm isotropic resolution). Simultaneous multislice diffusion-weighted MRI (dMRI) was performed with a spin-echo echoplanar imaging sequence applying threefold slice acceleration (Setsompop et al., 2012). A compressed sensing diffusion spectrum
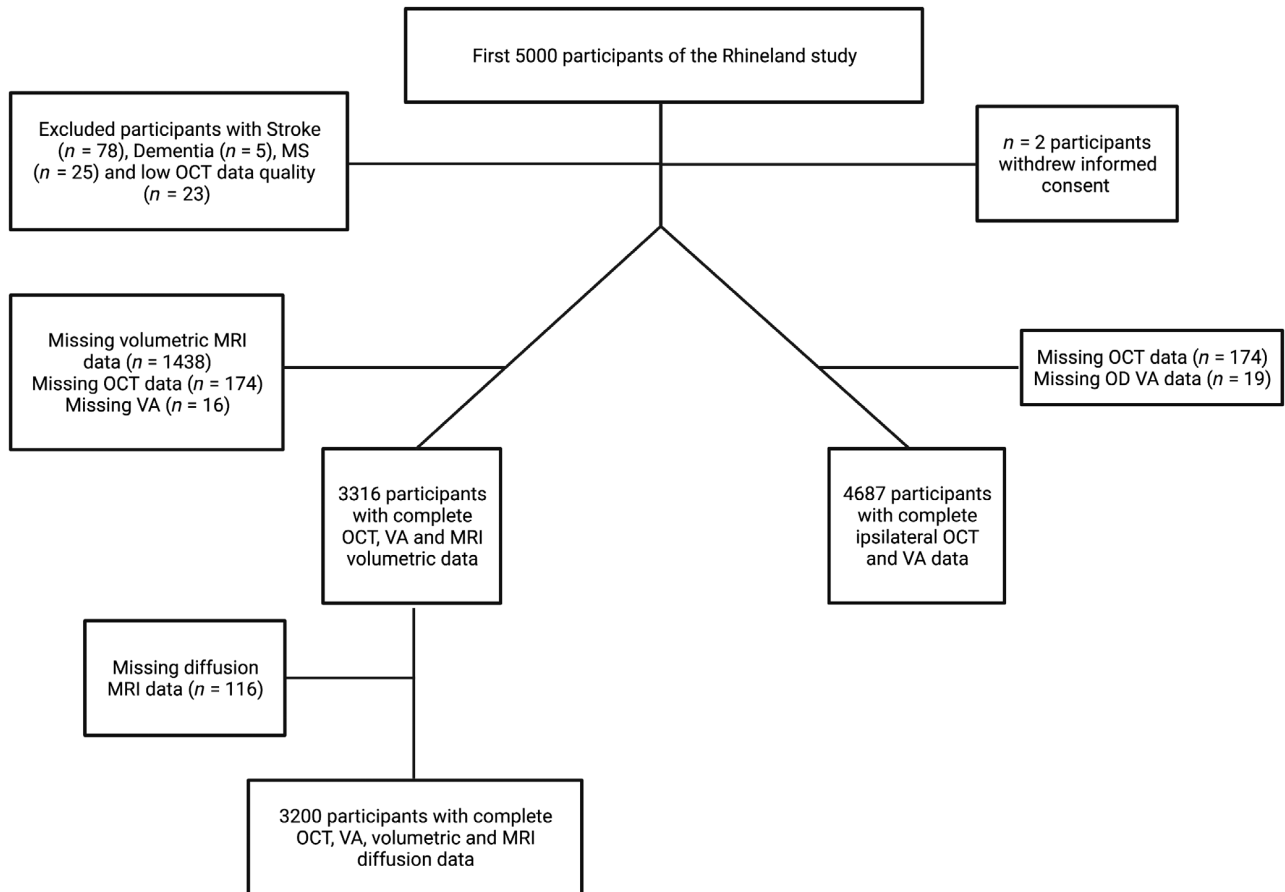
FIGURE 1 Flow chart of the study population. The most common reasons for missing volumetric brain magnetic resonance imaging (MRI) data were contraindications for MRI ($n = 789$, 52.8%), followed by refusal of brain imaging ($n = 556$, 37.2%), failed postprocessing ($n = 5$), and unknown reasons ($n = 64$). Further missings in diffusion MRI are due to postprocessing failure and drop-out of the diffusion part of the MRI examination. The most common reasons for missing spectral domain (SD)-optical coherence tomography (OCT) data were exclusion during quality assurance ($n = 75$, 43.1%), followed by technical issues ($n = 72$, 41.4%), and low participant compliance ($n = 10$, 5.7%). VA, visual acuity.

imaging protocol was used to collect dMRI scans at 1.5 mm isotropic spatial resolution (Harms et al., 2017; Lohner et al., 2022). The MRI protocol also included 3D sequences to acquire T2-weighted and FLAIR images (Lohner et al., 2022).

2.3 | MRI image processing

All T1-weighted images were processed using FreeSurfer version 6.0 (http://surfer.nmr.mgh.harvard.edu/) to derive quantitative volumetric measures (Fischl, 2012; Fischl et al., 2002). We used the estimated total intracranial volume generated by FreeSurfer as a proxy for head size (Buckner et al., 2004). Processing steps for diffusion MRI included the correction of susceptibility-induced and eddy current-induced distortions and head motion using FSL version 6.0 (www.fmrib.ox.ac.uk/fsl), compressed sensing reconstruction and subsequent estimation of fractional anisotropy (FA) from the diffusion tensor model through voxel-wise model fitting using the Microstructure Diffusion Toolbox framework (Andersson et al., 2003; Basser et al., 1994; Harms et al., 2017; Tobisch et al., 2018, 2019). A whole brain white matter mask

was obtained from the T1-weighted MRI data using the standard FreeSurfer processing pipeline, corrected for white matter hyperintensities determined based on T1-weighted, T2-weighted, and FLAIR images, and further refined through FA skeletonization. Using the Jülich histological atlas, white matter tract-specific and gray matter average FA values were derived for the optic radiation and the lateral geniculate nucleus, respectively (Figure 2; Bürgel et al., 2006).

2.4 | Brain regions of interest

We included brain areas known to be involved in visuosensory and cognitive processing. As measures of visual pathway integrity, we assessed the FA of the lateral geniculate nucleus, the optic radiation and the occipital lobe. As cortical areas involved in ventral stream higher order visual processing, we selected the inferior temporal, fusiform, and parahippocampal cortex (Aminoff et al., 2013; Zilles & Amunts, 2012). We also included the volume of the hippocampus, because of its importance as a cognitive biomarker (Jack et al., 1998), as well as total brain volume as a measure of brain atrophy.
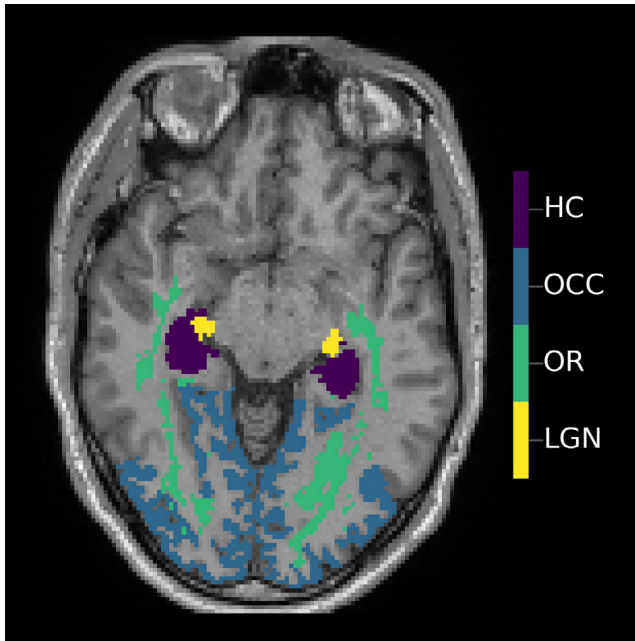
FIGURE 2 Axial view of brain regions for the lateral geniculate nucleus, optic radiation, pericalcarine cortex, and visual association areas obtained from diffusion magnetic resonance imaging and T1 FreeSurfer processing, and overlaid onto a T1-weighted scan. HC, hippocampus; LGN, lateral geniculate nucleus; OCC, occipital lobe; OR, optic radiation.

2.5 | SD-OCT image acquisition and processing

We assessed retinal layers using Spectralis SD-OCT (Heidelberg Engineering, Heidelberg, Germany) as described previously (Mauschitz et al., 2019). In brief, the SD-OCT imaging protocol includes a macular volume scan (97 horizontal B-scans, 20 automatic real-time [ART] frames per B-scan, $20° \times 20°$ field) and two circular OCT scans around the optic nerve head (3.5 mm diameter circular scan with 100 ART frames and 24 radial scans with 25 ART frames each). Volumes of six macular layers (RNFL, GCL, IPL, inner nuclear layer (INL), outer plexiform layer (OPL), outer nuclear layer (ONL), and retinal pigment epithelium (RPE)), total retinal volume, and peripapillary RNFL (pRNFL) thickness were computed using the inbuilt segmentation algorithm of the Heidelberg Eye Explorer (HEYEX). For each layer, we utilized total volume in mm^3 except for the pRNFL, which is computed as average thickness in μm. Corneal curvature of individuals was entered before scan acquisition to adjust for corneal refraction.

2.6 | Visual acuity and spherical equivalent

Refraction and VA were measured with an automated refractometer (Ark-1s; Nidek Co., Tokyo, Japan). Values <0.1 were manually assessed with a Snellen chart. Qualitative measurements of low-range VA ($n = 44$) were imputed as follows: perception of hand movements, finger counting, and light/nulla lux was set to 0.005, 0.014, and 0.001,

respectively (Schulze-Bonsel et al., 2006). Spherical equivalent was calculated as the spherical value and half of the cylindrical value. We utilized VA from the right eye when assessing the relationship with ipsilateral retinal measures (Table 2), and the average of the two eyes when assessing the relationship with brain measures, since each eye sends information to both ipsilateral and contralateral brain hemispheres. If VA was missing in one eye, we utilized VA from the contralateral eye. We utilized retinal measures from the right eye since it is the first examined eye in our imaging protocol, and therefore contains fewer missing values for retinal measurements.

2.7 | Statistical analysis

Descriptive statistics are presented as means and standard deviation for continuous variables and as frequency and percentages for categorical variables. VA is presented as the logarithm of the minimum angle of resolution (LogMar scale), with higher values indicating worse vision. All brain imaging measures were averaged between the two hemispheres. The variable "Higher-order visual areas" was a composite average of Z-scores of selected brain areas (i.e., inferior, middle temporal, and fusiform gyrus). We used multivariable linear regression models to investigate which retinal layer had the strongest association with VA and total brain volume. Similarly, we used multivariable linear regression to assess the associations between VA, GCL volume and optic radiation, lateral geniculate nucleus, occipital lobe, higher order visual association areas, hippocampal, and total brain volume.

In all models, VA was included as an independent variable; retinal measures were included as dependent variables when regressed on VA, and as independent variables when assessing their effect on brain structure. Statistical significance was inferred at a two-tailed, false discovery rate-corrected $q < 0.05$.

Structural equation modelling was used for mediation analysis. To investigate whether retinal neurodegeneration mediates the effect of VA on brain atrophy and hippocampal volume, we included GCL volume as a mediator. To assess whether the effect of retinal neurodegeneration on brain atrophy and hippocampal volume is mediated by transneuronal degeneration along the visual pathway, we included FA measures of visual pathway (lateral geniculate nucleus, optic radiation) and occipital lobe volume as potential mediators. For structural equation modeling, we standardized continuous variables using Z-scores to allow for estimate comparison. The 95% confidence intervals (CIs) of all the mediation analyses estimates were based on nonparametric bias-corrected bootstrapping with 1000 resamplings.

We adjusted all models, both in the regression analysis and in the structural equation modeling, for age, sex, systolic blood pressure, and spherical equivalent as a proxy of axial length when including retinal measures, and intracranial volume when considering brain volumetric measures (Mauschitz et al., 2019). We additionally adjusted the regression models for known cerebrovascular risk factors (including smoking status, diabetes mellitus, cholesterol levels, and body mass index) to ensure that the associations were independent of these cerebrovascular risk factors (Model 2 in Figure 3). Optic radiation FA

was further adjusted for global brain FA, to assess the effect of visual pathway degeneration independently from whole brain pathology.

2.8 | Sensitivity analyses

We assessed the robustness of our findings by excluding individuals with extreme values of VA, GCL, spherical equivalent, and self-reported age-related macular degeneration (AMD; $n = 69$) and glaucoma ($n = 65$). We also tested the robustness of our mediation analysis results by including models with "control" areas in the frontal lobe not in direct synaptic contact with visual pathway structures.

All statistical analyses were performed in R (base version 3.4), using the "lavaan" package for structural equation modeling (Rosseel, 2012).

3 | RESULTS

3.1 | Participant characteristics

An overview of the characteristics of the study participants is presented in Table 1.

Participants with missing data were significantly more often male, older, and had worse average vision and higher blood pressure. The majority of participants 2884 (91.4%), had good VA (-0.1–0.1), while it was reduced or poor in 270 participants (8.6%). Among 158 (4.8%) individuals with VA >0.2 (<0.63 on Snellen scale): 34 (21.5%) had been graded with early stages of AMD and 3 (1.9%) with late AMD. In total, 11 (7%) reported a diagnosis of glaucoma, 2 (1.3%) reported a history of uveitis, 12 subjects (7.6%) were graded with clinically significant lens opacities and 8 (5%) with epiretinal gliosis. In 2 individuals, retinal vascular disease and signs of myopic degeneration were graded, respectively.

3.2 | Association between VA, retinal layer measures, and total brain volume

All retinal layer measures were significantly associated with both VA and total brain volume, except the INL and the RPE, which were only associated with total brain volume. Standardized effect sizes, allowing for comparison of the strength of the associations between different retinal layers, are reported in Table 2. One-unit worse VA was associated with a 0.06 mm^3 thinner GCL [95% CI -0.08 to -0.04], while a 0.1 mm^3 decrease in GCL was associated with a 7524 mm^3 decrease in total brain volume [95% CI 6013–9035]. Among all inner retinal layer measures, VA had the largest effect on GCL, which in turn was most robustly associated with total brain volume. Other inner retinal layers showed similar trends, except for the OPL: one-unit better VA (decrease on LogMar scale) corresponded to a 0.046 mm^3 increase in OPL volume. Although a similar trend was discernible for the RPE, the association between its volume and VA did not reach statistical significance.

The trend of the association between all retinal layers and brain volume was positive (Table 2). The association between VA and GCL became nonsignificant after excluding participants in the smallest decile of GCL volume (E-Table 6), but remained robust in other sensitivity analyses, indicating that the effect of VA on GCL is likely driven by volumes in the lowest range.

3.3 | Associations among the different components of the visual system

Lower VA was associated with decreased occipital lobe, hippocampal, and total brain volume, as well as decreased FA of the optic radiation and the lateral geniculate nucleus (Figure 3). An association between VA and higher order visual areas was, however, not observed. GCL volume was strongly associated with all selected structural and FA

TABLE 1 Characteristics of the study population.

	Analytical population	MRI or OCT or VA missing data	p-Value
N	3316	1552	
Sex (male)a	1386 (41.8)	729 (47.0)	.001
Age (mean ± SD) (range)	54.49 ± 13.5 (30.2–95.4)	57.53 ± 14.6 (30.5–93.2)	<.001
Average VA from both eyes (mean ± SD)	$-0.01 ± 0.14$	0.03 ± 0.24	<.001
High (-0.1–0.1)[a]	2884 (87.0)	1244 (81.0)	
Middle (0.11–0.4)[a]	382 (11.5)	233 (15.1)	
Low (>0.41)[a]	50 (1.5)	59 (3.8)	
SBP (mean ± SD) (range)	125.9 ± 15.80	127.2 ± 16.46	.008
GCL volume (mean ± SD) mm^3	1.07 ± 0.10	1.06 ± 0.11	.072
TRET volume (mean ± SD) mm^3	8.65 ± 0.41	8.63 ± 0.41	.111
OR FA (mean ± SD)	0.63 ± 0.02	—	
TB volume (mean ± SD) mm^3	1,109,230 (117,960)	—	

Abbreviations: GCL, ganglion cell volume; OR FA, optic radiation fractional anisotropy; SBP, systolic blood pressure; SD, standard deviation; TB, total brain; TRET, total retinal volume; VA, visual acuity.

[a]Sex and strata of visual acuity are presented as counts (frequency as percentage). Two sample t-tests were used for intergroup comparisons.

measures of the visual pathway, including higher order visual association areas and hippocampus. Effect estimates changed little to none after additional adjustment (Model 2, Figure 3), indicating that these associations are independent from common cerebrovascular risk factors. Interestingly, VA also had a large effect on global FA, independent of its effect on optic radiation FA (Figure 4). Associations of VA and GCL with individual brain areas are reported in E-Table 1. Briefly, the association between VA and occipital lobe structures was most pronounced in the lateral occipital and lingual lobe, while GCL was robustly associated with selected brain areas involved in processing of visual information. Importantly, the observed associations remained robust in all sensitivity analyses (E-Tables 5, 7, and 8).

3.4 | GCL volume mediates the effect of visual acuity on brain measures

GCL volume significantly mediated the association between VA and structures of the visual pathway (percentages of mediated effect of 17.4% and 11.4% for occipital lobe and optic radiation FA, respectively; Figure 4). The percentage of mediated effect increased to 18.4% and 19.2% for hippocampal and total brain volume, respectively. Interestingly, we observed a strong association between VA and global FA (1 SD decrease in VA corresponded to 0.21 SD decrease in global brain FA 95% CI 0.16–0.27; Figure 4).

TABLE 2 Association between ipsilateral retinal measures, visual acuity, and total brain volume.

Retinal layer	Visual acuity[a]	Total brain volume[a]
pRNFL	−0.065 *** (−0.095 to −0.035)	0.047 *** (0.034–0.059)
GCL	−0.090 *** (−0.118 to −0.062)	0.066 *** (0.053–0.080)
IPL	−0.058 ** (−0.086 to −0.029)	0.062 *** (0.049–0.075)
INL	−0.004 (−0.033 to 0.026)	0.019 * (0.006–0.032)
OPL	0.095 *** (0.064–0.126)	0.018 * (0.005–0.030)
ONL	−0.055 ** (−0.085 to −0.025)	0.014 * (0.001–0.027)
RPE	0.026 (−0.005 to 0.058)	0.026 *** (0.014–0.038)
TRET	−0.041 * (−0.070 to −0.012)	0.050 *** (0.037–0.062)

Note: Each row represents one distinct regression model. Retinal measures were included as dependent variables when regressed on VA and as independent variables when assessing their effect on brain structure.

Abbreviations: FDR, false discovery rate; GCL, ganglion cell layer; INL, inner nuclear layer; IPL, inner plexiform layer; ONL, outer nuclear layer; OPL, outer plexiform layer; pRNFL, peripapillary nerve fiber layer; RPE, retinal pigmented epithelium; TRET, total retinal volume.

[a]Visual acuity was quantified as the logarithm of the minimum angle of resolution corrected for refractive error (LogMar scale), with higher values representing worse vision. All multivariable linear regression models are adjusted for age, sex, systolic blood pressure, spherical equivalent and, when including brain volume, also for intracranial volume. FDR *q < 0.05; **q < 0.001 ; ***q < 0.0001.
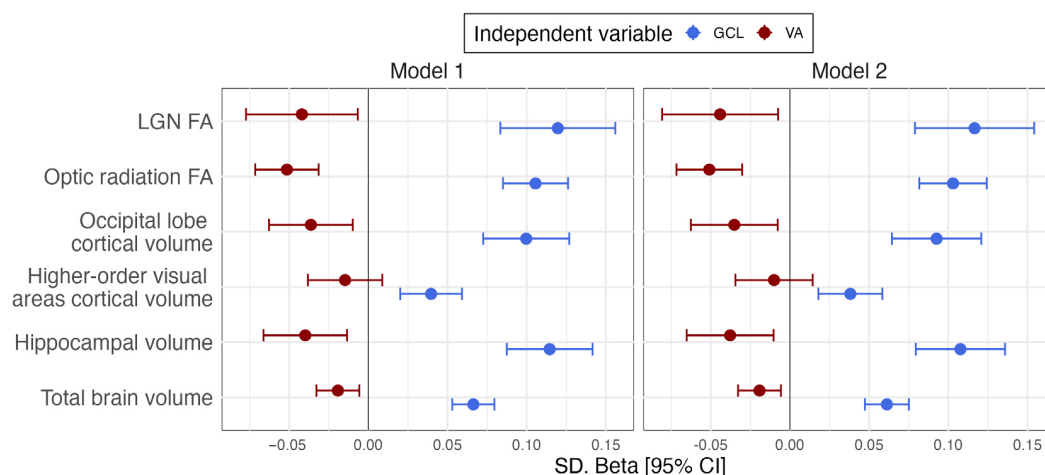
FIGURE 3 Associations between visual acuity, retinal volume, and cerebral measures. Each row represents one distinct regression model with dependent variables listed on the left side of the figure. Model 1 is adjusted for age, sex, intracranial volume for volumetric measures, global FA for optic radiation FA, SBP, and spherical equivalent for models including GCL. Model 2 is additionally adjusted for smoking status, diabetes mellitus, cholesterol levels, and body mass index. Visual acuity was quantified as the logarithm of the minimum angle of resolution with optimal correction of refractive errors. FA, fractional anisotropy; GCL, ganglion cell volume; LGN, lateral geniculate nucleus; VA, best-corrected visual acuity. FDR q *q < 0.05, **q < 0.01, ***q ≤ 0.0001.

3.5 | Visual pathway structures mediate the effect of GCL on total brain and hippocampal volume

The effect of GCL volume on total brain and hippocampal volume was mediated by all key structures of the visual pathway, including the lateral geniculate nucleus, the optic radiation and the occipital lobe (Figure 5). We observed the largest mediation effect sizes for the occipital lobe, accounting for 17.3% and 23.9% of the total effect for hippocampal and total brain volume, respectively. Importantly, apart from its relation to the optic radiation, smaller GCL volume was also independently associated with lower global brain FA (i.e., 1 SD increase in GCL volume corresponded to 0.22 SD increase in global brain FA 95% CI 0.18–0.26; Figure 5).

In the sensitivity analyses, we did not find an association of VA with two "control" brain areas in the frontal lobe not in direct synaptic contact with visual pathway structures. In the structural equation models, we observed a weaker association between GCL and the middle frontal lobe volume, which was not mediated by optic radiation

and lateral geniculate nucleus FA (E-Table 3). The occipital lobe volume fully mediated the effect of GCL on the middle frontal lobe volume (E-Table 4).

4 | INTERPRETATION

We present a large-scale population-based study in which we systematically assessed visual impairment in relation to the structural integrity of key components of the central visual system, including all retinal layers, visual pathway microstructure, as well as higher order cortical and subcortical visual association areas. We found that GCL is the inner neuronal retinal layer most robustly associated with both visual impairment and brain atrophy. This association was mainly due to individuals very low GCL volume, but was robust to exclusion of individuals with ophthalmological diseases, low VA, and large refractive errors. Interestingly, VA was also robustly associated with larger OPL; however, the direction of this association was opposite to that
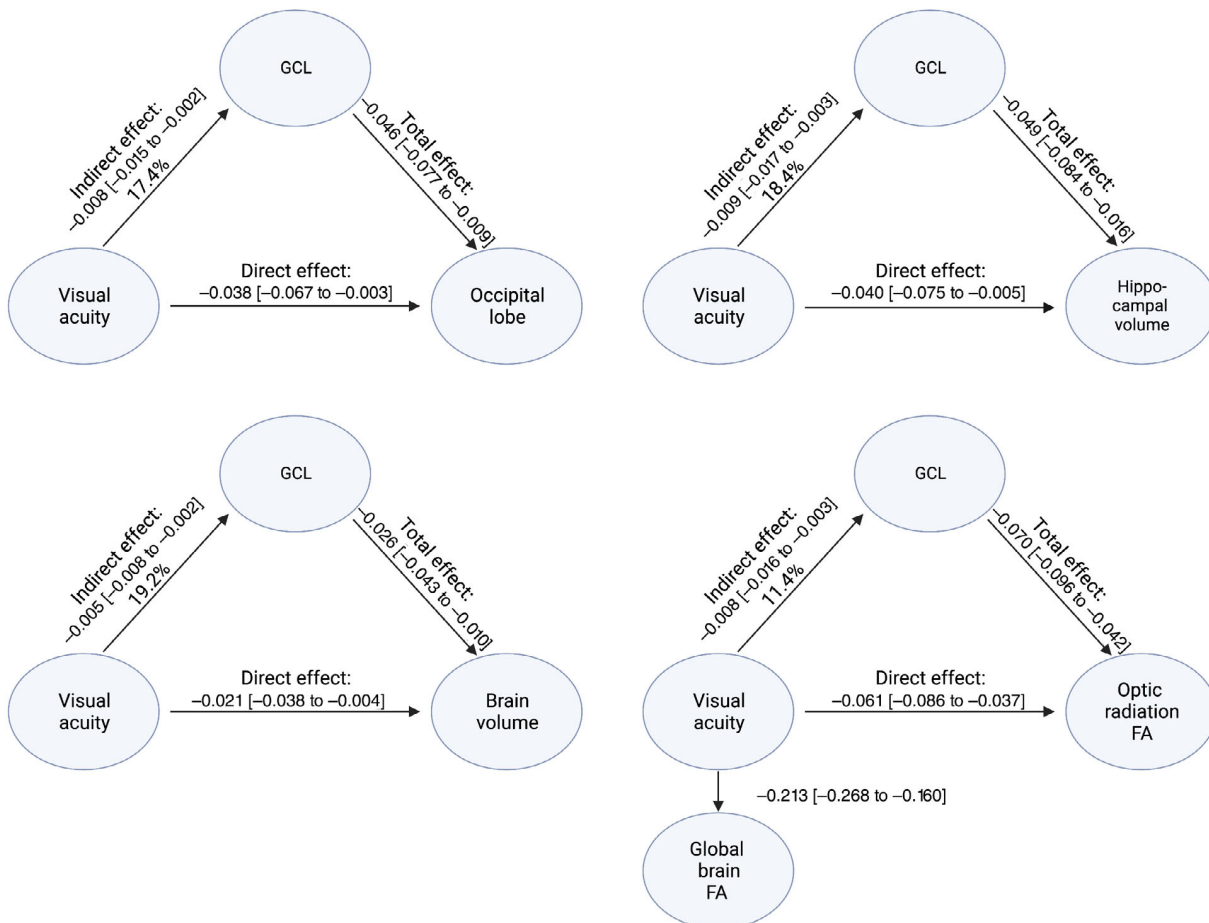
FIGURE 4 Inner retinal thinning mediates the effect of visual acuity on brain structural measures. All models are adjusted for age, sex, intracranial volume for volumetric measures, global FA for optic radiation FA, SBP, and spherical equivalent for models including GCL. Full lines indicate nominally significant effects, dashed lines are non-nominally significant effects. Visual acuity was quantified as the logarithm of the minimum angle of resolution at optimal correction of refractive errors. FA, fractional anisotropy; GCL, Ganglion cell layer; SBP, systolic blood pressure.

GARZONE ET AL.
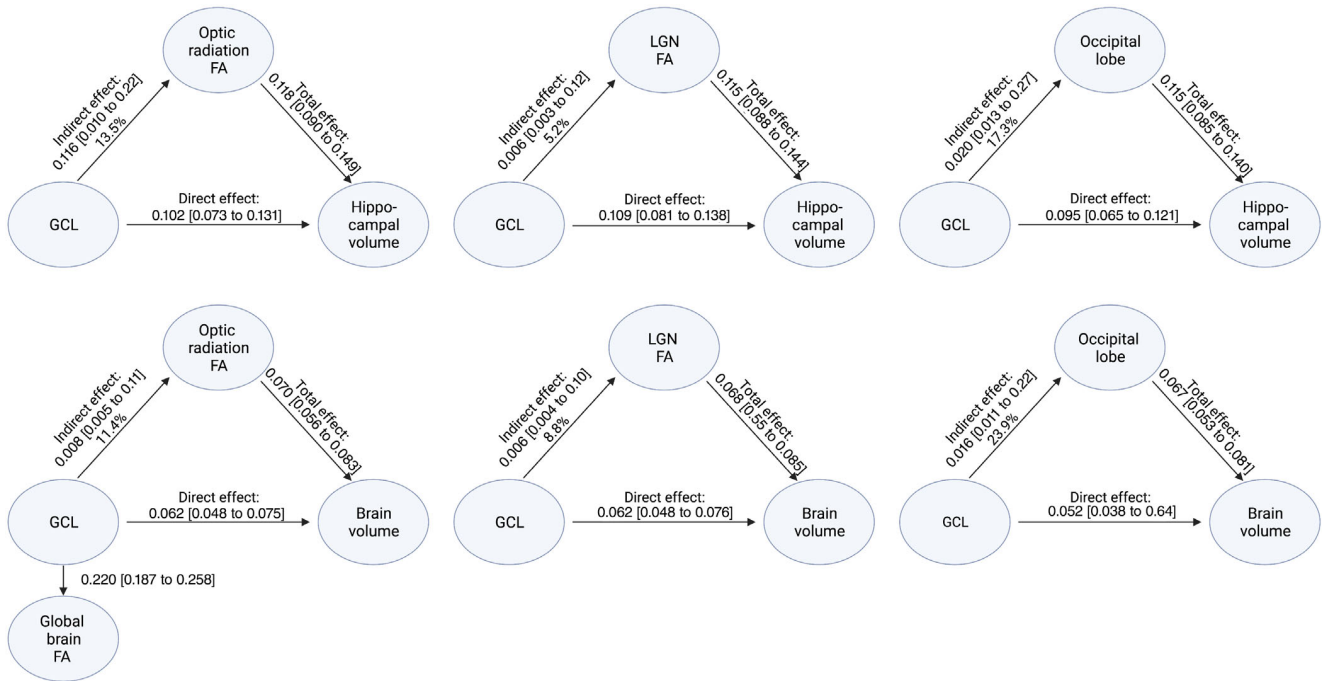
FIGURE 5 The effect of ganglion cell layer degeneration on total and hippocampal atrophy is mediated through disintegration of intermediate visual pathway tracts. All models are adjusted for age, sex, intracranial volume for volumetric measures, global FA for models including optic radiation FA, SBP, and spherical equivalent for models including GCL. All models are nominally significant. FA, fractional anisotropy; GCL, ganglion cell layer; SBP, systolic blood pressure.

for inner retinal layers. Moreover, we observed that visual impairment was associated with decreased structural integrity, measured as lower FA, of all major components of the visual pathway, as well as with lower total brain and hippocampal volume. VA had a much larger effect on optic radiation and global FA than on brain volumetric measures, indicating that microstructural changes might be more sensitive to visual impairment than atrophy. In additional sensitivity analyses, we observed that our findings were robust to exclusion of very low values of VA (LogMar 0.4), extreme refractive errors, and common ophthalmological conditions such as glaucoma and AMD, indicating that subclinical brain changes may occur at milder levels of visual impairment and might be a consequence of any visual impairment regardless of its cause. Importantly, conjoint modeling of the neuroanatomical connections between visual impairment and the different components of the central visual system indicated a pattern consistent with transneuronal degeneration. Thus, our findings imply that visual impairment and degeneration of retinal and central visual pathway structures are closely related, with pathology of any of these components likely to propagate along the entire chain through transneuronal degeneration.

Our findings are in line with previous studies reporting an association between visual impairment and transneuronal degeneration along the visual pathway (Boucard et al., 2009; Hanson et al., 2019; Hernowo et al., 2011, 2014; Malania et al., 2017). Our finding of an association between visual impairment and both total and hippocampal atrophy corroborates previous reports of a link between visual and cognitive impairment (Chen et al., 2017; Lee et al., 2021). We also

observed that retinal neurodegeneration partly mediates the association between visual impairment and brain structural integrity. Although the association between visual impairment and retinal neurodegeneration is likely to be bidirectional, we specifically assessed mediation through GCL volume, which can be interpreted as how visual impairment could affect brain structure independently of (causes related to) inner retinal thinning, such as transneuronal neurodegeneration. Indeed, retinal neurodegeneration was associated with decreased structural integrity measures across the entire visual pathway, which also partly mediated the association between retinal neurodegeneration and both total brain and hippocampal atrophy. Our findings support the notion that retinal neurodegeneration, in part reflecting visual impairment, may reflect changes in the visual pathway up to and including the occipital lobe, leading to decreased activation and degeneration of other interconnected brain regions, ultimately resulting in cerebral atrophy and cognitive decline.

Several studies describing retinal changes in neurological diseases such as Alzheimer disease and multiple sclerosis, have hypothesized involvement of the visual system in the pathophysiology of these disorders (Chan et al., 2018; Mckee et al., 2006; Mirzaei et al., 2020). For example, in Alzheimer disease, visual areas are a primary site of amyloid deposition, while visuospatial symptoms even predominate in the posterior cortical atrophy variant of the disease (Mckee et al., 2006; Mirzaei et al., 2020). Moreover, retinal and brain amyloid deposition might be correlated, with the highest correlation seen in the pericalcarine lobe (Koronyo et al., 2017). Our observation that the direct effect between retinal neurodegeneration and brain atrophy was

consistently larger in magnitude than the indirect effect through visual pathway structures, suggests that apart from transneuronal degeneration, other (shared) etiopathological mechanisms may also account for part of the association. Neuronal damage, due to aging or other pathologies, might lead to neuronal death which is reflected in degeneration of both retinal and cerebral structures. Retinal neurodegeneration therefore also likely reflects central neurodegeneration, independently of visual pathway decay (Garzone et al., 2022). Studies investigating retinal changes in brain diseases with predominant visual involvement and including more granular measures of visual function could further elucidate this relationship.

Indeed, a general neurodegenerative component may also explain the relatively weak direct effect of retinal neurodegeneration on one included "control" area (i.e., middle frontal lobe), although this effect was smaller in magnitude and less robust than for visual pathway areas.

Interestingly, a recent study found increased hippocampal amyloid clearance after exposing Alzheimer's disease transgenic mice to noninvasive light flickering at specific frequencies, thought to be due to restoration of local circuits of excitatory and inhibitory neurons (Iaccarino et al., 2016). Visual stimulation in patients with neurodegenerative diseases may also enhance the release of neurotrophic factors and thereby improve neuronal resilience and plasticity (Yang et al., 2021). In line with these findings, a recent study found a reduction in dementia risk after visual restoration through cataract surgery (Lee et al., 2021), while previous studies observed increased dementia risk in presence of ophthalmic conditions (Klaver & De Jong, 1999; Shang et al., 2021). Our results extend these previous findings by showing that in the general population, even relatively mild degrees of visual impairment and retinal degeneration are robustly associated with worse imaging indices of brain integrity, partly mediated through transneuronal degeneration. Therefore, our findings suggest that treatment of even mild degrees of visual impairment and retinal pathology might help warding off (age-associated) neurodegeneration and cognitive decline.

Our study has both strengths and limitations. Strengths of our study include the large sample size covering a wide age range, a relatively homogenous population-based sample, the employment of detailed imaging markers of both retinal layers and brain structure and connectivity, and concomitant assessment of visual impairment in relation to all key components of the central visual system, allowing for in-depth modelling of their neuroanatomical interconnections. Potential limitations of our study include the lack of more detailed measures of visual function, as VA was approximated using a per chart row and not per optotype. It has been observed that transsynaptic neurodegeneration in the visual pathway proceeds at a certain rate, implying different cerebral effects between early-onset and late-onset visual impairment (Dinkin, 2017; Jindahra et al., 2012). Unfortunately, due to lack of relevant data, we could not analyze the effects of onset and duration of visual impairment on brain integrity measures. Additionally, we accounted for common vascular risk factors that are associated with visual impairment, retinal, and brain changes in our analyses: we excluded individuals with stroke or large cerebral vascular lesions on MRI, adjusted our analyses for several cardiovascular risk factors, and only considered normally appearing white matter for DTI measures; however, some residual confounding might persist through small brain vascular lesions. Furthermore, to aid interpretability of our findings we modeled visual acuity as the average of the two eyes to capture decreased visual brain input, which is considered a valid approach when investigating outcomes operating at an individual level, such as brain areas atrophy. Although also more advanced and complex statistical methods of modeling information from the two eyes have been adopted and described before, the results are generally in line with the approach we have adopted (Murdoch et al., 1998; Ying et al., 2017). Finally, due to the population-based design of the study our disease assessment was based on self-reports, which may be subject to recall bias.

In conclusion, we found that both visual impairment and retinal neurodegeneration were associated with global as well as regional brain atrophy, partly mediated through disintegration of central visual pathways. Our findings thus not only support the use of OCT-derived retinal measures as markers of neurodegeneration, but also indicate that treatment of visual impairment and retinal pathology may be easily actionable, inexpensive measures for the maintenance of brain health and prevention of (age-associated) neurodegeneration and cognitive decline.

AUTHOR CONTRIBUTIONS

CONFLICT OF INTEREST STATEMENT

The author Robert P. Finger declares grants and personal fees from Novartis; grants from Biogen; personal fees from Bayer, Santen, Ophtea, Apellis, Roche/Genentech, Böhringer-Ingelheim, Novelion, ProQR, Oxford Innovation, Roche, Alimera, Santhera, Inositec, and Ellex. Other authors declare no conflict of interest.

DATA AVAILABILITY STATEMENT

The datasets for this article are not publicly available because of data protection regulations. Access to data can be provided to scientists in accordance with the Rhineland Study's Data Use and Access Policy. Requests for further information or to access the datasets should be directed to RS-DUAC@dzne.de.

ORCID

Davide Garzone 🆔 https://orcid.org/0000-0001-6209-117X

REFERENCES

Abdolrahimzadeh, S., Parisi, F., Marcelli, M., Giustolisi, R., & Gharbiya, M. (2019). Optical coherence tomography evidence of macular ganglion cell-inner plexiform layer thinning in eyes with subretinal drusenoid deposits. *Eye (London, England), 33,* 1290–1296.

Aminoff, E. M., Kveraga, K., & Bar, M. (2013). The role of the parahippocampal cortex in cognition. *Trends in Cognitive Sciences, 17,* 379–390.

Andersson, J. L. R., Skare, S., & Ashburner, J. (2003). How to correct susceptibility distortions in spin-echo echo-planar images: Application to diffusion tensor imaging. *NeuroImage, 20,* 870–888.

Basser, P. J., Mattiello, J., & LeBihan, D. (1994). MR diffusion tensor spectroscopy and imaging. *Biophysical Journal, 66,* 259–267.

Boucard, C. C., Hernowo, A. T., Maguire, R. P., Jansonius, N. M., Roerdink, J. B., Hooymans, J. M., & Cornelissen, F. W. (2009). Changes in cortical grey matter density associated with long-standing retinal visual field defects. *Brain, 132,* 1898–1906.

Brenner, D., Stirnberg, R., Pracht, E. D., & Stöcker, T. (2014). Two-dimensional accelerated MP-RAGE imaging with flexible linear reordering. *Magnetic Resonance Materials in Physics, Biology and Medicine, 27,* 455–462.

Buckner, R. L., Head, D., Parker, J., Fotenos, A. F., Marcus, D., Morris, J. C., & Snyder, A. Z. (2004). A unified approach for morphometric and functional data analysis in young, old, and demented adults using automated atlas-based head size normalization: Reliability and validation against manual measurement of total intracranial volume. *NeuroImage, 23,* 724–738.

Bürgel, U., Amunts, K., Hoemke, L., Mohlberg, H., Gilsbach, J. M., & Zilles, K. (2006). White matter fiber tracts of the human brain: Three-dimensional mapping at microscopic resolution, topography and intersubject variability. *NeuroImage, 29,* 1092–1105.

Chan, V. T. T., Sun, Z., Tang, S., Chen, L. J., Wong, A., Tham, C. C., Wong, T. Y., Chen, C., Ikram, M. K., Whitson, H. E., Lad, E. M., Mok, V. C. T., & Cheung, C. Y. (2018). Spectral-domain OCT measurements in Alzheimer's disease: A systematic review and meta-analysis. *Ophthalmology, 4,* 1–14.

Chen, S. P., Bhattacharya, J., & Pershing, S. (2017). Association of vision loss with cognition in older adults. *JAMA Ophthalmology, 135,* 963–970.

Chiang, T. T. K., Keenan, T. D., Agrón, E., Liao, J., Klein, B., Chew, E. Y., Cukras, C. A., & Wong, W. T. (2020). Macular thickness in intermediate age-related macular degeneration is influenced by disease severity and subretinal Drusenoid deposit presence. *Investigative Ophthalmology & Visual Science, 61,* 59.

Collignon, O., Dormal, G., Albouy, G., Vandewalle, G., Voss, P., Phillips, C., & Lepore, F. (2013). Impact of blindness onset on the functional organization and the connectivity of the occipital cortex. *Brain, 136,* 2769–2783.

Dinkin, M. (2017). Trans-synaptic retrograde degeneration in the human visual system: Slow, silent, and real. *Current Neurology and Neuroscience Reports, 17,* 16.

Fischl, B. (2012). FreeSurfer. *Neuroimage, 62,* 774–781.

Fischl, B., Salat, D. H., Busa, E., Albert, M., Dieterich, M., Haselgrove, C., van der Kouwe, A., Killiany, R., Kennedy, D., Klaveness, S., Montillo, A., Makris, N., Rosen, B., & Dale, A. M. (2002). Whole brain segmentation: Automated labeling of neuroanatomical structures in the human brain. *Neuron, 33,* 341–355.

Fleitas, M. F. G., Aranda, M. L., Diéguez, H. H., Milne, G., Langellotti, L., Miranda, M., Altschuler, F., Dorfman, D., & Rosenstein, R. E. (2020). The "Use It or Lose It" dogma in the retina: Visual stimulation promotes protection against retinal ischemia. *Molecular Neurobiology, 57,* 435–449.

Garzone, D., Finger, R. P., Mauschitz, M. M., Santos, M. L. S., Breteler, M. M. B., & Aziz, N. A. (2022). Neurofilament light chain and retinal layers' determinants and association: A population-based study. *Annals of Clinical Translational Neurology, 9,* 564–569. https://doi.org/10.1002/ACN3.51522

Hanson, R. L. W., Gale, R. P., Gouws, A. D., Airody, A., Scott, M. T. W., Akthar, F., Waterson, S., Wells, M. T., Wright, A. J., Bell, K., Silson, E., Baseler, H. A., & Morland, A. B. (2019). Following the status of visual cortex over time in patients with macular degeneration reveals atrophy of visually deprived brain regions. *Investigative Ophthalmology & Visual Science, 60,* 5045–5051.

Harms, R. L., Fritz, F. J., Tobisch, A., Goebel, R., & Roebroeck, A. (2017). Robust and fast nonlinear optimization of diffusion MRI microstructure models. *NeuroImage, 155,* 82–96.

Hernowo, A. T., Boucard, C. C., Jansonius, N. M., Hooymans, J. M. M., & Cornelissen, F. W. (2011). Automated morphometry of the visual pathway in primary open-angle glaucoma. *Investigative Opthalmology & Visual Science, 52,* 2758–2766.

Hernowo, A. T., Prins, D., Baseler, H. A., Plank, T., Gouws, A. D., Hooymans, J. M., Morland, A. B., Greenlee, M. W., & Cornelissen, F. W. (2014). Morphometric analyses of the visual pathways in macular degeneration. *Cortex, 56,* 99–110.

Huang, X., Li, S. H., Zhou, F. Q., Zhang, Y., Zhong, Y. L., Cai, F. Q., Shao, Y., & Zeng, X.-J. (2016). Altered intrinsic regional brain spontaneous activity in patients with comitant strabismus: A resting-state functional MRI study. *Neuropsychiatric Disease and Treatment, 12,* 1303–1308.

Iaccarino, H. F., Singer, A. C., Martorell, A. J., Rudenko, A., Gao, F., Gillingham, T. Z., Mathys, H., Seo, J., Kritskiy, O., Abdurrob, F., Adaikkan, C., Canter, R. G., Rueda, R., Brown, E. N., Boyden, E. S., & Tsai, L.-H. (2016). Gamma frequency entrainment attenuates amyloid load and modifies microglia. *Nature, 540,* 230–235.

Jack, C. R., Petersen, R. C., Xu, Y., O'Brien, P. C., Smith, G. E., Ivnik, R. J., Tangalos, E. G., & Kokmen, E. (1998). The rate of medial temporal lobe atrophy in typical aging and Alzheimer's disease. *Neurology, 51,* 993–999.

Jindahra, P., Petrie, A., & Plant, G. T. (2012). The time course of retrograde trans-synaptic degeneration following occipital lobe damage in humans. *Brain, 135,* 534–541.

Klaver, C. C. W., … De Jong, P. T. V. M. (1999). Is age-related maculopathy associated with Alzheimer's disease?: The Rotterdam study. *American Journal of Epidemiology, 150,* 963–968.

Koronyo, Y., Biggs, D., Barron, E., Boyer, D. S., Pearlman, J. A., Au, W. J., Kile, S. J., Blanco, A., Fuchs, D. T., Ashfaq, A., Frautschy, S., Cole, G. M., Miller, C. A., Hinton, D. R., Verdooner, S. R., Black, K. L., & Koronyo-Hamaoui, M. (2017). Retinal amyloid pathology and proof-of-concept imaging trial in Alzheimer's disease. *JCI Insight, 2,* e93621.

Kravitz, D. J., Saleem, K. S., Baker, C. I., & Mishkin, M. (2011). A new neural framework for visuospatial processing. *Nature Reviews. Neuroscience, 12,* 217–230.

Lee, C. S., Gibbons, L. E., Lee, A. Y., Yanagihara, R. T., Blazes, M. S., Lee, M. L., McCurry, S. M., Bowen, J. D., McCormick, W. C., Crane, P. K., & Larson, E. B. (2021). Association between cataract extraction and development of dementia. *JAMA Internal Medicine, 182,* 134. https://doi.org/10.1001/JAMAINTERNMED.2021.6990

Li, J., Zhou, Y., Chen, F., Li, Y., Zhou, R., Wu, C., Yu, H., Lin, Z., Shi, C., Zheng, G., Shao, Y., Chen, Q., Lu, F., & Shen, M. (2021). Visual acuity is

correlated with ischemia and neurodegeneration in patients with early stages of diabetic retinopathy. *Eye and Vision*, 8(1), 38.

Lohner, V., Enkirch, S. J., Hattingen, E., Stöcker, T., & Breteler, M. M. B. (2022). Safety of tattoos, permanent make-up, and medical implants in population-based 3T magnetic resonance brain imaging: The Rhineland study. *Frontiers in Neurology*, 13, 1–7.

Malania, M., Konrad, J., Jägle, H., Werner, J. S., & Greenlee, M. W. (2017). Compromised integrity of central visual pathways in patients with macular degeneration. *Investigative Opthalmology & Visual Science*, 58, 2939–2947.

Martorell, A. J., Paulson, A. L., Suk, H. J., Abdurrob, F., Drummond, G. T., Guan, W., Young, J. Z., Kim, D. N., Kritskiy, O., Barker, S. J., Mangena, V., Prince, S. M., Brown, E. N., Chung, K., Boyden, E. S., Singer, A. C., & Tsai, L. H. (2019). Multi-sensory gamma stimulation ameliorates Alzheimer's-associated pathology and improves cognition. *Cell*, 177, 256–271.e22.

Mauschitz, M. M., Bonnemaijer, P. W. M., Diers, K., Rauscher, F. G., Elze, T., Engel, C., Loeffler, M., Colijn, J. M., Ikram, M. A., Vingerling, J. R., Williams, K. M., Hammond, C. J., Creuzot-Garcher, C., Bron, A. M., Silva, R., Nunes, S., Delcourt, C., Cougnard-Grégoire, A., Holz, F. G., & Klaver, C. C. W. (2018). Systemic and ocular determinants of Peripapillary retinal nerve fiber layer thickness measurements in the European eye epidemiology (E3) population. *Ophthalmology*, 125, 1526–1536.

Mauschitz, M. M., Holz, F. G., Finger, R. P., & Breteler, M. M. B. (2019). Determinants of macular layers and optic disc characteristics on SD-OCT: The rhineland study. *Translational Vision Science & Technology*, 8, 34.

Mckee, A. C., Au, R., Cabral, H. J., Kowall, N. W., Seshadri, S., Kubilus, C. A., Drake, J., & Wolf, P. A. (2006). Visual association pathology in preclinical Alzheimer disease. *Journal of Neuropathology & Experimental Neurology*, 65, 621–630.

Mendola, J. D., Lam, J., Rosenstein, M., Lewis, L. B., & Shmuel, A. (2018). Partial correlation analysis reveals abnormal retinotopically organized functional connectivity of visual areas in amblyopia. *Neuroimage Clin*, 18, 192–201.

Mirzaei, N., Shi, H., Oviatt, M., Doustar, J., Rentsendorj, A., Fuchs, D. T., Sheyn, J., Black, K. L., Koronyo, Y., & Koronyo-Hamaoui, M. (2020). Alzheimer's retinopathy: Seeing disease in the eyes. *Frontiers in Neuroscience*, 14, 921.

Mishkin, M., Ungerleider, L. G., & Macko, K. A. (1983). Object vision and spatial vision: Two cortical pathways. *Trends in Neurosciences*, 6, 414–417.

Murdoch, I. E., Morris, S. S., & Cousens, S. N. (1998). People and eyes: Statistical approaches in ophthalmology. *The British Journal of Ophthalmology*, 82, 971–973.

Mutlu, U., Bonnemaijer, P. W. M., Ikram, M. A., Colijn, J. M., Cremers, L. G. M., Buitendijk, G. H. S., Vingerling, J. R., Niessen, W. J., Vernooij, M. W., Klaver, C. C. W., & Ikram, M. K. (2017). Retinal neurodegeneration and brain MRI markers: The Rotterdam study. *Neurobiology of Aging*, 60, 183–191.

Mutlu, U., Ikram, M. K., Roshchupkin, G. V., Bonnemaijer, P. W. M., Colijn, J. M., Vingerling, J. R., Niessen, W. J., Ikram, M. A., Klaver, C. C. W., & Vernooij, M. W. (2018). Thinner retinal layers are associated with changes in the visual pathway: A population-based study. *Human Brain Mapping*, 39, 4290–4301.

Pfeiffer, R. L., Marc, R. E., & Jones, B. W. (2020). Persistent remodeling and neurodegeneration in late-stage retinal degeneration. *Progress in Retinal and Eye Research*, 74, 100771.

Pillay, G., Ganger, A., Singh, D., Bhatia, R., Sharma, P., Menon, V., & Saxena, R. (2018). Retinal nerve fiber layer and ganglion cell layer changes on optical coherence tomography in early multiple sclerosis and optic neuritis cases. *Indian Journal of Ophthalmology*, 66, 114–119.

Prins, D., Hanekamp, S., & Cornelissen, F. W. (2016). Structural brain MRI studies in eye diseases: Are they clinically relevant? A review of current findings. *Acta Ophthalmologica*, 94, 113–121.

Rosseel, Y. (2012). Lavaan: An *R* package for structural equation modeling. *Journal of Statistical Software*, 48, 1–36.

Sabbah, N., Sanda, N., Authié, C. N., Mohand-Saïd, S., Sahel, J. A., Habas, C., Amedi, A., & Safran, A. B. (2017). Reorganization of early visual cortex functional connectivity following selective peripheral and central visual loss. *Scientific Reports*, 7, 43223.

Sanda, N., Cerliani, L., Authié, C. N., Sabbah, N., Sahel, J. A., Habas, C., Safran, A. B., & Thiebaut de Schotten, M. (2018). Visual brain plasticity induced by central and peripheral visual field loss. *Brain Structure & Function*, 223, 3473–3485.

Schulze-Bonsel, K., Feltgen, N., Burau, H., Hansen, L., & Bach, M. (2006). Visual acuities "hand motion" and "counting fingers" can Be quantified with the Freiburg visual acuity test. *Investigative Ophthalmology & Visual Science*, 47, 1236–1240.

Setsompop, K., Gagoski, B. A., Polimeni, J. R., Witzel, T., Wedeen, V. J., & Wald, L. L. (2012). Blipped-controlled aliasing in parallel imaging for simultaneous multislice echo planar imaging with reduced g-factor penalty. *Magnetic Resonance in Medicine*, 67, 1210–1224.

Shang, X., Zhu, Z., Huang, Y., Zhang, X., Wang, W., Shi, D., Jiang, Y., Yang, X., & He, M. (2021). Associations of ophthalmic and systemic conditions with incident dementia in the UK biobank. *British Journal of Ophthalmology*, 107, 275–282.

Silson, E. H., Zeidman, P., Knapen, T., & Baker, C. I. (2020). Representation of contralateral visual space in the human hippocampus. bioRxiv July 30, 2020.228361. https://doi.org/10.1101/2020.07.30.228361

Tobisch, A., Schultz, T., Stirnberg, R., Varela-Mattatall, G., Knutsson, H., Irarrázaval, P., & Stöcker, T. (2019). Comparison of basis functions and q-space sampling schemes for robust compressed sensing reconstruction accelerating diffusion spectrum imaging. *NMR in Biomedicine*, 32, e4055.

Tobisch, A., Stirnberg, R., Harms, R. L., Schultz, T., Roebroeck, A., Breteler, M. M. B., & Stöcker, T. (2018). Compressed sensing diffusion spectrum imaging for accelerated diffusion microstructure MRI in long-term population imaging. *Frontiers in Neuroscience*, 12, 650.

van Dijk, H. W., Verbraak, F. D., Stehouwer, M., Kok, P. H., Garvin, M. K., Sonka, M., DeVries, J. H., Schlingemann, R. O., & Abràmoff, M. D. (2011). Association of visual function and ganglion cell layer thickness in patients with diabetes mellitus type 1 and no or minimal diabetic retinopathy. *Vision Research*, 51, 224–228.

Ward, D. D., Mauschitz, M. M., Bönniger, M. M., Merten, N., Finger, R. P., & Breteler, M. M. B. (2020). Association of retinal layer measurements and adult cognitive function: A population-based study. *Neurology*, 95, e1144–e1152.

Yang, H., Luo, Y., Hu, Q., Tian, X., & Wen, H. (2021). Benefits in Alzheimer's disease of sensory and multisensory stimulation. *Journal of Alzheimer's Disease*, 82, 463–484.

Ying, G. S., Maguire, M. G., Glynn, R., & Rosner, B. (2017). Tutorial on biostatistics: Linear regression analysis of continuous correlated eye data. *Ophthalmic Epidemiology*, 24, 130–140. https://doi.org/10.1080/09286586.2016.1259636

Zilles, K., & Amunts, K. (2012). Architecture of the cerebral cortex. In J. K. Mai & G. Paxinos (Eds.), *The Human Nervous System* (3rd ed., pp. 836–895). Elsevier. https://doi.org/10.1016/B978-0-12-374236-0.10023-9

SUPPORTING INFORMATION

Additional supporting information can be found online in the Supporting Information section at the end of this article.

6. Discussion and outline of future work

In this chapter I will summarize and discuss the implications of my research, and provide an outlook for future research.

6.1 Age-related macular degeneration

My thesis largely focused on AMD, the leading cause of blindness in Western countries. AMD burden is expected to increase in the next decades due to an aging population.(Colijn et al. 2017) This calls for more AMD research, which in early AMD stages should aim at 1) better stratifying the risk of AMD progression and 2) to generate clinical endpoints for therapeutic interventions aimed at preventing or delaying AMD progression.(Finger et al. 2019)

The Rhineland Study is one of the first population-based studies integrating multimodal imaging and can provide significant steps forward in this direction. In this thesis, I first described grading methods and prevalence data of AMD in the Rhineland Study cohort. The prevalence of AMD was comparable to that of other population-based studies. Particular attention was given to the role of high-risk markers in AMD, RPD and LDA. RPD were identified in 93 (1.9%) of the population sample and 87 (9.3%) of individuals with AMD, while LDA in 78 (8.3%) of individuals with AMD, indicating these individuals are at higher risk of progression to late AMD. Risk stratification in e- and iAMD is crucial, since as showed in Chapter 2, they are common in the general population. I have also highlighted how multimodal imaging is crucial for deeper AMD phenotyping. This is also exemplified by the case of pachychoroid lesions, for which in the Rhineland Study cohort I observed a prevalence of 2.8%. Several studies highlighted how these two phenotypes might have different etiology and markers, which might translate as different therapeutic options. This was also shown in this thesis, as the GRS for AMD was negatively associated with pachychoroid diseases. Furthermore, associations with younger age and hyperopia were noted. However, in many cases a distinction is not possible only based on CFP and currently, epidemiological data on pachychoroid diseases are missing.

We also highlighted how ML-based imaging analysis provides great potential for automation of grading tasks; this provides an opportunity for great breakthroughs in AMD and ophthalmological research in the next years, such as in the transition from AMD

Beckmann stages to a multi-modal AMD classification including OCT-derived drusen volume, but its implementation should be gradual and careful. This was the main rationale behind the assessment of automated drusen volume measurements in the MACUSTAR Cohort, which not only provided data on drusen volume distribution across different AMD stages with two methods of automated drusen volume measurements, but also highlighted how different methods for imaging markers detection might be not fully interchangeable. Next step is the implementation of automated drusen volume assessment in the Rhineland Study cohort, whose validation I worked on in the last year of my PhD. This might provide for a first study showing the distribution of drusen volume in a population-based cohort. Furthermore, as mentioned in Chapter 5, RPE elevations are filtered out in both algorithms employed if smaller than 5 µm of height; interestingly, this threshold is purely based on empirical observations and its performance in terms of accuracy of drusen delineation has not been assessed yet. An objective threshold to distinguish significant RPE elevations in the future is needed. Other next steps should also include the necessary further grading and expansion of the Rhineland Study cohort and assessment of the association between AMD and many cutting-edge biomarkers available in the Rhineland Study, as well as data integration in longitudinal analyses, which will allow AMD progression assessment as outcome.

6.2   Retinal markers of brain´s health and disease

We have shown that, after taking ocular and systemic factors into account, OCT-derived retinal layers´ atrophy were associated with important neurological markers, such as plasma NfL and both regional (visual and cognitive brain areas) and general brain atrophy. After adjustment for relevant confounders (mainly GFR, blood volume and age), plasma NfL levels can be interpreted as a sensitive and disease-unspecific proxy of neuroaxonal damage and thus indirectly, of neurodegeneration. We observed that in a population-based cohort, mainly ageing, and secondarily neurological diseases and cardiovascular risk factors are the main determinant of an association between the two markers.

Interestingly, we also observed that inner retinal neurodegeneration is associated not only with general markers of brain and neuronal integrity such as plasma NfL and brain atrophy, but also with visual acuity and integrity of brain areas deputed to visual (occipital lobe) and cognitive (hippocampus) functions. The retinal layers in direct synaptic connection

with brain visual pathway structures showed the strongest connection in our analyses (namely GCL and pRNFL). The study attempted to determine if the associations were due to trans-neuronal degeneration along the visual pathway or generalized neuronal damage. Trans-neuronal degeneration had been mainly documented in small, selected cohort with visually impaired individuals; our results indicate it might play a role also in a population-based sample with relatively low prevalence of visual impairment. However, it must be noted that a common neuronal injury theory accounted for most of the association between retinal and both global brain and hippocampal atrophy.

Visual impairment was linked to a reduction in the integrity of both visual and cognitive brain regions. These encompass key areas such as the occipital cortex and white matter tracts, along with global measures like whole brain atrophy and white matter integrity. This underscores the crucial role of visual acuity as a potentially modifiable risk factor in preventive strategies targeting cognitive impairment. The ultimate goal is to enhance the quality of life through interventions that can also address visual impairment.

A main limitation of these analyses was their cross-sectional nature: temporal relationships can help identify causal relationships. This is particularly relevant in the case of our analysis on the association between plasma NfL and retinal layers atrophy, which paves the way for a longitudinal analysis. The Rhineland Study is planned longitudinally; hence this limitation will be overcome in the next years. Another limitation is given by previous authors recommending caution in utilizing mediation analysis in cross-sectional settings, but a strong hypothesis and evidence of causal relationship from previous literature support this.

Based on my analyses and on previous literature, I conclude that OCT-based imaging of retinal layers provides great potential for the assessment of brain´s health and disease, and implementation in real-life clinical scenarios is possible, but more research is needed, involving close collaboration between ophthalmology and neurology specialists. It must be noted that the implementation of imaging-based markers in real-life scenarios does not follow strict guidelines and is therefore somewhat more arbitrary than, for example, the approval of a new drug for a medical condition, for which clinical phases are clearly delineated. (Fryback and Thornbury 1991; Nierenberg 1988)

I hypothesize that possible roles of retinal markers include:

1) Monitoring
2) Diagnostic
3) Screening

Integrating retinal imaging in real-life scenarios: Diagnostics

Different cellular pathophysiology underlies different neurological diseases, which might also be reflected as retinal structural changes. The hypothesis that specific patterns of retinal changes might occur in different neurological diseases, needs to be further explored and assessed in clinical studies. This should involve different layers at different locations in the retina, assessed through different OCT scans, and possibly other imaging methods. An example of a disease-specific retinal thinning pattern is provided by Glaucoma, in which the primary event is the loss of GCL and RNFL, starting in the inferonasal quadrant and later involving other retinal quadrants.

Nowadays, literature available from large studies is mainly based on cross-sectional analyses. For achieving this, large, longitudinal cohorts are needed, employing different retinal scans and imaging methods. Examples in AD are AlzEye and Atlas of retinal Imaging in Alzheimer´s Study (ARIAS). (Alber et al. 2020; Wagner et al. 2022) Despite my analyses being based on cross-sectional data, the design of the Rhineland Study is longitudinal, which might allow to overcome these limitations in the literature.

In this context, newer retinal imaging such as adaptive-optics OCT or ultra-wide field might provide deeper phenotyping than SD-OCT. Adaptive-optics has the potential to directly resolve single retinal neurons. For example, in Parkinson disease dopaminergic neurons are affected, and adaptive optics might allow the observation of retinal dopaminergic inter- and horizontal neurons in vivo. (Zhang, Zhou, and McMahon 2007)

Furthermore, our analyses and previous studies showed that retinal layers´ atrophy, in particular GCL, might be more closely associated with atrophy in visual brain areas than whole brain areas; given the high variety of visual symptoms and visual variants in some neurological diseases, a possible use of retinal neurodegeneration to assess cerebral visual areas integrity deserves further consideration. In this regard, a previous meta-analysis already observed that among individuals with a diagnosis of multiple sclerosis, retinal atrophy is predictive of optic nerve involvement. (Petzold et al. 2017)

Integrating retinal imaging in real-life scenarios: Monitoring

In virtue of retinal and brain neurons undergoing similar pathology and as highlighted in our analyses, retinal neurodegeneration might be an easily accessible proxy to track cerebral neurodegeneration, for example as a secondary end-point in clinical trials. However, as mentioned, large longitudinal studies are needed to further clarify their relationship, both population-based and in specific pathologies.

Integrating retinal imaging in real-life scenarios: Screening

While retinal OCT-derived biomarkers can be used as a window to the brain, nowadays OCT is also a first-line diagnostics for retinal diseases. By performing SD-OCT in selected groups of at-risk individuals based on age or risk factors, " two (or more) birds with one stone could be killed": namely screen for ophthalmological diseases and neurodegeneration. For example, an inner retina that is thinner than normal for age and for spherical equivalent in an elderly individual might prompt a referral to a neurology department or a memory clinic.

Furthermore, the advent of more advanced imaging beyond OCT and the integration of AI-algorithms for automated markers extraction provide overarching potential. For example, enhanced depth imaging can fully resolve the choroid on OCT, whose thickness has been explored as a marker of cardiovascular and renal function. (Choi & Kim, 2020; Choi et al. 2009)

Markers such as arterioles or venules calibers and fractal dimension have been already largely explored as predictive of cardio- and cerebrovascular risk; OCT-Angiography, whose implementation in the second round of the Rhineland Study I worked on in the last year of my PhD, provides for new, more granular vascular biomarkers. Wide- and ultrawide-field imaging allows to visualize a 180° image of the retina in a single shot, hence displaying markers and lesions in the peripheral retinal. Adaptive-optics can increase OCT resolution up to a cellular level.

Point-of-care imaging centers that provide retinal imaging outside of hospitals could be worth exploring for emergency triage but also screening purposes. However, it must be noted that screening is based on a cost-benefit analysis basis: effective therapeutic and preventative strategies are needed for the outcomes that are screened for, which in the

cases of neurodegeneration, cognitive impairment or early AMD are at the moment lacking.

6.3 General conclusion

I described the grading of AMD data in the Rhineland Study and how utilizing state-of-the-art multimodal retinal imaging can allow for deeper AMD phenotyping. This is showcased by the examples of RPD detection and differentiation from pachychoroid manifestations. I also described my research on how OCT-derived markers can be provide useful markers for brain structure and disease, and I highlighted possible future research in this direction. Finally, I showed how visual impairment can be also detrimental for brain structure.

In conclusion, integration of retinal imaging in population-based studies holds significant potential for advancing our understanding of retinal diseases and for investigating overarching markers of brain structure and the aging process.

Bibliography

Alber, Jessica, Edmund Arthur, Louisa I Thompson, Danielle Goldfarb, Brian M Fernandez, Stephen P Salloway, Stuart Sinoff, and Peter J Snyder. 2020. "The Atlas of Retinal Imaging in Alzheimer's Study (ARIAS): Study Design and Objectives." *Alzheimer's & Dementia* 16 (S5): e045325. https://doi.org/10.1002/ALZ.045325.

Choi, Min Gyu, and Jee Taek Kim. 2020. "Strong Correlation of Renal Function with Choroidal Thickness in Patients with Type 2 Diabetes: Retrospective Cross-Sectional Study." *Journal of Clinical Medicine* 9 (7): 1–12. https://doi.org/10.3390/JCM9072171.

Colijn, Johanna M, Gabriëlle H S Buitendijk, Elena Prokofyeva, Dalila Alves, Maria L Cachulo, Anthony P Khawaja, Audrey Cougnard-Gregoire, et al. 2017. "Prevalence of Age-Related Macular Degeneration in Europe: The Past and the Future." *Ophthalmology* 124 (12): 1753–63. https://doi.org/10.1016/j.ophtha.2017.05.035.

Finger, Robert P., Steffen Schmitz-Valckenberg, Matthias Schmid, Gary S. Rubin, Hannah Dunbar, Adnan Tufail, David P. Crabb, et al. 2019. "MACUSTAR: Development and Clinical Validation of Functional, Structural, and Patient-Reported Endpoints in Intermediate Age-Related Macular Degeneration." *Ophthalmologica. Journal International d'ophtalmologie. International Journal of Ophthalmology. Zeitschrift Fur Augenheilkunde* 241 (2): 61–72. https://doi.org/10.1159/000491402.

Fryback, Dennis G., and John R. Thornbury. 1991. "The Efficacy of Diagnostic Imaging." *Medical Decision Making* 11 (2): 88–94. https://doi.org/10.1177/0272989X9101100203.

Nierenberg, Andrew A. 1988. "How to Evaluate a Diagnostic Marker Test." *Jama* 259 (11): 1699. https://doi.org/10.1001/jama.1988.03720110061036.

Petzold, Axel, Laura Balcer, Peter A. Calabresi, Fiona Costello, Teresa Frohman, Elliot Frohman, Elena H. Martinez-Lapiscina, et al. 2017. "Retinal Layer Segmentation in Multiple Sclerosis: A Systematic Review and Meta-Analysis." *The Lancet Neurology* 16 (10): 797–812. https://doi.org/10.1016/S1474-4422(17)30278-8.

Uk Choi, Sang, Ja Young, & Jee, and Taek Kim. 123AD. "Correlations between Choroidal Thickness and Renal Function in Patients with Retinal Vein Occlusion." *Scientific RepoRtS* | 10: 16865. https://doi.org/10.1038/s41598-020-74058-0.

Wagner, Siegfried Karl, Fintan Hughes, Mario Cortina-Borja, Nikolas Pontikos, Robbert Struyven, Xiaoxuan Liu, Hugh Montgomery, et al. 2022. "AlzEye: Longitudinal

Record-Level Linkage of Ophthalmic Imaging and Hospital Admissions of 353 157 Patients in London, UK." *BMJ Open* 12 (3): e058552. https://doi.org/10.1136/BMJOPEN-2021-058552.

Zhang, Dao Qi, Tong Rong Zhou, and Douglas G. McMahon. 2007. "Functional Heterogeneity of Retinal Dopaminergic Neurons Underlying Their Multiple Roles in Vision." *Journal of Neuroscience* 27 (3): 692–99. https://doi.org/10.1523/JNEUROSCI.4478-06.2007.